Contraction dynamics of biological muscles: mechanical and thermodynamical prediction, and experimental verification

Von der Fakultät für Mathematik und Physik der Universität Stuttgart
zur Erlangung der Würden eines Doktors
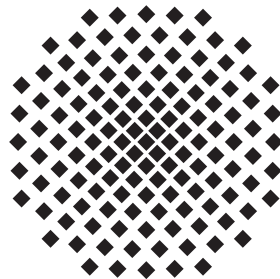der Naturwissenschaften (Dr. rer. nat.) genehmigte Abhandlung

Vorgelegt von

Daniel Florian Benedict Häufle

aus Filderstadt

Hauptberichter:	Prof. Dr. Günter Wunner
1. Mitberichter:	Prof. Dr. Jörg Wrachtrup
2. Mitberichter:	Jun.-Prof. Dr. Syn Schmitt

Tag der mündlichen Prüfung: 18. Dezember 2012

1. Institut für Theoretische Physik der Universität Stuttgart
2013

Contents

Contents

Abstract

When looking back on the recent Olympic Games in London (2012) there is something absolutely fascinating in how elegant, diverse, and complex human movement is: running, swimming, rowing, throwing, jumping, fencing, and so on. It is an inspiring challenge to investigate how humans and animals generate and organize movement. It is the aim of this thesis to add a few pieces to this puzzle.

Both humans and animals alike live in a universe which is governed by fundamental laws and principles. Physics is dedicated to reveal and quantify these fundamental principles that ultimately result in such a great diversity. The great success of physics lies in the interplay of theoretical predictions using mathematical models, and experimental verification or falsification of which. This will work particularly well, if the object of study can be isolated and thus investigated independent of all other phenomena. Unfortunately, isolating the fundamental structures that govern biological movement generation is very difficult for two reasons. Firstly, from an ethics perspective it is unacceptable to isolate relevant structures in living humans to study them independent of the rest of the body. Secondly, movement generation is a dynamical process involving not only biomechanical structures, e.g., muscles, bones, ligaments, etc. but also metabolic energy processing, physiological sensing, and neuronal control. Thus, isolating the object of study means to destroy the complex dynamics, in which it might play a crucial role. In recent years, it has become more and more clear that movement generation can only be understood if it is investigated in an integrated approach.

The work presented in this thesis aims towards such an integrated approach. It builds upon the results of physiological experiments with isolated animal muscles over the course of which their distinct dynamic properties have been described in great detail. Derived from previous simulation studies, the hypotheses posed were that (1) the dynamic properties of muscles strongly contribute to generation and control of movements, (2) they allow very simple control strategies, (3) and thus reduce control effort in comparison to (technical) systems whose actuators do not have similar dynamic properties.

Hypotheses (1) and (2) were substantiated in the **1$^{\text{st}}$ study** of this thesis. Here, hopping was used as a template model to study the relation of muscle properties, control strategies, and interaction with the environment. In a numeric hopping model the level of represented detail of the muscle's material properties (force-length-velocity relation) was varied to test their influence on periodic hopping. It was found that the typical non-linear force-velocity relation of the biological muscle improves hopping stability as compared to a linear approximation. Additionally, hopping stability could be further improved by combining feed-forward and feedback control. The results highlight the importance of the muscle properties, especially that of the force-velocity relation for the control of periodic movements. They also emphasize the ability of organisms to exploit the stabilizing properties of intrinsic muscle characteristics.

Hypothesis (3) was substantiated in the **2$^{\text{nd}}$ study**: If an organism exploits the dynamic properties of muscles, the control effort will be less than in a comparable (technical) system without these properties. Beforehand, a quantitative comparison between biological and technical actuators has not been possible because definitions of control effort were based on system specific measures, such as voltages, pressure, muscle activity, etc. Therefore, a new measure of control effort based on information theory was developed. Applied to the hopping

models this method revealed that the required information to control hopping can be as low as $I = 34$ bit with a muscle vs. $I = 798$ bit with a DC-motor. Concerning the muscle, the control strategy was particularly designed to exploit the muscle properties. In case of the DC-motor, a typical engineering control approach was chosen, where a negative-feedback controller was used to enforce a predefined trajectory regardless of the actuator properties. This shows that the approach to control effort based on information theory is applicable to and comparable across completely different actuator designs and control approaches.

Both studies emphasize the importance of the hyperbolic force-velocity relation. It helps to stabilize periodic movements and allows reducing the control effort. Therefore, the following two studies focus on the investigation of the physical origin of the force-velocity relation.

3$^\text{rd}$ study: So far, biomechanical muscle models incorporated the force-velocity relation as a phenomenological fit to experimental data, i.e. a hyperbolic function. Only microscopic muscle models proposed a physical origin of the hyperbolic force-velocity relation. However, microscopic muscle models can neither be used in simulation studies of complex human movements, nor as a blueprint for the construction of artificial muscles. A different macroscopic model predicted the hyperbolic force-velocity relation from an arrangement of three macroscopic physical components: a mechanical energy source (active element AE), a parallel damper element (PDE), and a serial element (SE) that exhibits operating points with hyperbolic force-velocity dependency. The open question addressed in the 3$^\text{rd}$ study was, whether this analytical model works in reality. To verify the contraction dynamics of this model, the analytical model was compared to a numerical simulation and a hardware implementation. The analytical model only predicts the operating points at steady state, whereas the numerical model includes the dynamics of the contraction, and the hardware implementation is used to verify the real world functionality of the concept. The same experiments as usually performed with biological muscles were conducted, i.e. quick release experiments against different loads. A similar hyperbolic force-velocity relation was found in the numerical model and the hardware implementation. However, deviations from the analytical prediction were found.

To resolve these discrepancies, two types of quick release experiments were performed in the **4$^\text{th}$ study**. These experiments represent two extreme cases of the contraction dynamics, i.e. against a constant force (isotonic) and against an inertial mass. Both experiments revealed hyperbolic force-velocity relations. Interestingly, the analytical model not only predicts these extreme cases, but additionally all contraction states in between as well. It was possible to validate these predictions with the numerical model and the hardware experiment. These results prove that the origin of the hyperbolic force-velocity relation can be mechanically explained on a macroscopic level by the dynamical interaction of three mechanical elements. Thus, the concept can be seen as a starting point for the development of muscle-like bionic actuators.

With these studies, this thesis contributes to the understanding of the role that muscles play in the control of periodic movements, and proposes a design concept allowing a transfer of their beneficial properties into technical systems. By using information theory to quantify the control effort, technical biological systems can be compared and key characteristics can be identified. These new insights and methods contribute to the integrated view of biological movement generation – a few pieces of the big puzzle.

Kurzbeschreibung

Wenn man an die Olympischen Spiele des vergangenen Sommers in London (2012) zurückdenkt, erinnert man sich voller Faszination daran, wie elegant, vielfältig und komplex menschliche Bewegung ist: Laufen, Schwimmen, Rudern, Werfen, Springen, Fechten und so weiter. Es ist eine inspirierende Herausforderung zu untersuchen, wie Menschen und Tiere solche Bewegungen erzeugen und organisieren. Ziel dieser Arbeit ist es, dieses Puzzle um ein paar Teile zu ergänzen.

Menschen und Tiere leben in einem Universum, das von fundamentalen Gesetzen und Prinzipien bestimmt ist. Die Physik widmet sich der Entdeckung und Quantifizierung dieser Prinzipien, die am Ende zu dieser Vielfalt führen. Der Erfolg der Physik beruht auf dem Zusammenspiel von Theorie und Experiment. Es werden Vorhersagen mit mathematischen Modellen generiert und durch Experimente verifiziert oder falsifiziert. Diese Methode funktioniert besonders gut, wenn ein Phänomen unabhängig von allen anderen Effekten untersucht werden kann. Leider ist eine solche Isolierung der grundlegenden Strukturen, die für die biologische Bewegung verantwortlich sind, sehr schwer. Das liegt zum Einen daran, dass es ethisch inakzeptabel ist Strukturen am lebenden Menschen zu isolieren. Zum Anderen beruht die Erzeugung von Bewegungen gerade auf der Kopplung unterschiedlicher Strukturen und Effekte. So spielen neben der Dynamik biomechanischer Strukturen wie Muskeln, Knochen, Bänder etc. auch metabolische Energieumsetzung, physiologische Sensorik sowie neuronale Kontrolle eine wichtige Rolle. Diese Überlegungen zeigen, dass Bewegungserzeugung nur in einem integrativen Ansatz untersucht und verstanden werden kann.

Diese Arbeit folgt dem integrativen Ansatz. Sie baut auf den Ergebnissen physiologischer Experimente mit isolierten Tiermuskeln auf, in denen die besonderen dynamischen Eigenschaften der Muskeln bestimmt wurden. Folgende Hypothesen wurden aus vorherigen Studien abgeleitet: (1) Die dynamischen Eigenschaften der Muskeln tragen maßgeblich zur Erzeugung und Kontrolle von Bewegungen bei. (2) Sie erlauben dadurch sehr einfache Kontrollstrategien. (3) So wird der Kontrollaufwand gegenüber (technischen) Systemen ohne diese Eigenschaften erheblich reduziert.

Hypothesen (1) und (2) konnten in der **1. Studie** dieser Arbeit untermauert werden. Hier wurde Hüpfen als Beispiel genommen, um die Beziehung zwischen Muskeleigenschaften, Kontrollstrategien und Interaktion mit der Umwelt zu untersuchen. Dazu wurden in eine Hüpfmodell die Materialgesetze des Muskels (Kraft-Längen-Geschwindigkeits-Relation) in unterschiedlicher Genauigkeit modelliert. Es zeigte sich, dass mit der typischen nichtlinearen Kraft-Geschwindigkeits-Relation die Stabilität beim Hüpfen besser ist als mit einer linear genäherten Variante. Die Stabilität konnte weiter verbessert werden, wenn einfache Kontrollstrategien kombiniert wurden. Diese Ergebnisse zeigen die Bedeutung der Kraft-Geschwindigkeits-Relation für die Kontrolle periodischer Bewegungen. Sie zeigen außerdem die Fähigkeit des Organismus, die stabilisierende Eigenschaften der Muskeln auszunutzen.

Hypothese (3) wurde in der **2. Studie** bestätigt: Ein Organismus, der die dynamische Eigenschaften des Muskels ausnutzt, hat einen geringeren Kontrollaufwand im Vergleich zu einem (technischen) System ohne diese Aktuatoreigenschaften. Bisher war ein quantitativer Vergleich zwischen biologischen und technischen Systemen nicht möglich, da Kontrollaufwand immer auf der Basis systemspezifischer Größen wie elektrische Spannung, Druck oder Muskelaktivität definiert wurde. Um dieses Problem zu lösen, wurde ein neues Maß für Kon-

trollaufwand entwickelt. Es basiert auf der Informationstheorie. Angewandt auf Hüpfmodelle zeigte sich, dass der Kontrollaufwand für stabiles Hüpfen mit einem Muskel bei gerade mal $I = 34\,\text{bit}$ liegt – mit einem Elektromotor hingegen bei $I = 798\,\text{bit}$. Die Kontrollstrategie für den Muskel war speziell entworfen um die Muskeleigenschaften auszunutzen. Die Kontrollstrategie für den Elektromotor hingegen war eine typische Robotiklösung, bei der ein Regler eine vorgegebene Trajektorie, unabhängig von den Aktuatoreigenschaften, erzwingen sollte. Diese Ergebnisse zeigten, dass der informationstheoretische Kontrollaufwand auf unterschiedlichste Aktuatoren und Kontrollansätze angewandt werden kann und diese quantitativ vergleichbar macht.

Beide Studien zeigen die Bedeutung der hyperbolischen Kraft-Geschwindigkeits-Relation. Diese hilft bei der Stabilisierung periodischer Bewegungen und reduziert den Kontrollaufwand. In den folgenden Studien wurde deshalb der physikalische Ursprung der Kraft-Geschwindigkeits-Relation untersucht.

3. Studie: Bisher wurde die Kraft-Geschwindigkeits-Relation in biomechanischen Muskelmodellen immer als phänomenologischer Fit an die Experimentaldaten implementiert. Nur mikroskopische Muskelmodelle konnten die Relation biophysikalisch erklären. Allerdings sind mikroskopische Modelle weder für komplexe biomechanische Simulationen geeignet, noch kann man sie als Vorlage für die Konstruktion künstlicher Muskeln verwenden. Erst ein kürzlich veröffentlichtes makroskopisches Modell führt die hyperbolische Kraft-Geschwindigkeits-Relation auf drei physikalische Elemente zurück: Eine mechanische Energiequelle, einen dazu parallelen Dämpfer und ein in Serie geschaltetes Element. Für dieses Konstrukt wurden Arbeitspunkte auf einer hyperbolischen Kraft-Geschwindigkeits-Relation vorhergesagt. In der 3. Studie wurde nun untersucht, ob diese Arbeitspunkte in einer dynamischen Kontraktion erreicht werden. Dazu wurden ein numerisches und ein mechanisches Modell entwickelt. Mit beiden Modellen wurden "quick-release" Experimente gegen eine Masse durchgeführt, wie sie in der Physiologie mit Tiermuskeln durchgeführt werden. Das numerische und das mechanische Modell zeigten beide eine ähnliche hyperbolische Kraft-Geschwindigkeits-Relation. Allerdings wich diese quantitativ von der analytischen Vorhersage ab.

Um diese Diskrepanz aufzulösen, wurden in der **4. Studie** zwei unterschiedliche "quick-release" Experimente durchgeführt. Diese Experimente untersuchen zwei Extreme der Kontraktionsdynamik: Gegen eine konstante Kraft (isotonisch) und gegen eine träge Masse. In beiden Experimenten wurde eine hyperbolische Kraft-Geschwindigkeits-Relation nachgewiesen, deren Parameter jedoch nicht identisch sind. Interessanterweise sagt das analytische Modell beide Hyperbeln und zusätzlich weitere dazwischenliegende vorher. Auch die dazwischenliegenden Hyperbeln konnten in den Experimenten nachgewiesen werden. Diese Ergebnisse stellen zum Einen die Interpretation biologischer Experimente in Frage. Sie bestätigen aber zum Anderen, dass die hyperbolische Kraft-Geschwindigkeits-Relation mit der dynamischen Interaktion dreier makroskopischer Elemente erklärt werden kann. Daher kann dieses Konzept als Startpunkt für die Entwicklung von muskelähnlichen bionischen Antrieben gesehen werden.

Diese Studien zeigen, welche Rolle Muskeln bei der Kontrolle von periodischen Bewegungen spielen. Außerdem stellen sie einen Ansatz dar, deren vorteilhafte Eigenschaften in die Technik zu übertragen. Das neu entwickelte informationstheoretische Maß für den Kontrollaufwand erlaubt es auch, technische Lösungen mit der Biologie zu vergleichen. Diese neuen Einsichten und Methoden tragen zum integrierten Bild biologischer Bewegungserzeugung bei – ein paar Teile des großen Puzzles.

Symbols and abbreviations

This list only contains symbols and abbreviations being used several times throughout the thesis.

$\mathcal{A}$	Hill constant		F_L	leg force
A	muscle activation		F_M	muscle force
AE	active element (part of CE)		$F_{\max}$	maximum isometric force
A_{opt}	optimal activation pattern		Fv	force-velocity relation
$\mathcal{B}$	Hill constant		G	feedback gain factor
CDSM	cascaded damped spring model		g	gravitational constant
CE	contractile element		ALLFB	combined F-, v-, and L-feedback
CoM	center of mass		$\mathcal{H}$	enthalpie rate
CPG	central pattern generator		H	entropy
δ	feedback signal delay		h	hopping height
Δt	time resolution		I	information
Δu	signal resolution		$I_{\min}$	minimal required information
E	Energy		k	spring constant
ECC	excitation contraction coupling		κ_v	gearing ration $\dot{l}_{SE}/\dot{l}_{CE}$
η	efficiency		k_{SE}	serial element stiffness
F	force		l	muscle length
f	frequency		L_0	reference length
F_{ext}	external force		LFB	length feedback
FFB	force feedback		l_{opt}	optimal muscle length
Fl	force-length relation		m	mass

11

Symbols and abbreviations

PDE	parallel damping element (part of CE)	T	cycle duration
p_i	probabilities of sensor measurements	τ	ECC time constant
		t_{QR}	time of quick release
P	hopping performance	u	measurement variable
Q	heat	v	velocity
QR_F	quick release against an external force	VFB	velocity feedback
		$v_{\max}$	maximum contraction velocity
QR_m	quick release against an inertial mass	W	work
R	robustness	w_{BF}	weighting factor feedback/feedforward
SE	serial element (part of CE)	$\vec{x}$	system state vector
SLIP	spring loaded inverted pendulum	y	position
STIM	muscle stimulation signal	y_0	release height
*STIM*0	pre-contact stimulation	y_{fix}	periodic hopping height

1

Introduction

The main subject of this thesis is the biological muscle. The research presented here is driven by the urge to understand how muscles work and why they are so well suited to generate the diversity, the elegance, and the power of biological movements. It is the goal to expand knowledge from isolated muscle experiments to an integrated movement control view. Deeper knowledge about muscles and movement generation on the one hand satisfies scientific curiosity, but is on the other hand a prerequisite and foundation for future developments in the field of prosthetics and robotics. This research contributes to the understanding of muscle dynamics and is intended to facilitate the peaceful and humanitarian application of biomechanical research.

The work presented in this thesis emerges from the interdisciplinary research between physics, biology, physiology, engineering, and cybernetics. This introduction chapter is intended to provide background knowledge on these different disciplines and introduce the reader to the research questions addressed in this thesis. As the topics and references selected for this chapter are only a small digest of the scientific knowledge in the field, this selection mostly represents my point of view and my research focus. Chapters 2 - 6 report five studies. The results are discussed in each chapter in the context of the study. Chapter 7 finally summarizes the findings and puts them in context.

1.1 My approach

In physics, it is well known that four distinct forces control all observed interactions of matter[1]. Strong (Gross and Wilczek, 1973; Politzer, 1973) and weak forces (Fermi, 1934) on the one hand certainly contribute to our existence but play a minor role on the scale of our perception ($\approx 1\,\mathrm{m}$). Electro-magnetic (Maxwell, 1873) and gravitational forces (Newton, 1802; Einstein, 1916) on the other hand dominate our daily life. Gravity e.g., is the necessary "opponent" in locomotion and will be treated as such in this thesis. The electro-magnetic force governs the interaction with our environment, allows transmission of information, and is the agent for chemical and molecular bindings resulting in vast and complex structures, such as the human organism.

---

[1]At least in the current state of the universe.

One fascinating characteristic of the human organism is that our biological structure allows us to acquire information on our environment and generate active forces for goal oriented motions, e.g., locomotion. This is a capability we humans have in common with animals, and with an increasing number of technical automata too. The research field of *Cybernetics*[2] is dedicated to such systems. It might seem a little far sketched relating the function of complex cybernetic systems to the fundamental physical forces, especially as cybernetics per definition is more concerned with the *behavior* of the system than with its material properties (Ashby, 1956). However, real cybernetic systems are fundamentally bound to these forces. To understand how biological organisms generate behavior, the approach in this thesis is to identify fundamental relations on the level of forces, energy, entropy, as well as basic mechanical structures and elements with physics methods.

We follow the principles of science with quantitative measurements on the one hand and modeling and predicting natural behavior on the other hand to develop and test theories (Feynman, 1994). This is especially challenging as humans cannot be disassembled like e.g., protons in the Large Hadron Collider to identify the governing principles and structures. To develop an understanding of how movement is generated, a synthetic approach has to be taken incorporating at least muscles, neuronal control, and interaction with the environment. For this purpose, reduced[3] physical models of muscles and cybernetic systems are developed predicting key aspects of natural behavior. These models are then transferred to hardware models and the results are compared to the biological counterpart (Kalveram and Seyfarth, 2009).

In the following sections, relevant background for modeling and simulating cybernetic systems is discussed with a focus on biomechanical systems.

1.2 Forward dynamic biomechanical simulations

For a formalized analysis of cybernetic systems, it is assumed that the state of a system can be described by a state vector $\vec{x}(t)$. Entries of $\vec{x}$ describe kinematic variables, such as the current location, orientation, and velocities of structures, but also chemical states like muscle activation levels. In order to conduct computer simulation experiments, the time development of the system state $\vec{x}(t)$ has to be predicted by a mathematical-physical model. In general, this time development is described by differential equations.

The differential equations for the mechanical state are based on newtonian mechanics. In short[4], the dynamics are described by equations of motion of the form

$$\ddot{x}_i = \frac{F_i}{m_i} \ .$$

Hopping for example can be described in a general approach by the differential equation

$$m\ddot{y} = -mg + \begin{cases} 0 & y > L_0 \quad \text{flight phase} \\ F_L & y \leq L_0 \quad \text{ground contact} \end{cases} . \tag{1.1}$$

---

[2] Wiener (1948) defined Cybernetics as "control and communication in the animal and the machine".

[3] Meaning few parameters and few degrees of freedom (in contrast to complex models).

[4] For further reading on multi body dynamics, especially in the context of biomechanics, I recommend: van den Bogert (1994); Schiehlen (1997); Nigg and Herzog (2007).
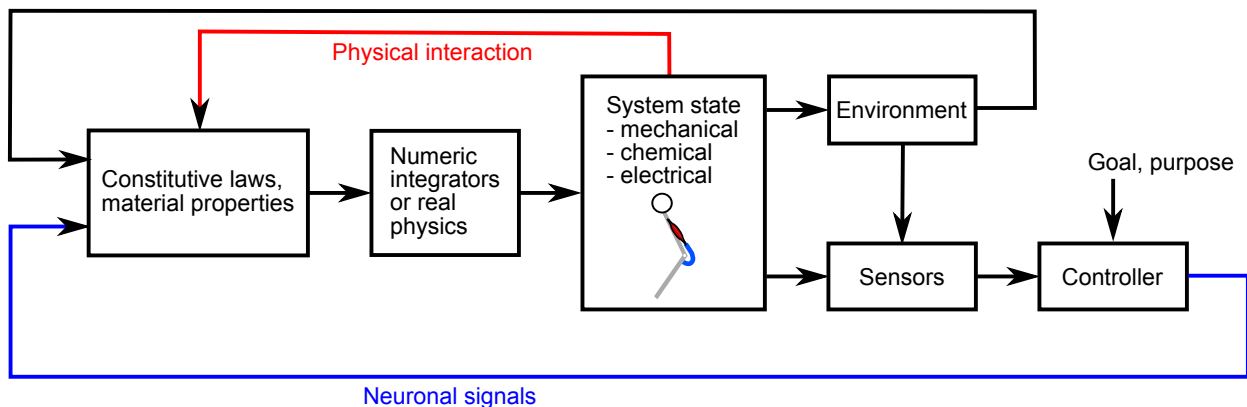
Figure 1.1: A cybernetic view on human movement generation. The system state results in certain sensor signals, which can be used by the controller to determine required actions (neural pathway). Additionally, the system state directly influences the environment and the material properties which also influence the system state (physical interaction). In a numerical simulation, the loop is closed by solving the equations of motion, while in the real world this "integration" is done by physics itself.

Here, hopping is analyzed in only one dimension (y). The body is idealized as a point mass m which is always accelerated by gravitation (g) in negative y direction, and additionally by the leg force F_L during ground contact ($y \leq L_0$) in positive y direction. To generate a periodic hopping movement alternating stance- and flight phases have to be generated by the leg force. This one-dimensional approach to hopping will be used in Chapters 2, 3, and 6 of this thesis.

The main challenge is to find accurate constitutive laws to describe the forces F_i (or F_L) generated by the biological structures. Sources of the forces F_i can be either passive or active structures. Passive structures are e.g., tendons (internal forces) and heel-pads (external forces); active structures are the muscles. The difference between passive and active is that the force of passive structures solely depends on the system state, while muscle force additionally depends on a neuronal stimulation signal $STIM$ transmitted through nerves:

$$
\begin{aligned}
F_{\text{passive}} &= F(\vec{x}) \\
F_{\text{active}} &= F(\vec{x}, STIM) \ .
\end{aligned}
\tag{1.2}
$$

Passive forces are therefore a solely mechanical reaction to the system dynamics, while active forces allow a goal oriented motion.

For goal oriented motions, the neuronal signals have to control the muscle forces appropriately. To do so, they may utilize information about the current state of the system and the environment. Many sensors distributed throughout the biological system provide this information. The output signal of these sensors obviously depend on the state $\vec{x}$ of the system[5] and $STIM$ can therefore be a function $STIM(\vec{x})$.

---

[5]The focus is here on proprioception, meaning the sensors sensing the internal state, such as segment orientations, forces, velocities, etc. Other senses used to perceive the outside world (exteroceptors), however, can be covered by this approach too: any interaction with the environment has an effect on the physical state of the sensors detecting it and thus can be represented in $\vec{x}$.
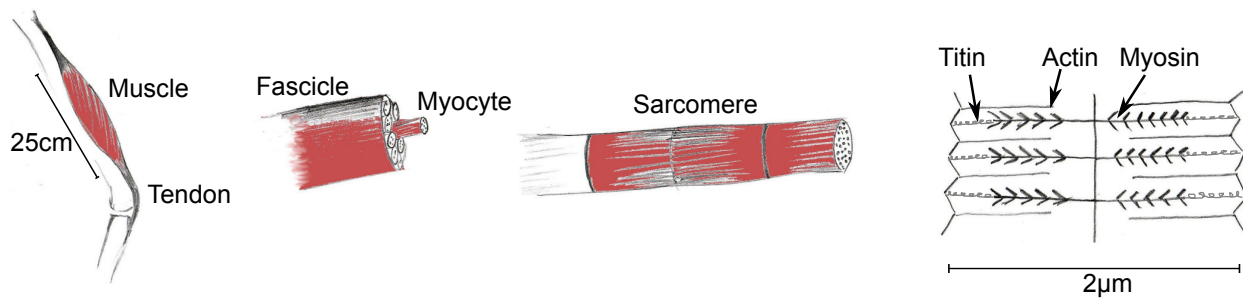
Figure 1.2: Internal structure of biological muscles. From left to right, the scale decreases. The sarcomere length is only about $1.6 - 2.6\,\mu$m. Adapted from Nigg and Herzog (2007).

Figure 1.1 sketches the complex interdependencies leading to the movement. Actuator, mechanical structure, neuronal signal processing, sensors, and interaction with the environment contribute to the movement generation. In this thesis, the interplay of these contributions is studied with special emphasis on the role of the muscle.

1.3 Macroscopic and microscopic muscle models

A glance at the complexity and diversity of muscle generated movements shows that muscle is a versatile, powerful, and flexible actuator (Sandow, 1970; Close, 1981; McMahon, 1984). This is achieved because muscles can operate in different modes depending on the contraction dynamics and the structural implementation (Lieber, 1999; Ahn and Full, 2002).

For an accurate prediction of the muscle force, muscle models have to be derived from muscle experiments. There exist various experimentally validated models on either a macroscopic scale, taking only gross effects into account or a microscopic scale, including even molecular phenomena. First quantitative empiric studies in the 19th century tried to measure the gross physical properties of biological muscle (e.g., Weber, 1846; du Bois-Reymond, 1848; Fick, 1892). Since then, both muscle experiments and mathematical formulations of muscle function iteratively improved.

Today, it is known that skeletal muscles have a distinct internal structure and arrangement of contractile proteins[6] (Figure 1.2): Muscles consist of many bundles (fascicles) of muscle cells (myocytes). Each muscle cell contains several myofibrils arranged in parallel. The myofibril consists of a serial arrangement of sarcomeres, arguably the smallest functional unit within the muscle. Within a sarcomere, the contractile proteins actin, myosin, and titin generate the forces. In microscopic pictures of myofibrils, filaments can be seen, which slide relative to each other upon contraction. The apparently thicker filament consist of myosin molecules, the thinner filament of actin molecules. Active regions (cross bridges) of the myosin can bind to actin and generate longitudinal forces causing the sliding of the filaments and ultimately the muscle contraction (first proposed by Huxley, 1957). The chemical processes resulting in the binding of actin and myosin are governed by the calcium ion (Ca^{2+}) concentration. Each cell is electrically isolated from the neighboring cells (by the endomysium). Groups of cells are recruited for contraction by motor neurons in the spinal

---

[6]For a detailed description of muscle physiology see Nigg and Herzog (2007) and Sherwood (2011).
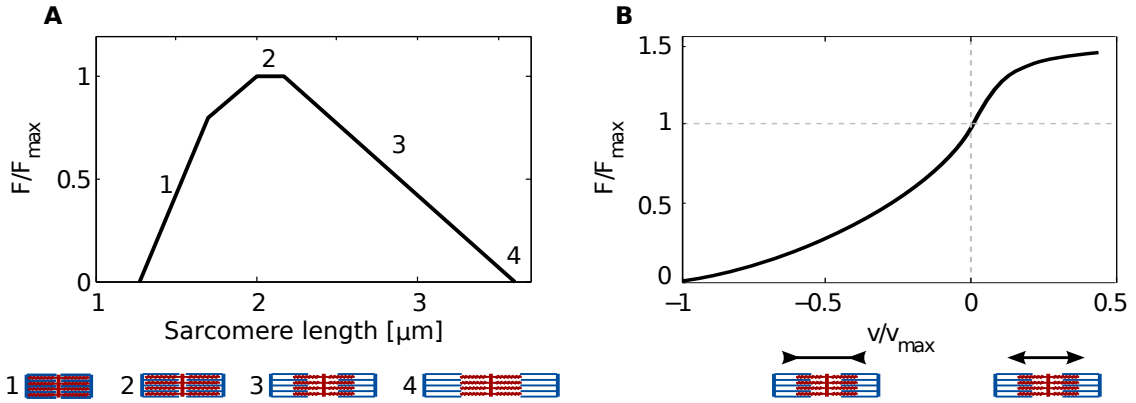
Figure 1.3: **A:** Force-length relation of a sarcomere. The approximate overlap of actin (blue) and myosin (red) is sketched at the bottom of the figure. **B:** Force-velocity relation of a muscle. In concentric contractions (shortening muscle: $v < 0$), the muscle exhibits a hyperbolic force-velocity relation. In eccentric contractions, the muscle is stretched with higher force than it exhibits itself ($v > 0$). Here the muscle can generate more force than in the isometric state ($v = 0$). Adapted from Nigg and Herzog (2007).

cord which cause the release of Ca^{2+} into the myofibrils. Such a group of cells innervated by one motor neuron is called a motor unit. The force output of the muscle can be modulated very precisely by recruiting few or many motor units, and by individually varying the neuronal spike rates (Hatze, 1978, 1977b).

These physiological structures and processes result in distinct characteristics of muscle contraction dynamics, which have to be measured for and considered in muscle modeling. From experiments with whole dissected muscles, it is known that muscle force depends on the current muscle length l, the contraction velocity v, and the muscle activation A (roughly the percentage of recruited motor units) (McMahon, 1984). Under the assumption that these dependencies do not influence each other, the behavior of the active part of muscles can be described by a model of the form

$$F_M = A \cdot Fl \cdot Fv \cdot F_{max} \ , \tag{1.3}$$

where the force-length relation $Fl = F(l)$ (Aubert et al., 1951) and the force-velocity relation $Fv = F(v)$ (Hill, 1938) are empirically measured and fitted functions. Both are normalized to the maximum isometric (measured at constant length) force F_{max}.

The force-length relation can be measured in isometric muscle experiments. These experiments reveal that active muscle force reaches a maximum at a certain length termed optimal length l_{opt} (Aubert et al., 1951). This behavior cannot only be found in the whole muscle, it is already present on the level of sarcomeres (Gordon et al., 1966). It is related to the overlap of thick and thin filament (Figure 1.3A).

The force-velocity relationship was determined by Hill (1938) from heat measurements during concentric contractions (Figure 1.3B). This relation constitutes a hyperbola

$$(F + \mathcal{A}) \cdot v = -\mathcal{B} \cdot (F_0 - F) \ , \tag{1.4}$$

with three parameters $\mathcal{A}$, $\mathcal{B}$, and F_0 which he named "constants of muscle". These constants can be determined in muscle experiments. Based on his work, a whole class of macroscopic

"Hill-type" muscle models emerged. Hill-type models are identified as macroscopic muscle models. They mainly consist of three elements: a contractile element incorporating force-length and hyperbolic force-velocity dependencies (Equation (1.3)), a serial, and a parallel elastic element in diverse configurations (Zajac, 1989; Winters, 1990; van Soest and Bobbert, 1993; Günther and Ruder, 2003; Houdijk et al., 2006; Kistemaker et al., 2006; Siebert et al., 2008). In this thesis, the focus will be on the contractile element. Various extensions account for physiologically observable effects, such as contraction history effects (Meijer et al., 1998; Rode et al., 2009a), high frequency oscillation damping (Günther et al., 2007), recruitment patterns of slow- and fast twitch fibers (Wakeling et al., 2012), and eccentric contractions[7] (Till et al., 2008; van Soest and Bobbert, 1993).

In the first comprehensive theoretical muscle model by Huxley (1957), the "sliding filament theory", the force-velocity relationship was derived solely from mapping the state of the art knowledge about the structure of the crucial molecules involved in the mechanism of muscular force production. Altogether, he needed to set nine microscopic parameters to fit the Hill relation. The Huxley model is identified as a microscopic muscle model. Huxley-type muscle models, nowadays, account for the detailed knowledge gained from microscopic morphological studies and explain the physiology in detail (Cooke et al., 1994; Piazzesi and Lombardi, 1995, 1996; Barclay, 1999; Lan and Sun, 2005; Chin et al., 2006; Walcott and Sun, 2009). With at least 30 parameters in the more recent approaches and several coupled differential and rate equations such models can predict, e.g., the force-velocity characteristics of a sarcomere.

In this thesis, the focus is on macroscopic muscle models. They allow to investigate movement control (Chapters 2 and 3) and are the basis of a new design concept for artificial muscles (Chapters 4 and 5).

While Fl and Fv in macroscopic models represent the mechanical properties of the muscle, the variable muscle activation A (Equation (1.3)) introduces the possibility to control muscle force via a neuronal stimulation signal $STIM$. This is represented by the blue arrow in Figure 1.1. As $STIM$ is used for a whole muscle, it represents the net-effect of the number of recruited motor units and the motor neuron spike rates in form of one neuronal stimulation signal. The connection between $STIM$ and muscle activation A is the excitation contraction coupling (ECC). ECC models the biochemical processes involved in the process initiated by muscle stimulation via motor-neurons and resulting in change in muscle force[8]. These processes can be approximately described by first order differential equations (e.g., Hatze, 1977a; Zajac, 1989) and have an effect similar to a low-pass filter. In this thesis, excitation contraction coupling was modeled as

$$\frac{dA(t)}{dt} = \frac{1}{\tau}(STIM(t) - A(t)) \tag{1.5}$$

where τ is a time constant (Geyer et al., 2003). $STIM$ could either be modeled as a neuronal spike train or a neural current defined as "the number of impulses passing through a cross section of all parallel redundant fibers in a given bundle per unit time" (Powers, 1973). The latter is very useful in macroscopic musculo-skeletal simulations: sensor signals can simply

---

[7]Eccentric contractions are contractions in which the muscle is stretched with a force higher than the current muscle force.

[8]For a detailed description of these processes see e.g. (Nigg and Herzog, 2007).
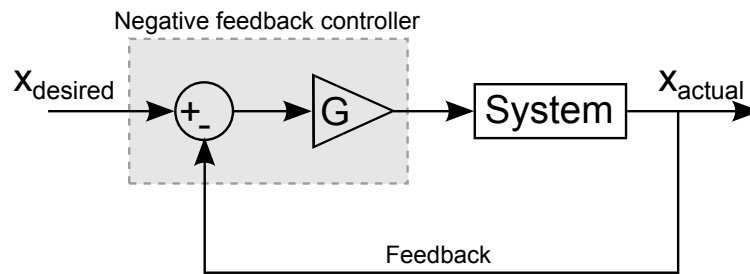
Figure 1.4: Operation principle of negative feedback control. A desired state of the system is given and compared to the actual state. If a deviation between actual and desired state is detected, this deviation will be gained by the factor G and used as control signal to the system.

be modeled as numeric values (e.g., $F = 10.3\,\text{N}$) and do not have to be translated into a spike signal. With this simplification and the model for the excitation contraction coupling, the signal path is "connected" by a mathematical model, allowing for defined muscle control.

1.4 Exploitive control

The above mentioned muscle models and muscle experiments mainly focus on the (isolated) muscle. To understand the functional role of muscles in the biological system, the control of movements has to be considered as well (Figure 1.1). Control theory in engineering[9] was greatly inspired by the work of early Cybernetics research:

> "We thus see that for effective action on the outer world, it is not only essential that we possess good effectors[10], but that the performance of these effectors be properly monitored back to the central nervous system, and that the readings of these monitors be properly continued with the other information coming in from the sense organs to produce a properly proportioned output to the effectors." [...] "The information fed back to the control center tends to oppose the departure of the controlled from the controlling quantity, but it may depend in widely different ways on this departure"(Wiener, 1948).

Although very openly formulated by N. Wiener (1948), this idea can be summarized by the term *negative feedback*. In the control of movements, the negative feedback approach requires a pre-defined/planned trajectory or time series of the controlling quantity. Typical examples are preplanned kinematics to generate a desired trajectory, or preplanned forces. Then, the deviation from this ideal trajectory is measured and the controller tries to minimize the deviation throughout the movement. Thus, "negative" stands for the difference between desired and actual state of the system (Figure 1.4) . Unknown effects like perturbations, friction, and damping can be compensated for. This approach has been very successfully implemented in industrial robots and automata[11].

---

[9]Control theory from an engineering point of view is described in detail in (Zacher and Reuter, 2011). For an interesting view on human control theory I recommend (Powers, 1973).

[10]e.g., motors, muscles etc. Also called actuators in this thesis.

[11]For an introduction to robot control see Siciliano et al. (2009).

In contrast to such control approaches, there exist mechanical systems that generate certain movements solely by the mechanical structure without any actuator or control. One example is an ideal spring-mass system (Figure 1.5), where the leg force is modeled as a purely elastic spring ($F_L = -k(y - L_0)$ in Equation (1.1)). Released above the floor, it generates a hopping movement by simply repeating the conversion of potential to kinetic energy and back. Inspired by this idea, a whole class of purely mechanical robots was constructed in the past and termed passive dynamic walkers (e.g., McGeer, 1990; Collins, 2001). Another aspect enriched this trend: interestingly, the simple spring-mass model[12] can predict the kinematic pattern of the center of mass (CoM) and the ground reaction forces of human and animal hopping, running (Blickhan, 1989), and walking (Geyer et al., 2006) quite well. Thus, the spring-mass model is a template model of the overall leg function during locomotion (Full and Koditschek, 1999). It is easy to implement in a computer simulation, can be analytically approximated (Geyer et al., 2005), and was studied extensively for its implications for locomotor control (Farley et al., 1998; Seyfarth et al., 2002; Rummel and Seyfarth, 2008; Blum et al., 2010; Rummel et al., 2010; Saranli et al., 2010; Peuker et al., 2012) and adapted for robot design and control (Poulakakis, 2010; Maufroy et al., 2011; Radkhah et al., 2011; Garofalo et al., 2012).

The spring-mass model assumes an ideal spring with no energy dissipation (conservative model). Every real world system, including the human leg, however, inevitably dissipates energy. This energy is lost for the hopping movement and has to be replenished for continuous hopping. To investigate how humans manage the movement energy in hopping, we furnished a spring-mass model with damping and allowed energy supply by means of spring-stiffness variation (Kalveram et al., 2012). A summary of this study is given in Chapter 6. The results suggest that humans might exploit the mechanical characteristics of the leg: by injecting the same amount of energy ΔE_{supply} in every cycle, friction and damping "passively control" the hopping hight. If for example the hopping height is very high, the energy dissipation E_{diss} will be high during the cycle ($E_{\text{diss}} > \Delta E_{\text{supply}}$). If the hopping height is very low, $E_{\text{diss}} < \Delta E_{\text{supply}}$. Naturally, the system will tend towards a hopping height, where $E_{\text{diss}} = \Delta E_{\text{supply}}$ and perturbations in the energy will be compensated for without the need of adaptation of the control. Additionally, hopping height in this regime can be easily adjusted by changing ΔE_{supply}.

This form of control does not require a preplanned trajectory. It still requires some proprioceptive sensory input[13], but not in the comparing sense of negative feedback. The movement pattern emerges from the dynamic interaction of the organism with its environment. Hereby, the intrinsic mechanical properties of the system play a crucial role and are exploited by the control regime. Therefore, this control approach was termed exploitive actuation[14] (Kalveram and Seyfarth, 2009). This term is biologically motivated: it implies a superordinate neural controller specifying discrete goals, for instance hopping with a certain height.

---

[12]There exist two terms for the same model: "Spring-mass model" was introduced by Blickhan (1989), "spring-loaded-inverted-pendulum (SLIP) model" was introduced by Schwind (1998).

[13]This is often also called feedback, as the proprioceptive signals are fed back to the motor controller. Unfortunately this causes a lot of confusion as engineers use feedback synonymous to "negative feedback".

[14]Other researchers termed different names for similar principles: morphological computation (Paul, 2006), embodied artificial intelligence (Pfeifer and Iida, 2004), intelligence by mechanics (Blickhan et al., 2007), or feed-forward preflex control (Cham et al., 2000). We prefer to simply call those processes exploitive control (Kalveram et al., 2005) or exploitive actuation (Kalveram and Seyfarth, 2009).
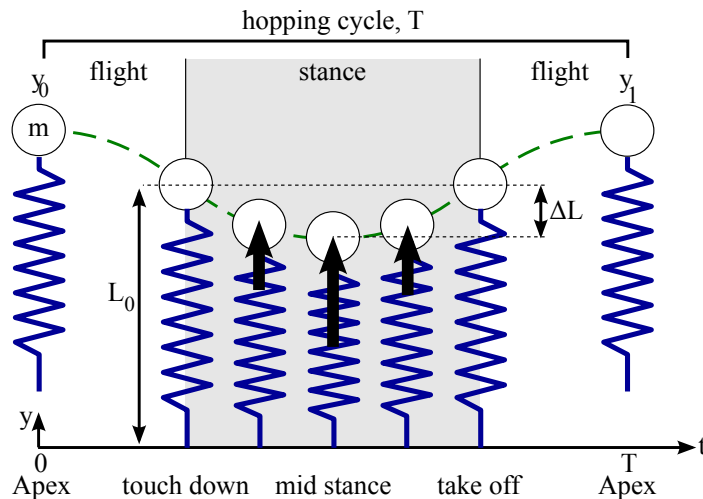
Figure 1.5: Spring-mass model for hopping (Blickhan, 1989). The point mass m represents the body, and the leg function is represented by a spring. The leg force is proportional to the leg deformation $F_L = -k(y - L_0) = -k\Delta L$. Force is only generated during stance phase (Equation (1.1)) as indicated by the black arrows. This model is a template for human and animal locomotion (Full and Koditschek, 1999).

On the continuous level of movement execution, however, the control instance leaves it to the physics of its own body to realize these goals (Kalveram et al., 2012). A characteristic of exploitive actuation is that it demands only minimal control effort compared to classical control solutions (see Chapter 3).

1.5 Exploitive muscular actuation in hopping

When muscles are used to generate movements, their distinct mechanical properties certainly play an important role[15]. In jumping simulations, van Soest and Bobbert (1993) found that perturbations have much less influence on take-off posture when the model is actuated by muscle dynamics instead of joint moment control. It appears that muscle properties are able to compensate for perturbations and facilitate the convergence of dynamic explosive movements. The authors concluded that the intrinsic muscle properties represented by the force-length-velocity relation in Hill-type muscle models (Equation (1.3)) act as a zero time delay peripheral feedback system. Thus, the mechanical properties of the muscle itself represent a functional "feedback" system. Because of the zero time delay, Brown et al. (1995) coined the term "preflex" for all mechanical actions, whether stabilizing or not, emerging from these intrinsic properties.

In hopping simulations, the interplay of predefined activation pattern and preflex properties of the mechanical system can be studied. It was found that they compensate for unexpected changes in surface stiffness by adjusting the leg stiffness (van der Krogt et al., 2009) as known from experiments (hopping: Moritz and Farley (2004), running: Ferris et al. (1999)). While van der Krogt et al. (2009) showed that passive preflex dynamics can ne-

---

[15]The following paragraphs are in essence a summary of my first article on this topic (Haeufle et al., 2010a).

gotiate such perturbations without any adaptation of the neural activation pattern, Geyer et al. (2003) demonstrated that a combination of muscle properties and simple proprioceptive feedback control can also generate stable periodic movements like vertical hopping. In addition, Geyer and colleagues discussed the necessity of specific muscle properties for the stabilization. They found that for hopping the force-length relationship can be neglected without losing periodic stability. In a similar way, McMahon (1984), Hogan et al. (1987) and Blickhan et al. (2007) mentioned a stabilizing effect of the force-velocity characteristic. Gerritsen et al. (1998) explicitly showed that a walking model with disabled force-velocity relation could not compensate for dynamic perturbations.

Based on these findings, we (Haeufle et al., 2010a) investigated which level of biologically observed complexity of the force-length and force-velocity curves (Equation (1.3)) is required for hopping. For this purpose, the leg force in Equation (1.1) was modeled as a muscle $F_L = F_M = A \cdot Fl \cdot Fv \cdot F_{\max}$ (Equation (1.3)). The approach was to stepwise increase the complexity of the force-length and force-velocity curves from constant ($= 1$, thus has no effect) to linear to non-linear phenomenological fit of the biological data. With this approach it was possible to show that the force-velocity relation is responsible for the stabilization of periodic hopping patterns. We found a faster convergence after perturbations with increasing complexity of the force-velocity relation. The characteristics of the force-length relation only marginally influenced hopping stability.

The main chapters of this thesis can all be seen as a consequence of these findings: In Chapter 2 the interaction of intrinsic muscle properties with different simple control approaches is investigated. In Chapter 3 a new method to quantify control effort is developed to evaluate the "exploitive" character of actuation. Both chapters again emphasize the importance of the force-velocity characteristics. Thus, Chapters 4 and 5 investigate the physical origin of the force-velocity relation on a macroscopic level in order to better understand muscle function and promote model based design principles for bio-inspired artificial actuators.

1.6 The test trilogy

In physics, experiments quantify nature, theory combines findings and predicts new results, which then have to be verified in experiments and so on (Feynman, 1994). This is the way how fundamental laws are discovered, formalized, and tested. In the study of human movement generation, this approach is very difficult for two main reasons: (1) The human organism is extremely complex and it is difficult to analyze single structures and theorize about their (isolated) function as it is often done and required in physics. (2) It is unethical to perform experiments by isolating structures from the living human organism to study their function. Thus, theories about movement generation are extremely difficult to validate in experiments.

Kalveram and Seyfarth (2009) proposed a strategy for a thorough investigation of movement generation theories: the "test trilogy". They demanded the following tests: a *simulation test* to verify that the theory is logically precise; a *hardware test* to verify that the theory is physically sound, and a *behavioral comparison test* to show the biological relevance of the theory.

From a physics point of view these demands seem almost self-evident, but they are often

difficult to realize in biomechanics. Nevertheless, the importance of the three tests can be seen already from the introduction above. Figure 1.1 represents primarily a verbal or graphical representation of a theory about movement generation. Only if it can be rewritten in a mathematical model and only if a simulation of such a model predicts the anticipated movement, the theory is logically sound and thus passes the simulation test.

The hardware test reveals whether the theory can work in the real world with real physical effects not considered in the simulation, e.g., friction, signal noise, gravity. Although the spring mass model passes the simulation test and is a valuable tool for analyzing legged locomotion, it cannot pass the hardware test as there exist no real purely elastic materials. Thus, it has to be discarded as an explanation, how locomotion is generated[16].

The basis for the behavioral comparison test is the Cybernetic analogy between biological and technical automata (Wiener, 1948), with additional guidance of the simulation results. If the systems perform similar tasks and react to perturbations in a similar way, the movement theory is adequate.

If all three tests are applied, the recursive interaction between theory and experiments can be established for the study of biological movement. This thesis follows the path of the test trilogy with a focus on simulation tests, but hardware and behavioral comparison tests are also presented. Additionally, the mechanical concept for an artificial muscle (Chapters 4 and 5) could lead to the development of robots used for the hardware test of complex biological behavior.

1.7 Robots as experimental tools

In recent years, robots have become more and more popular as tools to study human and animal movement. They can be used as tools for the hardware test. The benefit is clear: In a robot, it is possible to include only those structures that are hypothesized to play a functional role. It is also ethically unobjectionable to disengage parts and even approach structural limits in experiments with robots.

"The advantage of using robots is that embodiment can be investigated quantitatively: robots are much simpler to manipulate and monitor. That is, first, we can change the control structure without much effort, and we can even manipulate the morphology relatively easily. Second, all sensory stimulations, motor signals, and internal states can be recorded as time series for further analysis. Having discovered some principles or put forth some hypotheses, we can turn back into the biological realm and verify the ideas" (Hoffmann and Pfeifer, 2011).

When building humanoid or animal like robots, three approaches have to be distinguished[17]:

1. The engineering approach has the goal to build high performance robots with amazing new technology which imitate human or animal behavior. It is often inspired by new

---

[16]It has, by the way, never been intended to do so. It simply states that the overall leg behavior during locomotion can be described (not explained) by elastic behavior. This analogy was then used to investigate advantages of spring-like leg behavior (Blickhan, 1989).

[17]This classification originated from a personal communication with Prof. Kalveram.

sensor precision, new computational power and speed, or new mechanical design possibilities. Here, biology inspires the overall capabilities, the desired tasks, and the design criteria. Examples are the robots designed by Raibert (1986), Honda's humanoid robot Asimo (Hirose and Ogawa, 2007), humanoid robot Lola (Buschmann et al., 2007), or humanoid manipulator Justin (Albu-Schäffer et al., 2008).

2. The biomimetic or bio-inspired approach is to transfer biological principles of structure and function to robots. Here, biology offers input for new technologies which may even outmatch the biological role model. Examples are the caterpillar-inspired robot "GoQBot" (Lin et al., 2011), the cat like robot "Cheetah" with springs in the legs representing major muscle groups (Rutishauser et al., 2008), the "athlete robot" using two spring-like legs similar to state of the art sprinting prosthesis actuated by pneumatic muscles (Niiyama et al., 2012), or the BioBiped with series elastic actuators representing the nine major muscle groups in the human leg (Radkhah et al., 2011).

3. The inverse biomimetic approach focuses on the function and diversity of human or animal behavior. Here, biology is the actual object of the study, not the robot. Engineering techniques are simply used to derive and test concepts which explain observed behavior. In this approach, reduced robots are required that are confined to express the function under consideration. Examples are the walking robot used to validate models of the function of ankle push-off in walking (Renjewski and Seyfarth, 2012), and PostuRob, a robot build to test models on human stance control (Mergner et al., 2006; Mergner, 2010).

The three aspects are, of course, closely related to each other and some of the given examples may also partially belong into other categories. For the purpose of the test trilogy, only the inverse biomimetic approach (3) leads to suitable test platforms for the hardware test.

In this thesis, two hardware platforms were used. The first is a hopping monopod robot called "Marco" (Kalveram et al., 2008), which was developed at the Locomotion Lab, University of Jena. This robot was used to test the hopping regimes based on the spring-mass model with different energy supply methods (Section 1.4 and Chapter 6). A second platform was used to test the real world functionality of mechanical macroscopic muscle models (Chapters 4 and 5).

1.8 Artificial muscles and muscle like actuators

As stated earlier, the goal of this research is to expand knowledge from isolated muscle experiments towards an integrated movement control view. In the end, we would like to understand human locomotion. With respect to the test trilogy, comprehensive musculoskeletal models of legged locomotion (e.g., Günther and Ruder, 2003; Geyer and Herr, 2010) present successful simulation tests for movement control hypotheses. They can already be compared to detailed datasets of human locomotion (e.g., Lipfert, 2010), but the hardware test is not quite possible yet. One reason is that no muscle-like artificial actuator exists that can drive the test-robots adequately. The mechanical concept presented in Chapters 4 and 5 could lead to such artificial muscles.

As described in Section 1.3, biological muscles have a distinct microscopic structure, which cannot be replicated in technical actuators. But the microscopic structure and the way how the active forces are generated on the molecular level, result in specific macroscopic characteristics that are important for biological movement control (Section 1.5). These are (1) the contraction dynamics approximated by the force-length-velocity relation (Equation (1.3)), (2) almost no damping forces when the muscle is not activated ($A = 0$ in Equation (1.3)) and (3) the inherent compliance due to elasticity of muscle belly and tendon, represented by serial elastic elements in macroscopic muscle models.

In literature, various types of, and construction principles for muscle-like actuators are documented. One approach to achieve compliant joint behavior is active torque-based control (e.g., Albu-Schäffer et al., 2008). Here, the position y of a stiff actuator, e.g., an electro motor with gear, is measured and the actuator output torque is controlled proportional to the position ($T = -k\Delta y$) mimicking elasticity. In theory, the whole muscle function could be mimicked just by controlling the actuator force according to a muscle model Hannaford et al. (2001); Klute et al. (2002); Seyfarth et al. (2007). Problems arise, however, from the limitations of sensor and actuator precision, control loop time delays, and sampling time (Albu-Schäffer et al., 2008). Although electro-magnetic drives show hyperbolic speed-torque characteristics (Frank and Schilling, 1998), the fast rotating electric drives are normally combined with gearing mechanisms to adapt moments and velocities of walking machines and robots to commonly used values. However, the friction of the actuators themselves and their gearing mechanisms as well as their inertial properties (reflected inertia) inhibit muscle-like performance.

To overcome these limitations, recently, a variety of actuators have been coupled to serial elasticities implementing mechanical elastic properties as e.g. known from tendons in biology (Pratt and Williamson, 1995; Pratt et al., 2002; Chee-Meng et al., 2004; Albu-Schäffer et al., 2008; Hurst and Rizzi, 2008; Wyeth, 2008; Ham et al., 2009; Taylor, 2011). The benefits of such series elastic actuators as compared to traditional "stiff" actuator design concepts are shock tolerance, lower reflected inertia, more accurate and stable force control, less damage to the environment, and energy storage (Pratt and Williamson, 1995). The actuators themselves, however, do not yet incorporate muscle-like contraction dynamics.

Pneumatic artificial muscles (*McKibben muscles*), are inherently compliant (Chou and Hannaford, 1996; FESTO, 2000; Daerden and Lefeber, 2002) and were already used to drive a walking robot (Vanderborght et al., 2006a). These actuators produce maximum shortening ranges of $\approx 30\%$ (i.e. not more than half the value of biological muscles) and damping characteristics during concentric contractions are also traceable (Tondu and Lopez, 2000; Kerscher et al., 2006). To mimic muscle contraction dynamics even closer, Klute et al. (2002) used a non-linear damping element in parallel, and a non-linear elastic tendon in series to a pneumatic actuator. Even muscle-like hyperbolic force-velocity characteristics have been shown (Tondu and Zagal, 2006). Nevertheless, pneumatic actuators have inherent problems that are difficult to overcome: non-constant volumes during contractions, significant hystereses already at low velocities and pressures, lower maximal shortening values compared to biological muscles, lower energy efficiency and the incorporation of non-physiological masses. Thus, they require "extra design and control effort" (Vanderborght et al., 2006a).

There is a large variety of new materials for actuators (Madden, 2007; Karpelson and Wood, 2008). Examples are dielectric elastomers (Pelrine, 2002; Carpi et al., 2010; Chuc

et al., 2011), shape memory alloys (Lin et al., 2011), piezoelectric cantilevers (Wang and Cross, 1998), carbon nano tubes (Foroughi et al., 2011), and others. For most of these, the term "muscle" applies only in the sense that they contract, or even only generate controllable force.

All these approaches try to mimic the phenomenological characteristics of biological muscles to some extent. As will be discussed in detail in Chapters 4 and 5, a new mechanical muscle model (Günther and Schmitt, 2010) could serve as a design concept for functional artificial muscles.

Finally a note on new possibilities of tissue engineering. It is nowadays possible to cultivate animal heart- or skeletal muscle cells to engineer actuators (e.g., Akiyama et al., 2010). These approaches, however, will not help to understand the principles of movement generation and will in the foreseeable future not allow to build prosthetic devices replacing lost limbs as a whole. In the long term this might offer a possibility to regenerate or even replace muscle tissue. Whether this is desirable or not has to be determined in discussions within ethical boards.

1.9 Quantification criteria

If biological systems have and can exploit beneficial intrinsic characteristics the question arises, how their benefit could be quantified? Several criteria known in physics have already been adapted and used for this purpose. Most commonly these are *performance measures,* such as velocity or jumping height; e.g., Usain Bolt reached an average speed of $10.4\,\text{m/s}$ during his $100\,\text{m}$ world record of 2009 (IAAF, 2010) compared to the peak speed the fastest humanoid robot Mabel reached, namely $3.1\,\text{m/s}$ (Sreenath et al., 2012). Physics offers many more quantitative criteria. However, even if the criteria are well defined, it is not always straightforward to apply them. In this section a few criteria are mentioned and discussed.

Mechanical efficiency is a simple, yet strong measure of advantages. It is the relation of mechanical work output W_{out} to energy input E_{in}

$$\eta = \frac{W_{out}}{E_{in}} \, . \tag{1.6}$$

If one type of actuator can generate movements more energy-efficiently than others, it could be more easily used in prosthetic devices or robots (smaller and lighter battery/energy harvester). Interestingly, the literature is contradictory in this measure with respect to muscles. On the one hand, isolated muscles were found to have a peak efficiency (positive work done divided by the energetic equivalent of the oxygen consumed) of approximately $\eta = 0.15$ for rat soleus muscle or $\eta = 0.25$ for frog sartorius muscle (Heglund and Cavagna, 1987). Electric motors, on the other hand, reach efficiencies of $\eta > 0.9$ (Hsu et al., 1998). Still, researchers use artificial muscles in robots and prostheses "in order to reduce energy consumption" (Vanderborght et al., 2006a). Apparently, they are expected to be more efficient in a natural movement like walking. One reason is the possibility of storing energy in the tendon and within the muscle fibers themselves (Cavagna, 1970; Heglund and Cavagna, 1985; Dickinson, 2000). In a study comparing experimental data to a macroscopic Hill-type muscle model (including tendon) it was shown that mechanical efficiency can be up to 0.92 in muscle stretch-shorten cycles (Ettema, 1996).

The **enthalpy rate** is a sum of rates of energy portions an actuator has to generate in order to gain its net mechanical power output. Barclay (1996) summed up the rates of heat $\dot{Q}$ and work output during shortening $\dot{W}$ to get the enthalpy rate $\dot{\mathcal{H}} = \dot{Q} + \dot{W}$ including the maintenance heat rate necessary to obtain muscle stress or force at rest. In a model approach Günther and Schmitt (2010) compared the enthalpy rate, defined as the theoretical minimum power input of an actuator, with other model approaches and experimental data:

$$\dot{\mathcal{H}} = |F_M \cdot \dot{l}_M| + \dot{h} + \dot{h}_0 \quad . \tag{1.7}$$

Here $|F_M \cdot \dot{l}_M|$ is the net mechanical power output of the muscle (muscle force times muscle contraction velocity), $\dot{h}$ the heat rate due to muscle shortening (dissipated energy), and $\dot{h}_0$ the maintenance heat rate. In the evaluation of actuator performance the maintenance heat rate, as considered in the enthalpy rate, is an important factor. For example, when holding a load, a muscle performs no mechanical work but takes up energy. The mechanical efficiency in this case is simply $\eta = 0$ independent of the mechanism and thus cannot be used to compare different mechanisms. Holding a certain quasi static position is, however, a common task for humans.

The enthalpy rate reveals differences between muscle models more clearly: The muscle model investigated in Chapters 4 and 5 allows to reproduce the force-velocity relation for different sets of parameters. Evaluating the enthalpy rate as another criterion allowed us to pinpoint one consistent parameter set (Schmitt et al., 2012).

Stability and robustness are criteria rather related to specific movements than to a muscle, an actuator, or a drive, which itself cannot per se be stable or unstable. These measures are derived from the study of nonlinear systems[18]. In engineering, they are used to describe the capability of a feedback control systems to generate and to stabilize state trajectories under the influence of perturbations. Perturbations can arise from external forces acting on a system, as well as deviations of the initial state, the system parameters, or the input/sensor signals (Hinrichsen and Pritchard, 2010).

If a system performs periodic movements, the current state $\vec{x}(t)$ describes a closed loop trajectory in state space. Such a closed loop trajectory is called a limit cycle. If the system is perturbed, it deviates from the limit cycle. With stability analysis it is possible to predict its capability to return to the original limit cycle. The stability analysis for a limit cycle can be quite complicated. It can be simplified if, instead of looking at the whole trajectory, one analyzes only a characteristic section through the state space, a so called Poincaré map (or return map). For the hopping model (Equation 1.1), a meaningful section can be obtained by mapping the apices of the hopping pattern (highest points, $\dot{y}(t) = 0$). This Poincaré section is called the "apex return map". The apex return map is the dependency of apex height y_1 on release height y_0: $y_1(y_0)$ (Full et al., 2002; Rummel and Seyfarth, 2008). For periodic hopping the apex height after one hopping cycle is identical to the release hight $y_1 = y_0$. In the apex return map such a periodic solution is represented as a fixed point y_{fix} with $y_1(y_0) = y_0 = y_{\text{fix}}$. A perturbation of release height ($y_0 = y_{\text{fix}} + \Delta y_0$) generally causes a deviation of the hopping height ($y_1 = y_{\text{fix}} + \Delta y_1$). For a stable fixed point the perturbation diminishes during the cycle ($|\Delta y_0| > |\Delta y_1|$). Thus, the slope $S = dy_1/dy_0$ of the return map

---

[18]For further reading on "nonlinear dynamics" I recommend (Vogel, 2006, chapter 20) and (Strogatz, 2001). This section is based on these references.

$y_1(y_0)$ in the neighborhood of a fixed point is a measure for stability against infinitesimal perturbations. The trajectory converges to its periodic solution after a small perturbations if $|S| < 1$. Therefore, we call hopping model solutions with $|S| < 1$ stable. A solution is unstable for perturbations growing from step to step ($|S| > 1$). If a perturbation remains constant from step to step ($|S| = 1$) the model has indifferent behavior (neutrally stable).

This concept of stability can also be applied to biological locomotion (Full et al., 2002). In this thesis it was applied to the one-dimensional hopping model (Chapter 2). Here, specific characteristics of the biological system can be tested for their contribution to movement stability (Blickhan et al., 2007; Grimmer et al., 2008). For a biological system it is important to generate stable and robust movements. As described in Section 1.5, muscles play an important role in the stabilization of movements. In the sense of exploitive actuation, the stabilizing capability of an actuator is therefore an important measure.

In this thesis we use the term "robustness" (R) as a measure of how large a perturbation can be before the system gets unstable. With this approach robustness is similar to the "basin of attraction" or the "stability radius" (Qiu et al., 1995) known from nonlinear dynamic methods.

Control effort: The term exploitive actuation implies reduced requirements for the control algorithm in a well-designed system compared to one without suitable mechanical properties. This difference in control effort is considered an important feature of biological systems. Especially as the number of degrees of freedom seems to be excessive. Additionally, control in a real system is not an abstract mathematical rule, it has to be physically implemented. Such a physical implementation costs energy (Polani, 2009) and therefore has to be quantified somehow. In Chapter 3, a new measure for control effort is introduced. In contrast to the previously used measures of control effort, it allows the quantitative comparison of very different actuation systems like muscles and electric DC-motors.

Integration of intrinsic muscle properties, feed-forward, and feedback signals in hopping

As discussed in Chapter 1, the mechanical design, the control method, and the interaction with the environment contribute to the movement generation in a biological system. To investigate their interaction, a simulation study on hopping is presented in this chapter. A one-dimensional hopping model driven by a Hill-type muscle model was studied. It was investigated, whether a combination of feed-forward and feedback signals improves hopping stability compared to those simulations with one individual type of activation. Also, the muscles' contraction characteristics were varied to study their influence on hopping stability. Parts of this chapter have been published in the Journal of the Royal Society, Interface, 9(72), 2012.

2.1 Control schemes

In Hill-type muscle models, the muscle force depends on the current state of the muscle, i.e. muscle length, muscle contraction velocity, and muscle activation (see Equation (1.3)). Whereas force-length and force-velocity relations are intrinsic properties of a muscle, activation is an extrinsic variable that is considered to adjust the muscle for different tasks.

Physiologically, an appropriate muscle activation is generated via motor commands from the central nervous system consisting of brain and spinal cord. When coming from the brain via descending pathways, the motor commands could depend on a movement error signal, i.e. the current deviation from a planned movement trajectory, as the quantity to be minimized (Kawato, 1999). In engineering and cybernetics, this method is termed negative feedback control (Section 1.4). As an alternative to negative feedback control, generation of discrete and rhythmic[1] movements could be provided in a feed-forward manner. Rhythmical feed-forward activation patterns (e.g., Prochazka et al., 2002; Ijspeert, 2008; Dickinson, 2000) could be generated by central pattern generators (CPG's) (Loeb, 1989) which were

---

[1]Rhythmic patterns could also be seen as repeated discrete movements (Degallier and Ijspeert, 2010). Hogan and Sternad (2007) proposed a concept to define and distinguish the characteristics of rhythmic patterns. They stated that the complex biological movements may be a superimposition of both, discrete and rhythmic tasks.

proven to exist in biology and are conceptionally used in biomechanical models. CPG's are hierarchically on a lower level than the brain (Rybak et al., 2002) and presumably located in the spinal cord (Duysens, 1998).

The central nervous system incorporates peripheral sensory information from proprioceptive muscle sensor organs (Dickinson, 2000; MacKay-Lyons, 2002; Zehr, 2005), e.g., muscle spindles (measuring length and velocity of stretch and contraction) and GOLGI tendon organs (measuring muscle force). While negative feedback control necessarily depends on the feedback of sensory information (error signal), CPG feed-forward control may also require sensory information to reset or to adapt the phase of the rhythmic signal (e.g. Righetti, 2006; Ivanenko et al., 2006; Prochazka and Yakovenko, 2007; Aoi et al., 2010; Proctor and Holmes, 2010). Apart from this centralized incorporation of sensor signals, there is evidence of decentralized circuits, which directly couple sensor signals to muscle stimulation in direct feedback loops (Stein, 1974; Loeb, 1989).

Such decentralized proprioceptive feedback could also be responsible for generating a certain movement. For example, Geyer et al. (Geyer et al., 2003) showed that proprioceptive signals can produce a muscle activation pattern resulting in periodic human hopping. Here, the hopping movement is neither a result of a planned trajectory nor a predetermined pattern, but a result of the direct coupling of proprioceptive sensory signals to muscle activation. The hopping model of Geyer and colleagues consisted of a two-segment leg with one Hill-type knee extensor muscle (contractile and series elastic element). Three different proprioceptive signals (muscle force, length and contraction velocity) were delayed, gained and added or subtracted to a stimulation bias. The resulting stimulation was fed back to the muscle via excitation contraction coupling (ECC). Positive force feedback and positive length feedback were found to generate appropriate activation patterns for periodically stable hopping. Furthermore, such decentralized feedback could rapidly adapt to disturbances and thus, stabilize bouncing gaits. In contrast, in the literature several authors used feed-forward activation patterns to actuate models for human jumping (van Soest and Bobbert, 1993; van Soest et al., 1994; van der Krogt et al., 2009) and hopping (Haeufle et al., 2010a).

If it is assumed that biologically both actuation concepts are present and involved in locomotion (Delcomyn, 1980; Zehr, 2005; Paul et al., 2005), the question arises which functional benefit is achieved by the combination of these mechanisms (Dickinson, 2000)? In a model for insects Proctor & Holmes (Proctor and Holmes, 2010) found that an isolated antagonistic muscle system can partially compensate the effects of an additional load if feed-forward CPG activation is combined with tonic proportional force feedback. Also from an engineering perspective, Kuo (2002) demonstrated a performance advantage by the combination of feed-forward and feedback controllers. The advantage is that the sensitivity of feed-forward control against perturbations and the sensitivity of feedback strategies to sensor noise can be reduced. While this approach considers the combination of different control schemes, it does not consider the dynamics emerging from the interaction of the control system with intrinsic properties of the underlying musculo-skeletal system (Biewener and Daley, 2007; Dickinson, 2000).

Interestingly, the stability of human hopping models fundamentally relies on the representation of intrinsic muscle properties (e.g., constant, linear or non-linear force-length-velocity relation) and is less influenced by the activation pattern itself (Haeufle et al., 2010a). Furthermore, the force-velocity relation was found to be necessary for hopping stabilization

while the force-length relation could be removed. This result holds for optimized predetermined activation (Haeufle et al., 2010a) as well as proprioceptive feedback (Geyer et al., 2003) generated activation. It becomes obvious that a tight integration of intrinsic properties with feed-forward and feedback actuation is a key feature of locomotion (Paul et al., 2005; Pearson et al., 2006), especially in challenging environments, e.g. uneven terrain (Biewener and Daley, 2007).

Therefore, we hypothesize an improvement of stability in hopping movements through the integration of adequate representation of intrinsic muscle properties and the combination of feed-forward and feedback actuation.

To test this hypothesis we analyzed two template models for human hopping[2]. The intrinsic muscle properties were represented in different levels of detail, as proposed in (Haeufle et al., 2010a): a reduced model with only linear force-velocity relation and a complex model with Hill-type force-length and force-velocity relations. Both models were driven by different feedback modes as well as a combination of feedback and feed-forward activation, and investigated for stability.

2.2 Methods

2.2.1 Hopping model

The one-dimensional human hopping model used for this study has been published before (Haeufle et al., 2010a). It is based on the differential equation for hopping (1.1). The leg force was generated by a single muscle $F_L = F_M$ represented by a Hill-type contractile element (Equation (1.3)):

$$m\ddot{y} = -mg + \begin{cases} 0 & y > L_0 \quad \text{flight phase} \\ A(t)\, Fl\, Fv\, F_{\max} & y \leq L_0 \quad \text{ground contact} \end{cases}, \qquad (2.1)$$

where $A(t)$ was the activation state, $Fl(y)$ the force-length relation, $Fv(\dot{y})$ the force-velocity relation and $F_{\max}$ the maximal isometric contraction force of the muscle (see also Section 1.3). No gearing between leg force and muscle force was represented (Figure 2.1).

Force-length relation and force-velocity relation were represented in different approximations (linear, nonlinear) to the physiologically observed characteristics (Haeufle et al., 2010a, fig. 2). Here, we show the results for the simplest model allowing stable periodic hopping M[const, lin] and the most realistic model M[Hill, Hill] (Figure 2.2).

The simple model M[const, lin] had a constant Fl and a linear Fv dependency:

$$Fl_{\text{M[const, lin]}} = 1$$
$$Fv_{\text{M[const, lin]}} = 1 - \mu v$$

where μ describes the slope of the linear force-velocity curve. The more complex model M[Hill, Hill] had nonlinear Hill-type Fv and Fl dependencies:

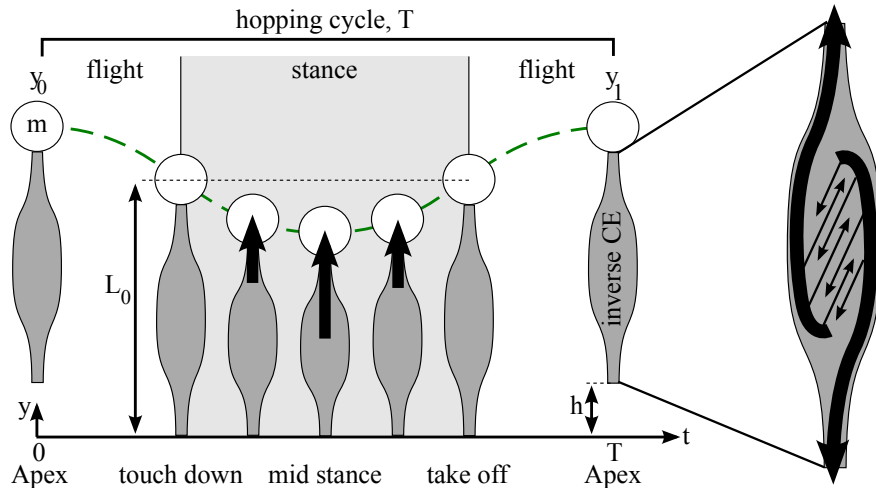[2]The concept of template models (Full and Koditschek, 1999) is discussed in Section 2.4.4.

Figure 2.1: Template model for hopping, scaled to human hopping. Hopping model consists of a point mass m representing the body and a conceptual 'leg muscle', which generates the force in positive y-direction (indicated by thick upward arrow). The 'leg muscle' is reduced to an inverse contractile element (inverse CE), which produces a pushing rather than pulling force during stance (indicated by the black arrows). The sketch on the right visualizes that this is equivalent to a pulling contractile element clamped in a stiff mechanical construction to redirect the force. Analyzed are hopping cycles defined by two subsequent apices and cycle time T. y_0 is the release height and $h = y_1 - L_0$ the hopping height. Stance phase occurs when the distance y of the mass to the ground is $y \leq L_0$ (indicated by the shaded area). From (Haeufle et al., 2010a).

$$
\begin{aligned}
Fl_{\text{M[Hill, Hill]}} &= \exp\left[-c\left|\frac{L - L_{\text{opt}}}{L_{\text{opt}}w}\right|^3\right] \\
Fv_{\text{M[Hill, Hill]}} &= \begin{cases} \frac{v_{\text{max}} + v}{v_{\text{max}} - Kv} & v > 0 \\ N + (N-1)\frac{v_{\text{max}} - v}{-7.56Kv - v_{\text{max}}} & v \leq 0 \end{cases}
\end{aligned}
\tag{2.2}
$$

where L_{opt} is the optimal length of the muscle for maximum force, w the width, and c the curvature of the bell-shaped force-length relation as described in Hill-type muscle models (e.g. Geyer et al., 2003). For the concentric phase ($v > 0$) K is the curvature parameter and v_{max} the maximum contraction velocity. The eccentric phase ($v \leq 0$) is characterized by an equation based on (Geyer et al., 2003), where N represents the dimensionless force F_M/F_{max} at $v = -v_{\text{max}}$. Parameter values were chosen to represent human hopping (Table 2.1).

The model was implemented in Matlab 7.4 (R2007a) using the Simulink 6.6 toolbox (Mathworks Inc., Natick, MA, USA). The embedded ODE45 integrator with a maximum step size of 10^{-3} s and absolute and relative error tolerance of 10^{-12} was used for the simulation.

2.2.2 Activation by proprioceptive feedback

Muscle activation state $A(t)$ is related to the neuronal stimulation input $STIM(t)$ by the excitation contraction coupling (Equation (1.5)), which basically acts as a low-pass filter
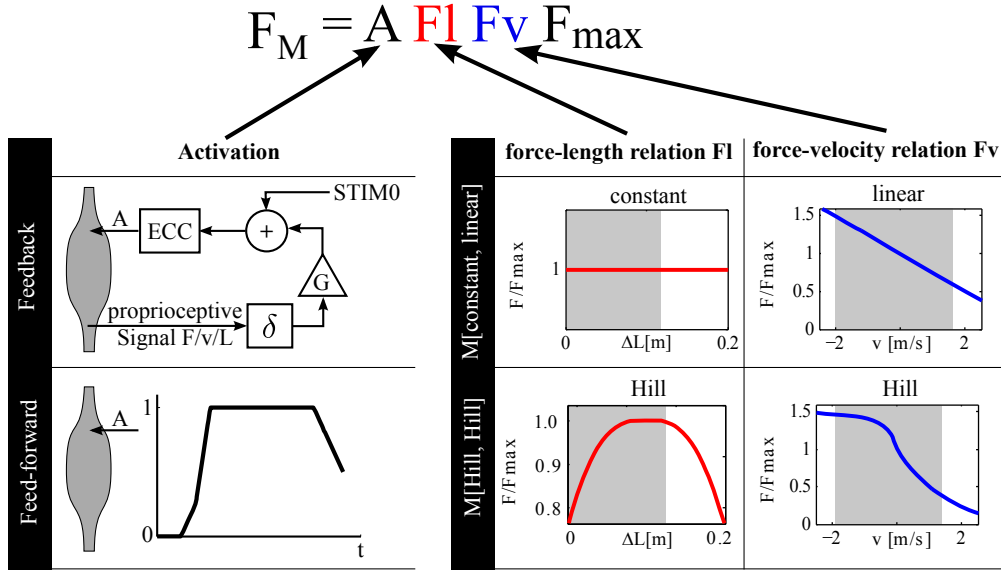
Figure 2.2: Muscle force F_M is defined by a Hill-type approach where A represents the muscle activation, Fl the force-length relation, Fv the force-velocity relation, and $F_{\max}$ the maximum isometric force (Haeufle et al., 2010a). The activation either is generated by proprioceptive feedback (figure adapted from (Geyer et al., 2003)) or is an optimized feed-forward pattern $A(t)$ or a combination of both. In the case of feedback, the stimulation is generated from force/velocity/length signals, which are delayed (by δ), amplified by the gain G, and added to the pre-stimulation $STIM0$ before being coupled to the activation (excitation contraction coupling ECC, Equation (1.5)). Force-length and force-velocity relation are represented in different levels of detail. In the simple model M[const, lin] there is no force-length dependency considered and the force-velocity relation is a linear approximation. In the more complex model M[Hill, Hill] Fv and Fl have nonlinear Hill-type dependencies. The maximum operating ranges during optimal periodic hopping are indicated by the grey areas. The force-length relation is plotted in reference to the leg compression $\Delta L = y - L_0$.

with the time constant τ. Muscle stimulation $0 \leq STIM(t) \leq 1$ is generated from the proprioceptive feedback signals muscle force F, contraction velocity v, and muscle length L. For this, these proprioceptive signals are multiplied by the gain factors G_F, G_v, G_L respectively and delayed by δ:

$$
STIM(t) = \begin{cases}
STIM0 + G_F F(t-\delta) & & & \text{FFB} \\
STIM0 & +G_v(v(t-\delta) - v_{\text{off}}) & & \text{VFB} \\
STIM0 & & + G_L L(t-\delta) - L_{\text{off}}) & \text{LFB} \\
STIM0 + G_F F(t-\delta) & +G_v(v(t-\delta) - v_{\text{off}}) & + G_L L(t-\delta) - L_{\text{off}}) & \text{ALLFB}
\end{cases}
\tag{2.3}
$$

$STIM0$ represents the pre-activation, v_{off} and L_{off} a muscle spindle signal offset (Geyer et al., 2003). Four feedback types are considered: force feedback (FFB), velocity feedback (VFB), length feedback (LFB) and the combination of all three signals in a hybrid feedback (ALLFB). In all feedback types the signal propagation delay δ was set to 15 ms as an estimate of afferent pathway properties from spinal cord to leg muscles (Geyer et al., 2003).

Table 2.1: Model parameters for human hopping. The biological relevance of these parameters is motivated in (Haeufle et al., 2010a).

parameter	value
leg rest length L_0	$1\,\mathrm{m}$
body mass m	$80\,\mathrm{kg}$
gravitational constant g	$9.81\,\mathrm{ms^{-2}}$
maximum isometric muscle force F_{max}	$2.5\,\mathrm{kN}$
optimal muscle length L_{opt}	$0.9\,\mathrm{m}$
width w	$0.45\,\mathrm{m}$
curvature c	30
maximum velocity v_{max}	$-3.5\,\mathrm{ms^{-1}}$
curvature constant K	1.5
eccentric force enhancement N	1.5
linearFv slope μ	$0.25\,\mathrm{ms^{-1}}$
excitation contraction coupling time constant τ	$10\,\mathrm{ms}$
feedback signal delay δ	$15\,\mathrm{ms}$

2.2.3 Combined feed-forward and feedback

We previously presented maximum height hopping generated by optimal activation patterns $A_{\mathrm{opt}}(t)$ (Haeufle et al., 2010a). These optimal activation patterns represent a feed-forward signal.

Here, feed-forward and proprioceptive feedback signals are combined:

$$A_{\mathrm{comb}}(t) = w_{\mathrm{FB}} \cdot A(F(t),\, v(t),\, L(t)) + (1 - w_{\mathrm{FB}}) \cdot A_{\mathrm{opt}}(t) \tag{2.4}$$

where $0 \leq w_{\mathrm{FB}} \leq 1$ is the weighting factor between feedback ($w_{\mathrm{FB}} = 1$) and optimal feed-forward ($w_{\mathrm{FB}} = 0$) activation.

2.2.4 Simulation protocol

To generate biologically relevant hopping patterns, the feedback parameters (gains and offsets) were optimized with respect to two criteria: periodic hopping height was chosen as the primary optimization goal in order to generate hopping patterns with enough ground clearance to allow for significant perturbations. The secondary criterion was a hopping frequency of $f \approx 2\,\mathrm{Hz}$, which corresponds to preferred human hopping frequencies (Melvill Jones and Watt, 1971; Farley et al., 1991). These criteria are represented in the fitness function P calculated from the hopping height $h = y_1 - L_0$ and hopping cycle duration T normalized to $1\,\mathrm{s}$:

$$\mathrm{P} = h \times \begin{cases} 1 & T \leq 0.5\,\mathrm{s} \\ 2(1 - T) & T > 0.5\,\mathrm{s} \end{cases}. \tag{2.5}$$

Performance P equals the hopping height for cycle durations of $T < 0.5\,\mathrm{s}$ and was penalized for cycle durations of $T > 0.5\,\mathrm{s}$. This restriction of hopping cycle time was necessary as the force-length relation in the model M[const, lin] included no physical limit for muscle

contraction and hopping height could have increased infinitely with longer hopping cycle duration.

A genetic optimization algorithm was used to find optimal parameters. Each individual represents a set of 5 parameters with the limits: $0.001 \leq \mathrm{STIM} \leq 1$, $0 \leq G_F \leq 2.5$, $0 \leq G_v \leq 1.2$, $-100 \leq G_L \leq 0$, $1 \leq v_{\mathrm{offset}} \leq 3$, and $-2 \leq L_{\mathrm{offset}} - 0.9$. In case of ALLFB, all parameters were optimized simultaneously. For the other feedback-types, the limits of the unnecessary parameters were set to 0. The initial population ($n = 0$) of individuals (parameter sets) was generated randomly. These parameter sets were applied to single-cycle hopping simulations from apex y_0 to apex y_1. Performance P of each individual was calculated.

Subsequent generations ($n + 1$) were derived from the 50 fittest individuals (with highest performance P). 50 % of the next generation ($n + 1$) were identical copies of the 25 fittest individuals of generation n, 25 % were created by randomly scattered pairwise recombination and 25 % by mutation with a mutation rate of one out of five genes. To favor periodic solutions the reached apex height y_1 was passed on as starting height y_0 for descendant individuals. Starting height of the initial population was $y_0 = 1.05\,\mathrm{m}$. The optimization was performed with 100 individuals for 100 generations and was repeated nine times. The best parameter set out of the nine repetitions was used for further analysis.

The resulting feedback driven hopping patterns were tested for stability against perturbations of the release height with return map analysis (see Section 1.9). The return maps were calculated for release heights of $1.01 \cdots 1.20\,\mathrm{m}$. If the return map $y_1(y_0)$ intersects the line $y_1(y_0) = y_0$, the hopping pattern exhibits a fixed point and the corresponding stability S was calculated. In addition, hopping patterns generated by the combination of feedback and feed-forward signals (according to Equation (2.4)) were tested for stability. The optimization process for the feed-forward patterns A_{opt} is described elsewhere (Haeufle et al., 2010a).

2.3 Results

2.3.1 Hopping with proprioceptive feedback

The direct feedback was found to be capable of producing activation patterns similar to the optimal activation pattern (Figure 2.3). For model M[const, lin] only minor deviations from the optimal activation pattern were found during stance phase (Figure 2.3a). For model M[Hill, Hill], force feedback FFB and the hybrid feedback ALLFB reproduced the optimal activation Aopt from (Haeufle et al., 2010a) fairly well (Figure 2.3b). Length feedback LFB activation pattern shows a similar shape but with shorter duration (resulting in reduced hopping height). Velocity feedback VFB cannot capture the quick rise of the optimal activation pattern after touchdown.

The resulting force patterns (Figure 2.3c and d) reflect the observations of the activation patterns described above. Peak forces of all activation schemes are similar in model M[const, lin] ($\max(F) \approx 3\,\mathrm{kN}$). In model M[Hill, Hill] peak forces rise up to $\max(F) \approx 3.6\,\mathrm{kN}$ for all activation types except for VFB with $\max(F) \approx 2.4\,\mathrm{kN}$.

Regarding the hopping height, model M[const, lin] reached with all four feedback types nearly the optimal feed-forward periodic hopping height of $h = 11.9\,\mathrm{cm}$ ($y_{\mathrm{fix}} = 1.119\,\mathrm{m}$) (Table 2.2). In the non-linear model M[Hill, Hill] force feedback FFB and the hybrid feedback

Table 2.2: Results of the optimization: For the characteristics of the periodic hopping patterns (stability S, periodic hopping height y_{fix}, and hopping frequency f) mean $\pm$ standard deviation of the optimization results (nine repetitions) are shown. The values for optimal feed-forward activation are taken from (Haeufle et al., 2010a). From all nine repetitions of the optimization, the feedback parameters resulting in the highest periodic hopping height were used for further analysis (§2.3.2). In this table these optimal feedback parameters are reported and additionally, the standard deviation of the optimization indicated by Δ. STIM is the stimulation bias, G_F, G_v, and G_L are the gains in the force, velocity, and length feedback circuits. v_{offset} and L_{offset} represent a signal offset. Please note, length gains G_L are negative due to the 'inverse' contractile element (Figure 2.1).

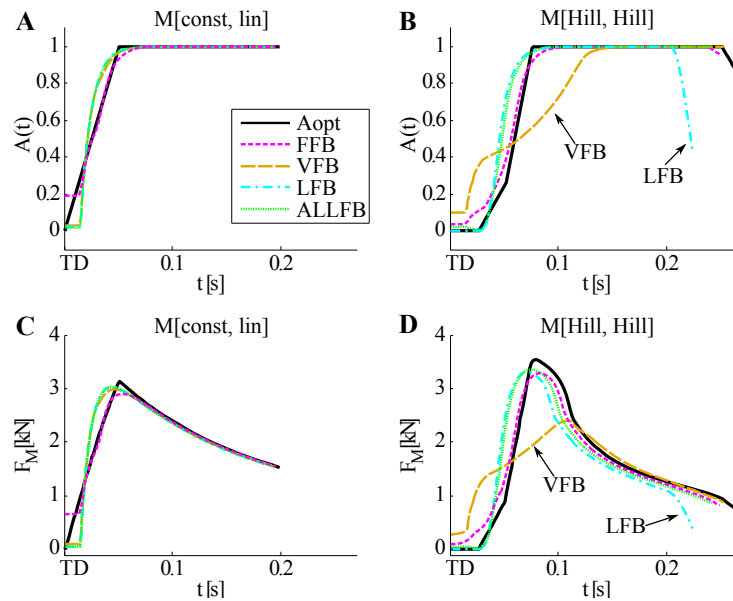| Muscle model		Feedback				Feed-forward
Fl	Fv	FFB	VFB	LFB	ALLFB	A_{opt}
const	lin	**S =0.4479 ± 0.0005** y_{fix} =1.1154 ± 0.0002 m f =2.001 ± 0.001 Hz STIM =0.186 Δ0.017 G_F =(7.11 Δ0.27) · 10⁻⁴	**S =0.62 ± 0.07** y_{fix} =1.1162 ± 0.0004 m f =2.001 ± 0.001 Hz STIM =0.007 Δ0.033 G_v =0.93 Δ0.13 v_{offset} =2.73 Δ0.19 ms⁻¹	**S =0.455 ± 0.006** y_{fix} =1.1164 ± 0.0002 m f =2.000 ± 0.001 Hz STIM =0.004 Δ0.018 G_L = − 9.59 Δ12.8 L_{offset} = − 1.62 Δ0.24 m	**S =0.51 ± 0.05** y_{fix} =1.1164 ± 0.0001 m f =2.0002 ± 0.0004 Hz STIM =0.006 Δ0.009 G_F =(2.25 Δ0.93) · 10⁻⁴ G_v =0.41 Δ0.29 G_L = − 26.3 Δ16.8 v_{offset} =1.72 Δ0.36 ms⁻¹ L_{offset} = − 1.03 Δ0.26 m	**S =-0.87** y_{fix} =1.119 m f =1.97 Hz
Hill	Hill	**S =0.26 ± 0.04** y_{fix} =1.066 ± 0.007 m f =2.1 ± 0.2 Hz STIM =0.027 Δ0.02 G_F =(9.71 Δ0.14) · 10⁻⁴	**S =0.8 ± 0.1** y_{fix} =1.063 ± 0.006 m f =2.1 ± 0.2 Hz STIM =0.054 Δ0.056 G_v =0.67 Δ0.15 v_{offset} =1.81 Δ0.30 ms⁻¹	**S =0.259 ± 0.005** y_{fix} =1.0545 ± 0.0002 m f =2.31 ± 0.02 Hz STIM =0.001 Δ0.003 G_L = − 49.8 Δ1.8 L_{offset} = − 0.980 Δ0.002 m	**S =0.24 ± 0.08** y_{fix} =1.067 ± 0.011 m f =2.1 ± 0.4 Hz STIM =0.002 Δ0.019 G_F =(8.48 Δ0.96) · 10⁻⁴ G_v =0.20 Δ0.35 G_L = − 36.0 Δ11.8 v_{offset} =2.14 Δ0.56 ms⁻¹ L_{offset} = − 0.97 Δ0.03 m	**S =-0.10** y_{fix} =1.070 m f =1.98 Hz

Figure 2.3: Comparison of the activation patterns resulting from the feedback parameters (Table 2.2) and the optimal activation (A and B). The resulting muscle forces are shown in C and D. The color indicates the type of activation (cf. legend in A). Activation pattern and resulting muscle force are very similar in the simple model (A and C). In the more complex model force feedback FFB and hybrid feedback ALLFB reproduce the optimal pattern better than LFB or VFB (B and D). Curves for optimal activation patterns Aopt are taken from (Haeufle et al., 2010a).

ALLFB reached the highest hopping height (FFB: $h = 6.6\,\mathrm{cm}$, ALLFB: $h = 6.7\,\mathrm{cm}$). Hybrid feedback does not reach much higher hopping heights in any model than a single feedback. Hopping height was lowest for all models with velocity feedback VFB.

When comparing muscle model complexity we found increasing model complexity to result in decreasing periodic hopping height (M[const, lin]: $11.5\,\mathrm{cm} \leq h \leq 11.6\,\mathrm{m}$, and M[Hill, Hill] $5.5\,\mathrm{cm} \leq h \leq 6.7\,\mathrm{cm}$, see Table 2.2).

2.3.2 Hopping stability with combined feedback and feed-forward

The return maps (Figures 2.4 and 2.5) show that optimal feed-forward activation as well as all feedback types result in stable hopping ($|S| < 1$). All pure feedback types ($w_{\mathrm{FB}} = 1$) showed a return map with positive slope ($0 < S < 1$) (thick colored lines) at the fixed point, while pure feed-forward activation ($w_{\mathrm{FB}} = 0$) resulted in return maps (thick black lines) with a negative slope ($-1 < S < 0$) (see also Figure 2.6). These two observations hold for both muscle models M[const, lin] and M[Hill, Hill].

The return maps further show that the whole range of investigated disturbances in release height ($y_0 = 1.0 \ldots 1.2\,\mathrm{m}$) were compensated as the hopping was attracted to the fixed point (undisturbed hopping pattern). Only VFB in the M[Hill, Hill] model has a limited range of release heights ($y_0 < 1.09\,\mathrm{m}$).
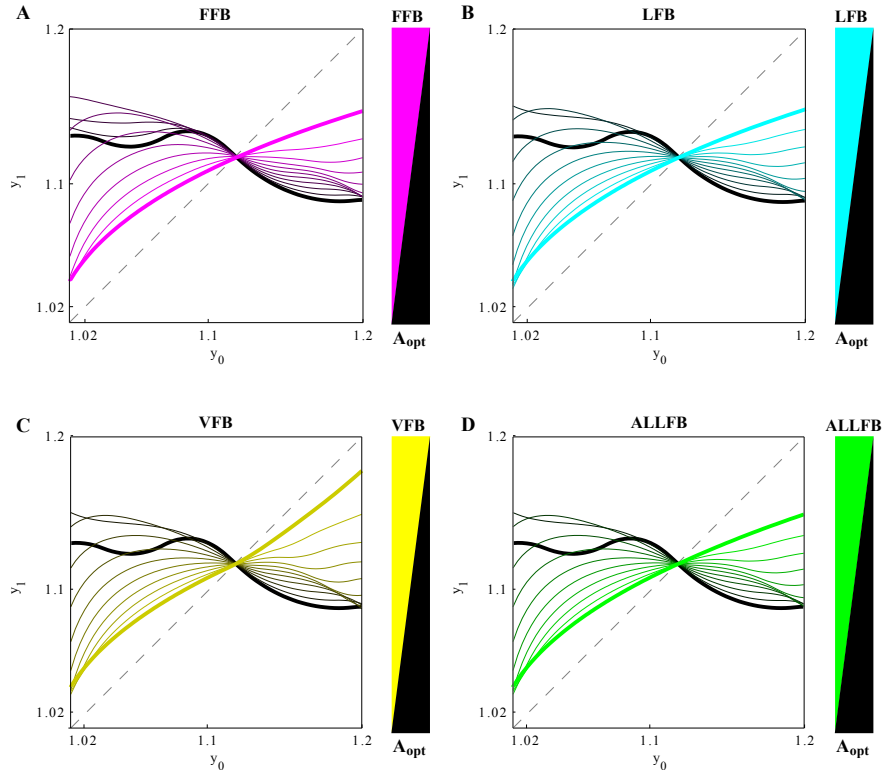
Figure 2.4: Return maps for model M[const, lin] show the model reaction to perturbations: $y_1(y_0)$ is the relation between release height y_0 and subsequent apex height y_1. Release height varied between $1.0\,\mathrm{m} < y_0 < 1.2\,\mathrm{m}$. Intersections of return maps with the diagonals (dashed lines) indicate fixed points y_{fix} (periodic solutions with $y_1 = y_0$). Here, all fixed points are stable as the slope $S = dy_1/dy_0$ of the return map at the fixed point is always $|S| < 1$. **A**: Comparison of return maps with force feedback FFB (thick magenta line) and optimal activation (thick black line). The thin lines represent the return maps for the combination of both activation types under different weighting w_{FB} as indicated by the color bar at the right: the brighter the lines are, the stronger is the contribution of the feedback (higher values for w_{FB}). The corresponding graphs for the other feedback schemes (LFB, VFB, and ALLFB) are shown in **B**, **C**, and **D**, respectively. For this analysis, the feedback parameters resulting in the highest periodic hopping height (out of nine repetitions of the optimization) were used (Table 2.2).

Combinations of optimal feed-forward activation and different feedback modes (Figures 2.4 and 2.5, thin lines) resulted in return maps with slopes S between the two extreme cases, namely pure optimal activation with $w_{\mathrm{FB}} = 0$ and pure feedback with $w_{\mathrm{FB}} = 1$.

Comparing the simple linear and the more complex non-linear model, we found smaller differences in the complex model between the return maps of optimal feed-forward and pure feedback activation. This becomes prominent by the closer alignment of the return maps (Figure 2.4 vs. Figure 2.5). Further, the perturbation is diminished faster in the complex model (flatter return maps). A higher hopping stability is indicated in the more complex model (except for VFB) by smaller values of $|S|$ (Table 2.2).
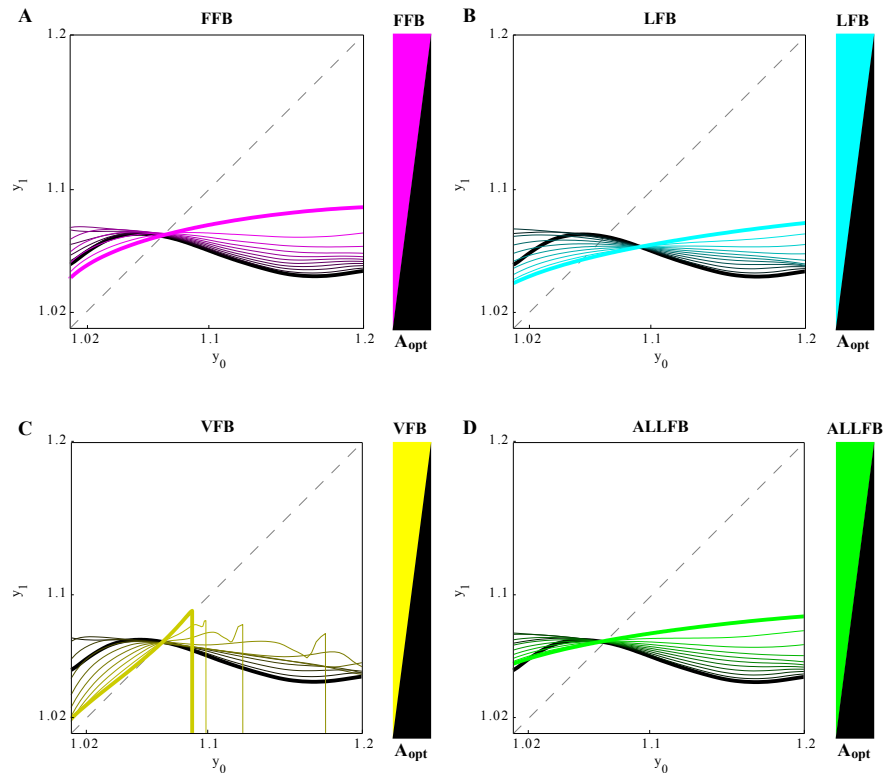
Figure 2.5: Return maps for model M[Hill, Hill] show the model reaction to perturbations in the apex height y_0 leading to a subsequent apex height y_1. Further description see Figure 2.4. The discontinuous return map with velocity feedback (**C**) results from the following situation: if the release height is too high, the contractile element driven by the velocity feedback does not produce enough force to generate the next push off and the model collapses.

2.4 Discussion

Dickinson (Dickinson, 2000) stated that "future studies of motor control should address the dynamic coupling among CPGs, sensory feedback, mechanical preflexes, and the environment." In this chapter we integrated mechanical muscle properties, feed-forward, and feedback signals, and tested their capabilities in generating and stabilizing hopping.

We were able to show that the combination of feed-forward and direct feedback improves hopping stability and that the more complex Hill-type representation of intrinsic muscle properties generally leads to a faster reduction of perturbations independent of the type of activation.

2.4.1 Performance of feedback modes

The results clearly prove that an optimal feed-forward activation pattern and a purely feedback driven activation lead to similar periodic hopping behavior. This becomes prominent since activation patterns and force patterns nearly remain the same for the feed-forward and feedback approaches (Figure 2.3). This result is surprising since it reveals that decentralized feedback modes are as effective as centralized feed-forward activation. This stands in

contrast to Geyer et al. (Geyer et al., 2003) where the optimal activation pattern clearly outperformed the best feedback type (FFB) in hopping height with 19.6 cm vs. 16.3 cm. Regarding the different feedback types we found only minor differences in hopping height in the M[const, lin] model (< 1 mm). The M[Hill, Hill] basically confirms the results of (Geyer et al., 2003) that force feedback FFB leads to highest periodic hopping. However, we found smaller differences in hopping height between force feedback FFB and length feedback LFB (≈ 1 cm in contrast to ≈ 7 cm for the model in (Geyer et al., 2003)). The differences observed here between the feedback types might be amplified by the more complex structures in the model of Geyer et al. (Geyer et al., 2003), i.e. segments, muscle acting over lever arm at joint, and tendons acting in series to the muscle.

The resulting hopping heights vary between 5.5 cm $\leq h \leq 11.6$ cm (Table 2.2). This is in accordance with a hopping height of up to $h \approx 8.6$ cm found for human periodic hopping at preferred hopping frequency (Farley and Morgenroth, 1999). In addition, the chosen hopping frequency of 2 Hz corresponds to the preferred frequency in human hopping (Melvill Jones and Watt, 1971; Farley et al., 1991). Therefore, the criteria used for the optimization in this study (periodic hopping, $f \geq 2$ Hz, maximum hopping height) led to biologically relevant hopping performance.

Regarding hopping stability, we found stable solutions for all feedback types. However, the capability to quickly reduce a perturbation is clearly better with force and length feedback than with velocity feedback, i.e., the slope of the return map $|S|$ at the fixed point is flatter for FFB and LFB (Figures 2.4 and 2.5). Furthermore, in the complex model M[Hill, Hill] VFB is not capable to reject perturbations larger than 2 cm. This means that FFB and LFB outperform VFB with respect to hopping performance. This behavior can be inherited by more complex models (Geyer et al., 2003).

2.4.2 Benefits of combining feedback and feed-forward

Both optimal feed-forward and feedback activation can produce the same periodic hopping patterns. However, when introducing perturbations, the stabilizing response can be clearly distinct. The return maps of feed-forward activation have a negative slope ($-1 < S < 0$) at the fixed point, while the return maps of all feedback modes have a positive slope ($0 < S < 1$) (Figure 2.4 and 2.5). Disturbances in case of a positive slope S are rejected in an monotonic manner (Figure 2.6). This means that with every hop, the perturbation is reduced by a certain fraction $\Delta y_{i+1}/\Delta y_i \approx S$. In case of feed-forward with a negative slope S the consecutive apices are alternatingly too high or too low and only the norm $|\Delta y_{i+1}/\Delta y_i|$ of the perturbation is reduced in every cycle (Figure 2.6). Despite this qualitatively different reaction to perturbations they diminish with both types of activation within a few cycles. Therefore, the type of stabilization (negative or positive slope) reflects system properties whose biological relevance is still unclear. Interestingly, only this difference facilitates a combination of feed-forward and feedback signals which results in optimal stability ($S = 0$).

In the literature, it is widely accepted that locomotion is controlled by a combination of feed-forward signals (e.g. from a CPG system) and direct proprioceptive feedback (e.g. from muscle sensor organs) (e.g., Dickinson, 2000; MacKay-Lyons, 2002; Nielsen, 2003; Zehr, 2005; Prochazka and Yakovenko, 2007; Friesen, 2009). For instance, in a simulation study on human walking Paul et al. (Paul et al., 2005) found indications that sensory feedback can
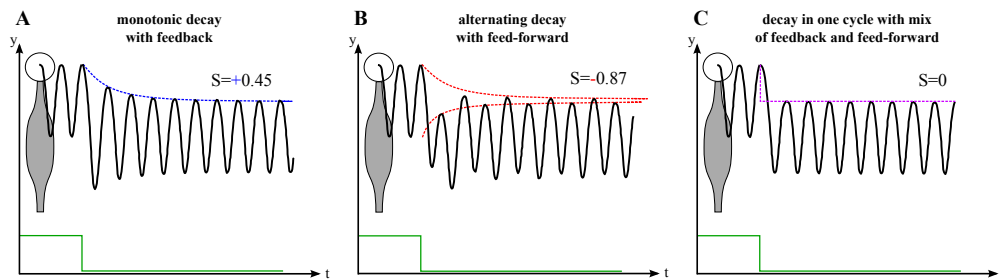
Figure 2.6: Stabilizing response of the model to a perturbation in ground level height (green). **A:** The response of the feedback driven model is a monotonic decay of the perturbation towards the periodic hopping with respect to the new (lower) ground level. **B:** With feed-forward activation A_{opt} the periodic hopping height y_{fix} is approached in an alternating pattern. **C:** Combined feedback and feed-forward activation can compensate the perturbation in one cycle. This behavior is indicated by the sign of the slope S of the return map ($S < 0$: alternating, $S > 0$: monotonic, $S = 0$: compensation in one cycle) (Figure 2.4). This figure symbolizes the principle and is not drawn to scale.

have a positive effect on the stability of a walking patterns generated by rhythmic activation. The stabilizing influence of feedback was also reported for feed-forward generated insect locomotion (e.g., Proctor and Holmes, 2010; Proctor et al., 2010). However, the interaction mechanisms and benefits are often unclear.

In our study, the improved stability of the hopping simulations driven by combined feed-forward and feedback actuation could be quantified and compared to those simulations using exclusively one actuation type. All return maps from combined activation lay within the range given by the pure signals (Figure 2.4 and Figure 2.5). At the fixed point the slope of the return maps is closer to zero, implying faster reduction of perturbations than the pure activation schemes. Interestingly, this is only possible because feed-forward and feedback actuated hopping results in alternating vs. monotonic rejection of the perturbation (Figure 2.6). In fact, only this difference allows selection of a weighting factor ω resulting in patterns with slope $S = 0$ and thus facilitates a combination of feed-forward and feedback signals which results in optimal stability. From these results it can be predicted that a combination of feed-forward and feedback is beneficial to all systems, reacting to perturbations in this opposing way.

There is also experimental evidence of simultaneous contributions of feedback and feed-forward signals. For example, in human hopping both contribute to the early EMG burst after landing (Zuur et al., 2010) or to adapt walking patterns against movement resistances (Lam et al., 2006). Our study shows that one resulting benefit of the combination is an improved disturbance rejection. We can speculate about other benefits of the combination of feedback and feed-forward signals. One advantage could be that the organism can rely on a well known and trained pattern but adds some flexibility by using sensory feedback. Also, the shape of the trained pattern could be much less critical if reflex pathways are provided at the same time. Or the redundancy of control possibilities could be a safety measure to compensate the (temporary) loss of one of the systems.

2.4.3 Stability arises from exploitive actuation

In the literature, the paradigm exists that a feed-forward strategy cannot generate adaptive movement patterns ensuring stability for uneven terrain (e.g., Daley et al., 2009; Friesen, 2009; Kuo, 2002). Our feed-forward driven model can reject perturbations of more than 13 cm (for a 1 m leg length). Therefore, we can dispel such doubts about the feed-forward strategy not being able to properly adapt to altering terrain in hopping. Another paradigm is that instabilities arise from the signal delays in a pure feedback strategy (e.g., Daley et al., 2009). Although our feedback driven model incorporates signal delays of 15 ms, it results in very stable hopping patterns. In both cases, the key is the integration of the control strategy with intrinsic muscle properties. Several other studies confirm the role of intrinsic muscle properties for compensating perturbations, e.g., variations in starting position for explosive jumping (van Soest et al., 1994), unexpected changes in surface stiffness during hopping (van der Krogt et al., 2009), sudden external forces during walking (Gerritsen et al., 1998), and perturbations while holding a load (Blickhan et al., 2003). These intrinsic muscle properties may provide rapid responses to perturbations, for instance mechanical preflexes as described by Brown & Loeb (Brown and Loeb, 2000). The control mechanism can rely on these mechanical properties and exploit them (Kalveram et al., 2005). In this concept of exploitive actuation, furthermore, the movement trajectory has not to be planned and compared to the current movement, but rather emerges from the intrinsic properties of the actuated mechanical system itself (Kalveram and Seyfarth, 2009; Kalveram et al., 2010) as discussed in Section 1.4.

The benefits of exploitive actuation for locomotion stability has also been demonstrated in several studies on insect locomotion (e.g., Schmitt and Holmes, 2003; Koditschek et al., 2004; Proctor et al., 2010; Proctor and Holmes, 2010). Furthermore, a recent model addresses the integration of feed-forward and feedback activation in the context of intrinsic muscle properties (Kukillaya et al., 2009). They found that feedback can modulate muscle force to counteract strong impulsive perturbations. However, for the high stride frequency in rapid insect locomotion, it seems not possible that direct proprioceptive feedback alone could generate adequate muscle activations because of the neural time delays. Therefore, exploitive actuation might be even more important in insects, whereas feedback might play a more important role in mammalian locomotion (Pearson et al., 2006).

In hopping, this exploitive actuation relies especially on the force-velocity relation. We observed that the nonlinear Hill-type force-velocity relation (Figure 2.5) always resulted in a faster reduction of perturbations (smaller values of $|S|$) than the linear approximation (Figure 2.4). Since this holds for all types of activation pattern generation – pure feed-forward (Haeufle et al., 2010a), or feedback, and their combination – our results reveal an independence of the activation type. Thus, the stabilizing capabilities seem to be mainly governed by the intrinsic muscle properties. And therefore, this hopping study is a strong case for the concept of exploitive actuation.

2.4.4 General implications for locomotion

The approach to understanding legged locomotion presented in this chapter is inspired by the concept of *templates & anchors* (Full and Koditschek, 1999). In this concept, the complexity
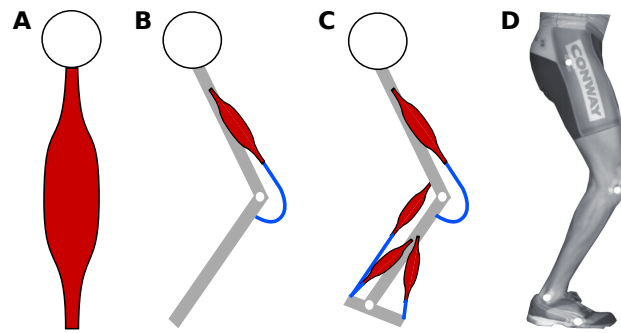
Figure 2.7: Model evolution - The path from a reductive model to elaborated representative models for human hopping. A: The one-dimensional neuromechanical template model used in this study incorporates muscle characteristics. This model predicts the centre of mass trajectory, ground reaction forces, and reactions to perturbations in landing height. B: Anchor model with two segments and one muscle-tendon complex. This model can accurately predict elastic leg behavior and vertical hopping stability (Geyer et al., 2003). C: More elaborate neuromechanical anchor models incorporate several muscles and segments (e.g., van Soest and Bobbert, 1993; van der Krogt et al., 2009; Geyer and Herr, 2010). D: The goal is to understand the functional characteristics of human and animal locomotion. Therefore, the more advanced anchor models implement the concepts found in the template models towards a specific human/animal and task.

of a biological system is reduced to a model that describes and predicts a target behavior with the least possible number of variables and parameters. Given the reductive nature, the analysis of such so-called template models facilitates the identification of underlying basic principles of locomotion. Template models can be anchored to be more representative of an organism by adding for example more morphological (segmentation of a leg, joints, muscles) and physiological details (muscle fibre orientation, behavior of motor neurons, proprioceptive sensor properties). While templates are oriented on the global behavior, anchors "provide causal explanations of detailed neural and musculo-skeletal mechanisms" (Full and Koditschek, 1999).

Following this concept, the model analyzed in this chapter reduces the neuromechanical function of a leg (Figure 2.7D) to a "muscle segment" with Hill-type muscle properties (Figure 2.7A). With this, it describes the basic function of legged systems in bouncing gaits, i.e., the vertical motion of the centre of mass, with alternating stance and flight phases. The muscle model itself represents the fundamental muscle characteristics and generates an active push off during stance phase. As the muscle operation requires a neural stimulation signal, we investigated two possibilities of neural movement generation for hopping. The major finding was that the simultaneous contribution of feed-forward and feedback could improve stability and reduce the response time to perturbations to one cycle.

We speculated that this result is a general feature of legged locomotion and can be inherited to more realistic anchor models for the following reasons:

1. The vertical oscillation of the centre of mass represents a movement primitive present in all legged gaits, whether it is hopping, running or walking (Blickhan and Full, 1993). Our reduced model predicts the global dynamics (centre of mass motion, ground reaction forces) for this vertical component and it further indicates how a muscle actuated legged system can

cope with perturbations in ground height. In this respect it fulfills the Full & Koditschek requirements of a template since it defines "the behavior of the body that serves as a target for control" (Full and Koditschek, 1999).

2. Although our analysis was done with parameters related to human hopping (Table 2.1), in principle a dimensionless analysis would lead to the same results and thus, could be applicable to animals of different size.

3. The literature already indicates that the mechanisms detected in our reduced model could be inherited by more complex musculo-skeletal models. For example, the hopping dynamics with force feedback remain very similar in a two-segmented leg model driven by one muscle-tendon complex (Geyer et al., 2003) (Figure 2.7B). There, the reaction to perturbations showed the same monotonic behavior found in our study. Furthermore, Geyer & Herr (Geyer and Herr, 2010) showed that this force feedback mechanisms could also generate and stabilize walking patterns in a more elaborate musculo-skeletal model with four segments and 14 muscles. This model could accurately predict human-like movement dynamics and even muscle activation patterns that remarkably resemble measured human EMG signals (cf. Fig. 4 in Geyer and Herr, 2010). Such an anchor evolution path towards human locomotion (Figure 2.7) indicates that the feedback properties investigated on a fundamental level might not only remain valid in a more realistic model, but also synthesize behavior observable in biology.

Therefore, we are confident that the advantages of combining feed-forward and feedback activation shown in this study is also advantageous for more complex musculo-skeletal systems. However, the proof of this speculation is open and could be tackled by the analysis of more elaborate (anchored) models.

3

Quantifying control effort of biological and technical movements: an information theory approach

In the previous chapter it was emphasized that the muscle's hyperbolic force-velocity relation contributes to the stabilization of hopping. Intuitively, hopping should be "simpler" in this case, and thus the "control effort" should be reduced compared to a system without these properties. However, a quantitative comparison to other (technical) actuators was not possible so far as previous definitions of control effort were based on system specific measures, such as voltages, forces, muscle activity, etc. In this chapter, a new system independent measure of control effort based on information theory is presented and exemplarily applied to the hopping model described in Sections 1.2 and 2.2.1.

3.1 Control effort

As stated in the introduction, the meaning of "exploitive actuation" is that a biological system with its well designed physical properties demands only minimal control effort compared to classical engineering control solutions (Section 1.4). This implies that part of the movement generation and control is done by the intrinsic mechanical characteristics of the system, and that the controller can rely on their beneficial character. One simple example to visualize this idea is a joint, a motor, and proportional-differential-controller (PD-controller) with the task of holding a desired joint position stable against external perturbations. If joint and motor are frictionless and ideal (as usually desired), the PD-controller can hold the position by measuring position and velocity of the joint. A joint with the right amount of internal viscous friction on the other hand could supersede the D-part of the controller, and measuring the velocity would not be required. If the engineer knows of such properties, he can exploit the mechanical characteristics of the system to simplify the control (Hoffmann and Pfeifer, 2011; Takuma et al., 2012).

It has been suggested that muscles and other biological or bio-inspired structures could reduce control effort or simplify control (Pratt et al., 2002; Seyfarth et al., 2006; Vanderborght et al., 2006b; Blickhan et al., 2007; Grimmer et al., 2008; Haeufle et al., 2010a; Walker and Niemeyer, 2010; Haeufle et al., 2012c; Schmitt et al., 2012; Peuker et al., 2012). But how is control effort quantified? In engineering control effort is a measure for the control

signal/input. Examples are output signal voltage of a controller (Goher and Tokhi, 2005; Nouri and Zaidan, 2006), motor armature voltage (Wai, 2006), motor torque (Bobrow et al., 2001), actuation voltage in polymer actuators (Fang, 2008), or pressure in pneumatic actuators (Lilly and Quesada, 2004). All these measures quantify the effort, in terms of force or energy, a system/controller has to apply in order to generate a desired movement. Such measures are often used as cost functions for control parameter optimizations (e.g., Neustadt, 1962; Johansson and Magnusson, 1991) and have been applied in a similar manner to biomechanical simulations (Neustadt, 1962; Nelson, 1983; Kawato et al., 1990). In some studies, control effort was also associated with muscle activation (Kuo, 1995; Schouten et al., 2001) or muscle electromyography (EMG) signal (Lockhart and Ting, 2007).

If control effort is measured in voltage, current, pressure, and muscle activation, different actuation principles can hardly be quantitatively compared. A measure, applicable to and comparable across completely different actuators and control approaches is required.

In this chapter, a method is proposed to quantify "control effort" based on information theory. The basic idea is that the amount of information required to generate a desired motion is a measure for control effort. This approach introduces a physics based measure, which allows one to compare structurally different realizations of the same movement. This concept is introduced and applied to the biomechanical model for periodic hopping described in Chapter 2.

3.2 Method: information in sensor measurements

In cybernetics, the analogy between humans and machines is that both are seen as control systems (Section 1.2). To achieve a goal, both use sensors to take measurements of their state and the environment, transmit and process the gathered information, and take actions accordingly (Wiener, 1948; Belis and Guiasu, 1968). But how can the amount of processed information be quantified? According to Shannon (1948) the prior uncertainty of the outcome when measuring the variable u can be quantified as the entropy of an information source (e.g., a sensor):

$$H(u) = -K \sum_{i=1}^{n} p_i(u = u_i) \log_2 p_i(u = u_i) \ , \tag{3.1}$$

where p_i are the probabilities of the possible sensor measurement results $u = u_i$, with $\Sigma p_i = \Sigma p_i(u = u_i) = 1$. The constant $K = 1$ bit defines the units of information.

Let us consider a linear sensor measuring a state variable u of a system. The sensor has a range $u_{min} \leq u \leq u_{max}$ and a resolution Δu and thus, $n = 1 + (u_{max} - u_{min})/\Delta u$ possible measurement results. In each measurement, it will measure one value $u_i = u_{min} + (i-1)\Delta u$, with the probability of p_i, with $i = 1 \ldots n$. The information gained in each measurement I_j is

$$I_j = - \sum_{i=1}^{n} p_{ji} \log_2 p_{ji} \ , \tag{3.2}$$

where we account for the possibility that the probability distribution may change between measurements.

To generate a movement, e.g., with a feedback loop, the measurement is repeated $j = 1 \cdots m$ times until the goal is reached. The total information processed in the task is

$$I = - \sum_{j=1}^{m} \sum_{i=1}^{n} p_{ji} \log_2 p_{ji} \quad . \tag{3.3}$$

For a real cybernetic system, the probabilities p_{ji} are a priori unknown and difficult to determine. In a typical sensor implementation, however, there is no prior assumption about the measurement outcome on the controller side. Thus, all sensor values are equally likely in each measurement: $p_{ji} = 1/n$. With this simplifying assumption, the total information is

$$I = -m \log_2 \frac{1}{n} = m \log_2 n \quad . \tag{3.4}$$

It can easily be shown that $0 \leq I_j \leq \log_2 n$ (Kolmogorov, 1965), hence $0 \leq I \leq m \log_2 n$. Therefore, the above assumptions result in an estimate of the maximum information. It will be discussed later that these assumptions only simplify the approach and do not limit its validity.

With Equation (3.4) the information provided by a sensor for movement generation can be determined from the duration of the movement T, the time resolution Δt, and the sensor properties:

$$I = \frac{T}{\Delta t} \log_2 \left(1 + \frac{u_{max} - u_{min}}{\Delta u} \right) \quad . \tag{3.5}$$

This simple measure can be applied to almost any type of sensor and requires only a discretized sensor output and discrete repeated measurements.

Here on the contrary, equal probability for each sensor value is assumed. Additionally, the possibility is neglected that subsequent measurements are related to each other. In real world systems, both assumptions must be dismissed: some sensor values are more likely to be measured than others ($p_i \neq 1/n$) and earlier measurements may carry some information about later measurements.

3.3 Application to models for hopping

To test its cogency, the proposed measure (Equation (3.5)) was applied to the biomechanical model for periodic human hopping described in Chapter 2. One-dimensional hopping is a good test scenario, as it is an easy to define motion (Equation (1.1)), which can be generated by many different actuation and control methods. To generate periodic hopping, alternating stance- and flight phases have to be generated by the leg force F_L (Equation (1.1)). The performance of hopping can be defined independent of the actual trajectory (Equation (2.5)) Three models for the leg force with appropriate (neural) controllers were investigated and the respective information (Equation (3.5)) was determined in dependence of the sensor resolutions for these three models:

Model MFF: Muscle model with feed-forward control strategy (Haeufle et al., 2010a). In the MFF model, the leg force is generated by a muscle, as defined in Equation (2.1) and described in Section 2.2.1. Here, the non-linear most realistic model M[Hill, Hill] was

chosen for the representation of the force-length and force-velocity relation (Equation (2.2)). The muscle was controlled by an optimized feed-forward muscle activation pattern $A(t)$ with $0 \leq t \leq T$ and T being the hopping cycle duration. The pattern was optimized on a grid of defined time and amplitude resolutions $\Delta t_{\text{pattern}}$ and ΔA. Detection of the take-off event in hopping triggers the feed-forward pattern. For more details on the feed-forward activation, see (Haeufle et al., 2010a). What is important is that the information required for generating hopping can be easily calculated. It is the sum of the information content of the feed-forward pattern and the information processed to measure the take-off event. The former can be directly calculated from the pattern resolution (Equation (3.5), $\Delta u_{\text{pattern}} = \Delta A$); For the latter, $u = 1$ only if take-off occurs and $u = 0$ in all other measurements, and the take-off detection measurement is performed with a time resolution $\Delta t_{\text{take-off}}$. The result is

$$I = \frac{T}{\Delta t_{\text{pattern}}} \log_2 \left(1 + \frac{1-0}{\Delta A} \right) + \frac{T}{\Delta t_{\text{take-off}}} \log_2 \left(1 + \frac{1-0}{1} \right) \ . \tag{3.6}$$

Model MFB: Muscle model with direct feedback control strategy. The muscle model is the same as in MFF, but the muscle activation A is now generated by a force feedback signal, as in Chapter 2. By focusing only on force-feedback, Equation (1.5) and (2.3) combined simplify to

$$A(t) = -\tau \frac{dA(t)}{dt} + G F_M(t - \delta) + STIM0 \ ,$$

where F_M is the muscle force multiplied by the gain factor G and delayed by δ. To allow a calculation of I, the resolutions of the signal $F_M(t)$ in amplitude Δu and time Δt were specified in the numerical simulation (independent of integrator time steps). Thus, I can be directly calculated using Eq 3.5.

Model EFB: Electric DC-motor model with PD-feedback-controller. To compare the biomechanical model of hopping with a technical control approach, a DC-motor-driven model was used. One-dimensional hopping can, with a coordinate transformation, also be modeled as a rotational system. The form of the differential equation for rotational hopping is the same (compare Equation (1.1))

$$J\ddot{\varphi} = -Jg_r + \begin{cases} 0 & \varphi > L_{0r} \quad \text{flight phase} \\ T_{\text{L}} & \varphi \leq L_{0r} \quad \text{ground contact} \end{cases} , \tag{3.7}$$

Only the units of the parameters and variables change. In this form, hopping can be modeled as generated by a DC-motor model applying the "leg"-torque T_L to de- and accelerate an inertia J:

$$\begin{aligned} \dot{I}_{\text{motor}} &= \frac{1}{\mathcal{L}} (U_a - k_T \dot{\varphi} - \mathcal{R} I_{\text{motor}}) \\ \ddot{\varphi} &= \frac{T_L}{J} = \frac{1}{J} k_T I_{\text{motor}} \ , \end{aligned} \tag{3.8}$$

where k_T is the motor constant, $\mathcal{R}$ and $\mathcal{L}$ resistance and inductance of the motor windings, I_{motor} the current through the motor windings and U_a the armature voltage of the motor, i.e. the control parameter. The motor parameters, including the maximally allowed voltage of $U_a \leq 48\,\text{V}$, were taken from a commercially available DC-motor typically used in

robotics applications (Maxon EC-max 40 283873). Back-transformation of the results allows a comparison to the linear hopping models.

Here, hopping is generated by enforcing a predefined desired hopping trajectory with a PD-feedback-controller. This resembles a traditional control theory approach. The desired trajectory was taken from previous results (Haeufle et al., 2010a) and encoded with resolutions $\Delta t_{\text{trajectory}}$ and $\Delta u_{\text{trajectory}}$. PD-controller signals position y and velocity $\dot{y}$ were measured by two "sensors" with the same resolutions to calculate I (Equation (3.5)).

To allow a comprehensive analysis and better interpretation of the resulting hopping patterns, additional characterizing quantities were calculated from the simulation results. Hopping performance P was determined with Equation (2.5). Also calculated were the stability S against small perturbations in ground level (Section 1.9) and the robustness R as a rough measure for how large a perturbation can be (similar to basin of attraction in nonlinear dynamics (Strogatz, 2001)). A perturbation range of $0.2\,\text{m}$ (20% of the leg length) was investigated, and if the model could reject these perturbations (return to the periodic hopping height, the fixed point), robustness is $R = 0.2\,\text{m}$. Furthermore, the elasticity coefficient C_{EL} (Geyer et al., 2003) was calculated to relate the hopping patterns to human hopping behavior. Human hopping is characterized by a nearly spring-like linear force-length behavior (Figure 1.5, and Blickhan (1989)). The quantity C_{EL} measures how closely the leg approximates perfectly elastic behavior:

$$C_{\text{EL}} = \left(1 - \frac{\mathcal{D}}{\mathcal{D}_{\text{max}}}\right)^2 \tag{3.9}$$

where $\mathcal{D}$ is the net area enclosed by the force-length trace and $\mathcal{D}_{\text{max}} = \max(F_{\text{M}}) \times \max(y - L_0)$ during stance. Perfectly elastic behavior corresponds to $C_{\text{EL}} = 1$.

In all models, hopping was first performed with high resolution sensors and patterns to determine the reference performance $P_{\text{max resolution}}$. Then, the resolution was decreased to minimize I, while the feedback parameters in the MFB and EFB model were adjusted to maximize performance at each investigated resolution. Stop criterion was either a reduction in optimal performance by about 10% ($P_{\text{min resolution}} \not< 0.9 \cdot P_{\text{max resolution}}$) or when hopping became unstable ($|S| \geq 1$). This was then called the "minimal information resolution" resulting in I_{min}.

3.4 Simulation results

In the **model MFF**, the feed-forward signal $A(t)$ was optimized for hopping performance P (Eq. 2.5) on grids of different resolution with the algorithm described in (Haeufle et al., 2010a) to find the resolution with the lowest encoded information ($\Delta t_{\text{pattern}} = 0.125\,\text{s}$, $\Delta A = 0.125$, therefore $I_{\text{pattern}} = 12\,\text{bit}$). Afterwards, the minimal required time resolution of the trigger event detection was searched ($\Delta t_{\text{take-off}} = 0.02\,\text{s}$). The minimal required information to generate hopping in this model was thus found to be $\mathbf{I_{\text{min}} = 34\,\text{bit}}$. The achieved hopping performance at I_{min} was $P = 0.06\,\text{m}$. Further reduction of the resolutions resulted in reduced performance and robustness. It can be seen from Table 3.1 that hopping with higher resolutions ($I > I_{min}$) only marginally effects other characterizing quantities of the movement.

Model and feedback resolution	I [bit]	P [m]	S []	R [m]	C_{EL} []
MFF [0.1, 0.015, 0.001]	597	0.0602	0.2566	0.2	0.54
MFF [0.125, 0.125, 0.001]	509	0.0617	0.3149	0.2	0.69
$I_{\min}$ MFF [0.125, 0.125, 0.02]	**34**	0.0566	0.3000	0.2	0.69
MFB [0.001, 0.001]	4980	0.0705	0.3557	0.2	0.56
MFB [0.01, 0.01]	332	0.0699	0.2220	0.176	0.58
$I_{\min}$ MFB [0.02, 0.02]	**136**	0.0666	0.3262	0.2	0.56
EFB [0.01, 0.01]	1961	0.0931	0.2475	0.2	0.75
EFB [0.2, 0.01]	1114	0.1009	0.8904	0.2	0.68
$I_{\min}$ EFB [0.3, 0.0125]	**798**	0.0914	0.0171	0.2	0.69

Table 3.1: Results: For each model the results are given for three resolutions with the minimal resolution depicted by $I_{\min}$. I is the neurally processed information per cycle, P the performance, S the stability, R the robustness, and E the elasticity coefficient (for details see Methods). **MFF:** The resolution of the feed-forward muscle activation pattern $A(t)$ was varied, as well as the time resolution of the trigger event (take off) detection. Resolutions are given as [ΔA, $\Delta t_{\text{pattern}}$, $\Delta t_{\text{take-off}}$]. **MFB:** Feedback resolution is given as [Δu, Δt]. **EFB:** The feedback and desired trajectory resolutions are given by [Δu, Δt].

In the **model MFB** model, the time and amplitude resolution of the force-sensor signal were manually tuned to find the minimal required information $\mathbf{I_{\min}} = \mathbf{136\,bit}$ to be transmitted from the sensor to the muscle ($\Delta t = 0.02\,\text{s}$, $\Delta u = 0.02$)[1]. The achieved performance was $P = 0.07\,\text{m}$. Further reduction of the resolution resulted in reduced performance and robustness, similar to the model MFF.

For the **Model EFB**, manual tuning of parameters resulted in a minimal required information of $\mathbf{I_{\min}} = \mathbf{798\,bit}$ to generate hopping with a PD-controller and a DC-motor. The achieved performance was $P = 0.10\,\text{m}$. Further reduction of the resolution results in unstable and non-robust behavior. Varying the resolution has a large effect on hopping stability (Table 3.1).

An overview of the $I_{\min}$ solution results for comparison between models is given in Figure 3.1.

3.5 Discussion

Information proves as a valuable measure of control effort, as it captures the simplicity aspect of motion control, and allows a quantitative comparison of structurally different realizations of the same movement. This approach reveals that the muscle model allows simpler control of hopping as it requires considerably less information to generate and stabilize the movement ($I_{\min} = 34\,\text{bit}$ or $I_{\min} = 136\,\text{bit}$), compared to the traditional engineering approach (model EFB) with a DC-motor and a PD-trajectory control method ($I_{\min} = 798\,\text{bit}$). This is achieved by the muscle's mechanical properties, namely the force-length-velocity relation of the muscle fibers. These properties act as a mechanical controller providing rapid mechanical

---

[1] u is considered the normalized force signal $u = F_M/F_{M,\max}$ and Δu is thus normalized accordingly, as is the sensor limit $u_{max} = 1$ in the calculation of I.
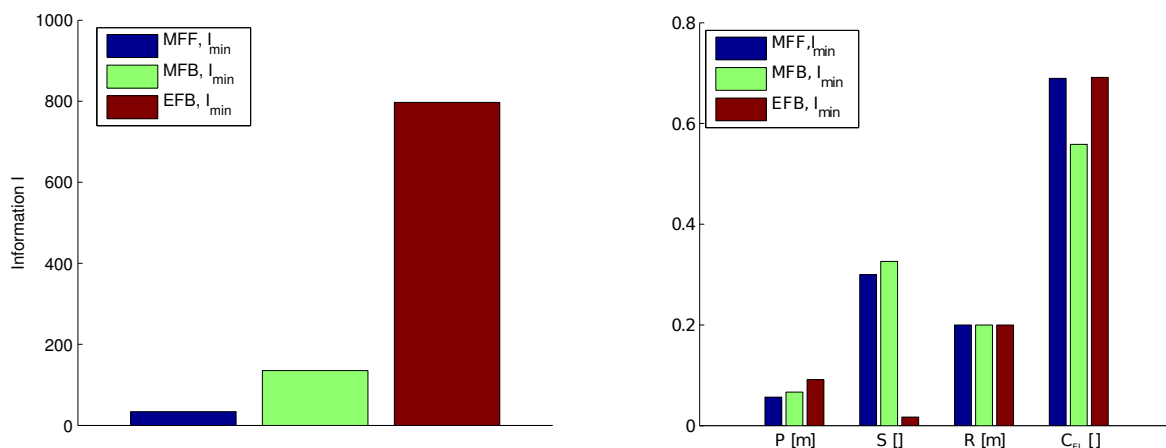
Figure 3.1: **A:** Minimal required information in all three models. **B:** Other quantities characterizing the resulting hopping patterns of the $I_{\min}$ solutions: hopping performance P, stability S, robustness R, and elasticity C_{EL}. This graphs visualizes the values in the lower rows of each section in Table 3.1.

reactions to perturbations without the need of any neurally mediated adaptation to the perturbation (Brown et al., 1995). Thus, they modulate muscle output force in a way that supports the generation and stabilization of hopping and jumping movements (van Soest and Bobbert, 1993; Gerritsen et al., 1998; Geyer et al., 2003; Haeufle et al., 2010a).

The concept of such beneficial properties has been termed "embodied artificial intelligence" (Pfeifer and Iida, 2004) (similar in its meaning to exploitive actuation (Section 1.4)). The concept of "embodiment" furthermore proposes to integrate physical and information processes Polani (2009); Hoffmann and Pfeifer (2011). Such neural information processing is closely related to energy consumption by the relation between entropy and information. Therefore, the information "metabolism" may play a crucial role in daily activities and the formation of evolutionary structures (Polani et al., 2007). The evolutionarily encoded muscle properties can non-neurally process much information in terms of Equation (3.5). First, their "resolution" is discretized not before the quantum-mechanical level (very large n). Second, any acting force is associated with structural changes and thus, very likely, with entropy changes. Leaving an enormous amount of information processing to the material substrate (exploitive actuation) may allow a reduction in neural information processing load. Biological evolution may favor such embodiment strategies for biological behavior (Polani, 2009).

An abstract approach to explain biological behavior is to investigate embodiment with perception-action loops in terms of causal Bayesian network models (Touchette and Lloyd, 2004, 2000; Capdepuy et al., 2008). The goal of that approach is to describe the behavior with emphasis on the role of information flow, but independent of the actual physical realization of sensors and actuators. By contrast, our approach focuses on the quantitative benefit of biological structures. It can be seen as a way to quantify the "active information metabolism" that is governed by the actual realization of the sensor-actuator dynamics and the interaction with the environment. By comparing different realizations of actuator-sensor-controller systems and calculating the related control effort, advantage from "embodiment"

can be quantified.

3.5.1 Information theoretical considerations

Information theory has developed many tools and approaches to quantify the information flow in cybernetic systems based on the probabilities $p(x)$ of certain signals, code words etc. However, the application of these tools to real cybernetic systems is often difficult as these probabilities are unknown a priori. From this perspective our implementation is an almost abecedarian implementation of Shannon's Information Theory (Shannon and Weaver, 1949). On the other hand, it practically allows one to use information theoretical tools to evaluate the function and design of cybernetic systems.

To calculate the real information gathered by the sensor, it would normally be necessary to know the real probability distribution p_i of the sensor values. Here on the contrary, equal probability for each sensor value is assumed. Additionally, the possibility is neglected that subsequent measurements are related to each other. In real world systems, both assumptions must be dismissed: some sensor values are more likely to be measured than others ($p_i \neq 1/n$) and earlier measurements may carry some information about later measurements. However, this approach is still valid from our point of view if the following facts are considered:

(1) In a typical feedback-loop in robotic systems a sensor value is usually directly transmitted to the controller with its full possible range of output values. Although some values may never be reached, the controller typically allows for their theoretical existence. Thus, each sensor value is equally likely from the controllers point of view and contributes to the control effort accordingly ($p_i = 1/n$).

(2) It can easily be shown (Volkenstein, 2009, p. 154) that the assumption of equal distribution ($p_i = 1/n$) gives the upper bound of the information compared to all other possible distributions ($p_i \neq 1/n$)

$$0 \leq - \sum_{i=1}^{n} p_i \log_2 p_i \leq \log_2 n \ \ .$$

Therefore our approach typically overestimates the transmitted information. Within the signal lies the relevant information for the movement, also called "pragmatic information" (Gernert, 2006). Pragmatic information is only the information that actually generates a measurable action or change in structure stripped of all the redundant and unnecessary information. Usually, the sensor transmits much more information. Decreasing the resolution (n) and with it the transmitted information to the limit where the task can just be performed, is a way to approach or determine the real distribution and thus the pragmatic information $\log_2 n \to - \sum_{i=1}^{n} p_i \log_2 p_i$.

Tishby et al. (1999) proposed to approach the question of "relevant information" quantitatively by "lossy source compression". In principle, their proposed "information bottleneck method" is equivalent to our approach in finding the minimal required information for the movement, as the reduction in sensor resolution is equivalent to a lossy source compression. However, the requirement in hopping is not to evaluate the complete time course of the force signal, but to extract the crucial information about the interaction with the environment in order to continue hopping.

3.5.2 Biological vs. technical actuator

To generate a generally definable movement such as hopping (alternating flight and stance phases at about 2 Hz), any actuator requires an actuator-specific control strategy. Both examined control strategies for muscle models (MFF and MFB) realize hopping with similar performance ($P = 0.06$ m and $P = 0.07$ m). The feed-forward strategy with an optimized activation pattern requires less control effort ($I_{min} = 34$ bit) than the feedback scheme ($I_{min} = 136$ bit). However, the feed-forward pattern only allows for one steady-state hopping height. If the hopping height has to be varied, the feedback scheme can be more easily adapted by only varying one parameter, the feedback gain (G), while in case of the feed-forward pattern, a new optimization would be required. This suggests that higher versatility requires to permanently process more information.

Higher versatility might also be a benefit of a DC-motor, at least it reached higher hopping performance ($P = 0.10$ m vs. $P = 0.06$ m or $P = 0.07$ m). In contrast to the muscles intrinsic modulation of the output force in a DC-motor the full force is always available. But again, this higher performance comes at the cost of higher control effort ($I_{min} = 798$ bit).

It can be seen that, although control effort may play an important role, it cannot be the only relevant criterion in actuator design. We approached this difficulty by incorporating other characterizing quantities in the analysis (Table 3.1). For example the stability S shows that the rejection of perturbations depends very little on the control strategy and resolution in the muscle model (Haeufle et al., 2012a), while the feedback parameters have a large influence on stability in the DC-motor model (EFB). From a biological point of view this suggests that a carefully tuned technical system might outmatch the biological system in terms of performance, but requires more fine tuning and is less reliable.

3.5.3 Relation to other quantification criteria

The previously suggested measures of control effort (voltage, current, forces, muscle activity, etc., see Section 3.1) are system specific measurable values, all ultimately related to energy or forces. Control effort in terms of information, however, is a system independent measure ultimately related to the physical quantity entropy, which is a priori independent of energy and forces. Additionally, information represents a characterizing quantity independent of all those commonly used to quantify cybernetic systems (energy efficiency, performance, stability, robustness, etc.). To compare different systems performing the same task, in biomechanics normalization to key characteristics of the system are typical (e.g. maximum ground reaction force in locomotion normalized to body weight). In the examples presented such a normalization was not necessary, as the system parameters were carefully chosen to allow for a direct comparison. However, in future studies information could also be normalized, e.g., to body weight (I/m) and time required for a movement (I/T), or could be related to time (dI/dt) or energy (dI/dE) as an information flow. This would allow e.g., to compare the control effort for locomotion of leopards, snails and robots on the level of information.

4

Proof of concept of an artificial muscle: theoretical model, numerical model, and hardware experiment

State of the art macroscopic muscle models incorporate the contraction properties of biological muscles as phenomenological functions (Section 1.3). In the previous chapters, such muscle models were utilized to investigate the benefits of contraction properties for movement stabilization (Chapter 2) and control effort (Chapter 3). The transfer of these properties to a technical artificial muscle for prosthetics, however, requires an understanding of their physical origin. A recently published study (Günther and Schmitt, 2010) proposed a model for the physical origin. In this chapter, this model is further investigated in a numerical simulation and a hardware implementation. Parts of this chapter have been published in the proceedings of the IEEE International Conference on Rehabilitation Robotics (ICORR), 2011 and the Journal of Applied Bionics and Biomechanics 9(3), 2012.

4.1 Concept of an artificial muscle

The contraction dynamics of muscles has been recorded and described in numerous muscle experiments. To interpret the results Hill (1938) proposed a macroscopic mathematical model. As outlined in Section 1.3 a whole class of "Hill-type" muscle models is based on these findings. They incorporate the force-length and the force-velocity relation of muscle fibers as phenomenological functions in one structural element, the contractile element (CE). For the force-velocity relation in concentric contractions (shortening muscle) Hill (1938) found that the muscle fiber shortening velocity depends on the contractile element force in a hyperbolic relation (Equation (1.4)). This hyperbolic relation is now known as the Hill relation. Various extensions account for physiologically observable effects, such as contraction history effects (Meijer et al., 1998; Rode et al., 2009a), high frequency oscillation damping (Günther et al., 2007), and eccentric contractions (Till et al., 2008).

In a bionics approach it is an enormous challenge to realize all these properties of biological muscles in one artificial muscle at once (Section 1.8). Fortunately, with knowledge about the task specific functional role of these properties it is possible to evaluate their importance. The previous chapters emphasize the beneficial influence of the hyperbolic force-velocity relation on movement stability and control effort. A biologically inspired artificial muscle
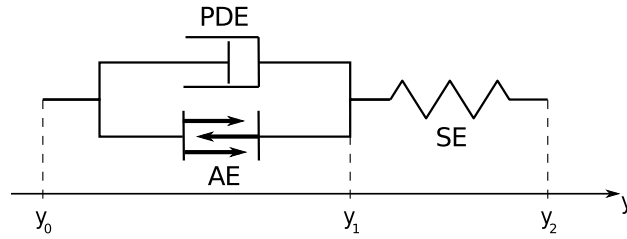
Figure 4.1: Theoretical construct of the contractile element CE (Günther and Schmitt, 2010). The contractile element consists of three elements: active element AE, parallel damping element PDE, and serial element SE. $y_0 = 0$ is the origin of the contractile element, y_1 represents the length of the AE/PDE and y_2 the length of the whole contractile element.

suitable for legged hopping and jumping should therefore feature (hyperbolic) force-velocity characteristics.

Recently Günther and Schmitt (2010) analytically derived a muscle-like Hill-type force-velocity relation from basic physical components. They showed that a contractile element (CE) consisting of a mechanical energy source (active element AE), a parallel damper element (PDE), and a serial element (SE) exhibits operating points with hyperbolic force-velocity dependency. In this concept, the force-velocity relation is no longer a phenomenological outcome of a black box (as in a Hill-type contractile element) but rather a physical outcome of the interaction of the three elements AE, PDE, and SE. Therefore, this concept can be interpreted as a basic engineering design for the contractile element of an artificial muscle.

This contractile element design concept was proven to work in a hardware prototype (Haeufle et al., 2010b). The prototype implemented AE and PDE as two DC motors and the SE as a metal spring. As expected, quick release experiments revealed qualitatively a hyperbolic force-velocity relation. Quantitatively the force-velocity relation deviated from the theoretical prediction. This was not very surprising as the characteristics of neither SE nor AE were specified by the theory (Günther and Schmitt, 2010) and were designed very simple in the prototype. Waiving the dynamics of masses the muscle acts upon, the analytical theory could not predict the actual time course of the contraction dynamics.

To further improve the understanding of the contraction dynamics and the differences between theoretical and experimental results we present here a numerical model of the contractile element, and compare it to analytical prediction and experimental results. With this we follow the test trilogy (Section 1.6).

4.2 Methods

4.2.1 Components of the contractile element

Günther and Schmitt (2010) derived a hyperbolic force-velocity relation for the construct drawn schematically in Figure 4.1. It consisted of three elements: active element AE, parallel damping element PDE and serial element SE making up together the contractile element CE of a Hill-type muscle. y_1 was the coordinate specifying the length of the PDE (and AE) and y_2 the length of the whole contractile element.

PDE: Günther and Schmitt (2010) specified the functional dependency of the PDE

$$F_{\mathrm{PDE}} = d_{\mathrm{PDE}} \cdot \dot{y}_1 \,, \tag{4.1}$$

where $\dot{y}_i = dy_i/dt$. The PDE force depended linearly on the contraction velocity of the AE with the damping coefficient

$$d_{\mathrm{PDE}}(F_{\mathrm{CE}}) = D_{\mathrm{PDE,max}} \cdot \left((1 - R_{\mathrm{PDE}}) \cdot \frac{F_{\mathrm{CE}}}{F_{\mathrm{AE,max}}} + R_{\mathrm{PDE}}\right) \tag{4.2}$$

depending linearly on the current force F_{CE} of the CE. $F_{\mathrm{AE,max}}$ was the maximum isometric force, $D_{\mathrm{PDE,max}}$ the maximum $d_{\mathrm{PDE}}(F_{\mathrm{CE}})$ value (at $F_{\mathrm{CE}} = F_{\mathrm{AE,max}}$) and R_{PDE} the minimum $d_{\mathrm{PDE}}(F_{\mathrm{CE}})$ value (passive damping in an inactive muscle) normalized to $D_{\mathrm{PDE,max}}$.

AE: The force produced by the active element is

$$F_{\mathrm{AE}} = A_{\mathrm{AE}} \cdot F_{\mathrm{AE,max}} \,, \tag{4.3}$$

where the parameter $0 \le A_{\mathrm{AE}} \le 1$ allows linear scaling of the AE force. This is taken from biology, where A_{AE} represents the activation state of a muscle (Zajac, 1989).

SE: For the SE we chose a mechanical spring which produces the force

$$F_{\mathrm{SE}} = \begin{cases} -k_{\mathrm{SE}} \cdot \Delta l_{\mathrm{SE}} & \Delta l_{\mathrm{SE}} > 0 \\ 0 & \Delta l_{\mathrm{SE}} \le 0 \end{cases}, \tag{4.4}$$

where k_{SE} is the spring constant, $\Delta l_{\mathrm{SE}} = y_2 - y_1 - l_{\mathrm{SE,0}}$, and $l_{\mathrm{SE,0}}$ the slack length of the spring.

4.2.2 Numerical simulation of contractions

The theory (Günther and Schmitt, 2010) assumes equilibrium of the forces generated by the three elements

$$F_{\mathrm{SE}} = F_{\mathrm{AE}} + F_{\mathrm{PDE}} \tag{4.5}$$

at the internal degree of freedom y_1. Together with the definition of F_{PDE} (Equation (4.1)) this gives a differential equation describing the internal movement

$$\dot{y}_1 = \frac{F_{\mathrm{AE}} - F_{\mathrm{SE}}}{d_{\mathrm{PDE}}(F_{\mathrm{CE}})} \,. \tag{4.6}$$

Contraction of the whole contractile element against a mass m is described by a second differential equation

$$\ddot{y}_2 = g + \frac{1}{m} F_{SE} \,, \tag{4.7}$$

where $g = 9.81\,\mathrm{ms}^{-2}$ is the gravitational acceleration. In contrast to the original analytical model, this numerical model includes the dynamics of the mass m attached to the end of the muscle. This set of differential equations was solved with Matlab Simulink embedded ODE45 (Dormand-Prince) solver with absolute and relative tolerance of 1×10^{-7}.

4.2.3 Parameter identification

For the elements described above the following Hill-type hyperbolic force-velocity relation (compare to Equation (1.4))

$$(F_{\mathrm{CE}} + \mathcal{A}) \cdot \dot{l}_{\mathrm{CE}} = -\mathcal{B} \cdot (F_{\mathrm{CE},0} - F_{\mathrm{CE}}) \tag{4.8}$$

is predicted (Günther and Schmitt, 2010), where the Hill parameters $\mathcal{A}$ and $\mathcal{B}$ are directly related to the parameters of the three components

$$\mathcal{A} = \frac{R_{\mathrm{PDE}}}{(1 - R_{\mathrm{PDE}}) \cdot (1 - \kappa_v)} \cdot F_{\mathrm{AE,max}} + \frac{\kappa_v}{1 - \kappa_v} \cdot F_{\mathrm{CE},0} \tag{4.9}$$

$$\mathcal{B} = \frac{1}{\frac{D_{\mathrm{PDE,max}}}{F_{\mathrm{AE,max}}} \cdot (1 - R_{\mathrm{PDE}}) \cdot (1 - \kappa_v)} \tag{4.10}$$

with

$$\kappa_v = \frac{(\dot{y}_2 - \dot{y}_1)}{\dot{y}_2} = \frac{\dot{l}_{\mathrm{SE}}}{\dot{l}_{CE}} \tag{4.11}$$

being the relation between the contraction velocity of the SE and the whole contractile element.

These relations can be transposed to determine the parameters of the PDE:

$$R_{\mathrm{PDE}} = \frac{1}{1 + \frac{F_{\mathrm{AE,max}}}{\mathcal{A}(1 - \kappa_v) - \kappa_v \cdot F_{\mathrm{CE},0}}} \tag{4.12}$$

$$D_{\mathrm{PDE,max}} = \frac{F_{\mathrm{AE,max}}}{\mathcal{B}(1 - R_{\mathrm{PDE}})(1 - \kappa_v)} \tag{4.13}$$

For a rat GM with $F_{\mathrm{AE,max}} = 13.39\,\mathrm{N}$ the constants $\mathcal{A}$ and $\mathcal{B}$ were experimentally determined to be $\mathcal{A} = 2.68\,\mathrm{N}$ and $\mathcal{B} = 4.16 \times 10^{-2}\,\mathrm{ms^{-1}}$ (van Zandwijk et al., 1996, Animal 1). With the assumptions $\kappa_v = 0.15$ and $F_{\mathrm{CE},0} = F_{\mathrm{AE,max}}$, the parameters of the PDE result in

$$R_{\mathrm{PDE}} = 0.02$$
$$D_{\mathrm{PDE,max}} = 386\,\mathrm{Nsm^{-1}}$$

4.2.4 Hardware model

AE and PDE: both AE and PDE were realized each with an electric motor (Maxon EC-max40) as shown in Figure 4.2. The motor torque (assuming motor torque is proportional to motor current $T \propto I$) was controlled by Maxon digital EC-motor control units (DEC 70/10). Both motors were mounted from opposite sites to the same disc with radius $r_{\mathrm{disk}} = 0.05\,\mathrm{m}$. The disc was used to coil up a steel rope and exert a force

$$F_{\mathrm{AE}} + F_{\mathrm{PDE}} = r_{\mathrm{disk}} \cdot (T_{\mathrm{MotorAE}} + T_{\mathrm{MotorPDE}}) \tag{4.14}$$

on the rope. The force characteristics of the PDE and AE (Equations (4.1) and (4.3)) were implemented in Matlab Simulink through Real Time Workshop and Real Time Windows
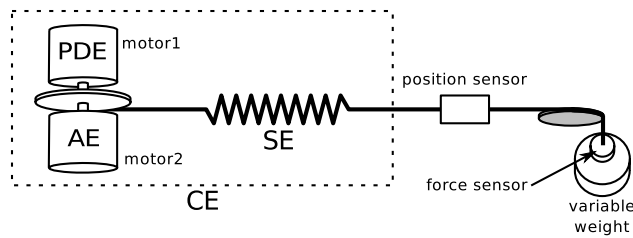
Figure 4.2: In the hardware design, the active element AE and the parallel damping element PDE were realized with electric motors, and the SE with a mechanical spring. A variable weight was used for the external loading of the contractile element CE.

Target. In this way the motors could exert the specified force on the steel rope and the SE as required by the theoretical construct. This was validated for the torques and speeds occurring during the experiments (current controller bandwidth $\approx 1\,\text{kHz}$, motor included $> 100\,\text{Hz}$, peak target frequencies $\approx 30\,\text{Hz}$).

SE: a metal spring with stiffness $k_{\text{SE}} = 2401\,\text{Nm}^{-1}$ was tight on one end to the steel rope of the motor disc and on the other end to a variable weight (Figure 4.2).

Sensors: the motor shaft position φ_{Motor} was recorded by an optical encoder (Scancon 2RMHF 5000 pulses/revolution) and represented $y_1 = 2r_{\text{disk}}\varphi_{\text{Motor}}$. An optical linear position encoder (Renishaw RGH24D $5\,\mu m$ resolution) recorded y_2. A load cell (Transducer Techniques MLP 25 with amplifier TM0-1-24) recorded the force F_{CE}. All sensor data was recorded with Matlab Simulink via a Sensoray 626 AD I/O at $1\,\text{kHz}$.

Test-bed: the motors were mounted to a table. A variable weight was attached to the SE via a wheel at the end of the table. An electromagnet was installed below the weight to restrain the movement of the weight for isometric and quick release experiments.

4.2.5 Experimental protocol

To investigate the force-velocity characteristics of the contractile element, **quick release contraction** experiments were performed in the numerical simulation and in the hardware model (experiments published in (Haeufle et al., 2010b)). For this purpose, muscle activation state was set to maximum ($A_{\text{AE}} = 1$) while the muscle length y_2 was held constant by fixing the mass. After the settlement of the initial isometric contraction movement (at $t_{\text{QR}} = 3\,\text{s}$) the mass was released. The recorded contractile element contraction velocity $v_{\text{CE}} = \dot{y}_2$ (Figure 4.4B) shows a global minimum shortly after t_{QR} at $t_{v\text{CE\_min}}$. The values $v_{\text{CE}}(t_{v\text{CE\_min}})$ and $F_{\text{CE}}(t_{v\text{CE\_min}})$ were extracted. This experiment was performed with different weights $0.2\,\text{kg} \leq m \leq F_{\text{CE,max}}/9.81\,\text{ms}^{-2}$ in steps of $\approx 0.08\,\text{kg}$ (five times per weight for the hardware model). The curve $F_{\text{CE}}(t_{v\text{CE\_min}})$ vs. $v_{\text{CE}}(t_{v\text{CE\_min}})$ for all weights represents the force-velocity characteristics of the artificial contractile element.

4.3 Results

We can now compare **force-velocity relations** (Figure 4.3) predicted by theory, calculated with the numerical model, and measured in the hardware experiments. The numerical simulation showed a hyperbolic force-velocity relation with higher velocities for the same
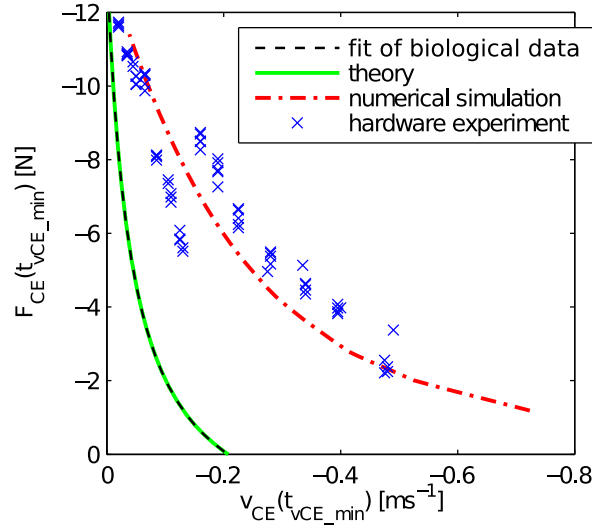
Figure 4.3: Comparison of theoretical, numerical, and experimental contractile element CE force-velocity relation. The experimental data (Haeufle et al., 2010b) is scattered around the numerical prediction (quality of the fit: $R^2 = 0.85$); both show hyperbola-like force-velocity characteristics, but deviate from the theoretical prediction. The theoretical prediction is based on biological data of a rat gastrocnemius muscle (van Zandwijk et al., 1996).

forces than the theory predicted. So did the hardware experiment. Hardware quick release measurements resulted in reproducible clusters of five data points for each load in the force-velocity graph. These clusters align in fairly good agreement to the numerical prediction (quality of the fit: $R^2 = 0.85$), but are scattered around the numerical force-velocity relation.

Contraction characteristics of the numerical simulation and the hardware experiment were in principle the same, although deviations were existent (Figure 4.4). Compared to the numerical simulation the hardware experiment showed **I** slower peak contraction velocities ($\approx 20\%$) of both contractile element CE and AE/PDE (Figure 4.4A and B); **II** slower change in contraction velocities after QR (4.4A and B); **III** two minima of contractile element contraction velocity v_{CE} around t_{vCE_min}, separated by $\approx 20\,\text{ms}$ (4.4B); **IV** additional features in the contractile element force drop after QR (4.4D); **V** noise in the PDE force which is larger for higher loads (4.4C).

4.4 Discussion

The test trilogy introduced by Kalveram and Seyfarth (2009) (see Section 1.6) is a guideline to verify that a biomechanical concept is logically precise, physically sound, and biologically relevant. The biomechanical concept in question in this chapter is the construction/working principle of the contractile element CE in muscles, based on simple physical components (Günther and Schmitt, 2010). In this chapter, we follow the test trilogy and presented a numerical model (simulation test) and a hardware experiment (hardware test) and compared them to a biological rat gastrocnemius muscle (behavioral comparison test).
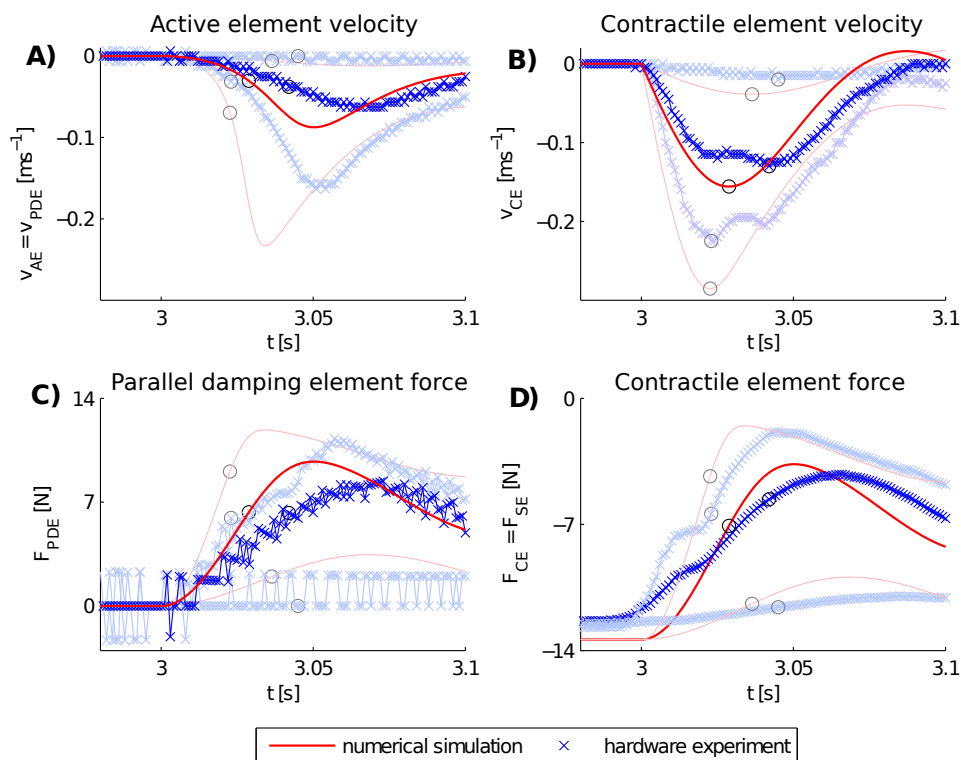
Figure 4.4: Contractile element (CE) contraction dynamics for loads of $m_1 = 0.44\,\text{kg}$, $m_2 = 0.72\,\text{kg}$ (thick strong lines), and $m_3 = 1.16\,\text{kg}$ in the numerical simulation (red) and the hardware experiment (blue x). The force-velocity relation (Figure 4.3) is extracted for the instant $t_{v\text{CE\_min}}$ where v_{CE} reaches a minimum (B: black circle). The load is released at $t_{\text{QR}} = 3\,\text{s}$.

4.4.1 Differences between numeric and hardware

Simulation test and hardware test show similar force-velocity characteristics, but deviations were identified. They emerge from additional aspects of physical reality which were not represented in the numerical model. In contrast to the numerical model, in the hardware experiment a position sensor is integrated into the SE by using steel wires with knots at their end (Figure 4.2). Thus, an additional mechanical degree of freedom (lever mass) is introduced into the SE, leading to further oscillations at frequencies above 30Hz (20-30ms period; Figure 4.4B and D). These result in two v_{CE} minima around $t_{v\text{CE\_min}}$ (4.4B) instead of one distinct minimum as in the numerical model. Sometimes the first one is lower, sometimes the second, causing the algorithm (Section 4.2.5) to extract very different CE forces for the force-velocity relation as the CE force rises quickly during the contraction. This explains the scattered data in the force-velocity relation (Figure 4.3). The amplitudes of such oscillatory disturbances could be reduced along with minimizing the mass of any potential sensor integrated into the serial muscle arrangement.

In the numerical model AE, PDE, and SE are assumed to be massless and free of internal friction. In reality the rotors of the motors, the axes, and the transmission disc (Figure 4.2) together have an inertia of $J \approx 1.97\,\text{kgm}^2$ which has to be accelerated during the contraction. Frictional forces in the bearings additionally hinder the acceleration. This is the main reason for the slower peak contraction velocities and the slower acceleration of the AE/PDE complex

observed in the hardware experiment (Figure 4.4A). The slower acceleration of the whole contractile element (Figure 4.4B) is partly a result of the slower acceleration of the AE/PDE and partly of the friction in the position sensor at y_2 and the bearing holding the load (Figure 4.2).

The oscillations of the PDE force could be reduced if the PDE were an actual passive damping element and not a hardware in the loop motor generating damping forces on the basis of a noisy velocity signal (time derivative of discrete encoder signal). Internal properties of the motor/controller unit have no influence on the force-velocity characteristics of the contractile element, as they produce a torque proportional to the controller set value (current control mode). This was validated for the torques and speeds occurring during the experiments (current controller bandwidth $\approx 1\,\mathrm{kHz}$, motor included $> 100\,\mathrm{Hz}$, peak target frequencies $\approx 30\,\mathrm{Hz}$).

In summary, three additional physical aspects in the hardware experiment were identified: elasticity, friction, and internal inertia. Elasticity and external friction can partly be accounted for in the numerical model and might explain some of the deviation in the force-velocity relation (Figure 4.5). Internal inertia is not considered and should be minimized in future experiments (see setup in Chapter 5).

4.4.2 Differences to biology

Comparing the numerical (and hardware) results to the biological data of rat gastrocnemius muscle (van Zandwijk et al., 1996) reveals that the qualitative hyperbolic shape of the force-velocity relation is represented, but there are quantitative deviations (Figure 4.3). This is a first behavioral comparison test (Kalveram and Seyfarth, 2009) based only on literature data. A better behavioral comparison test should be performed in the same experimental setup.

From a robotics point of view the difference between theory and experiment would not be a problem, especially, as the numerical model predicts the experimental results. An engineer could choose the right properties to match his design criteria. From a biomimetics point of view, the difference is not tolerable. It reveals that the theoretical model does not completely describe the real physical properties of biological muscles.

The observed deviations could originate in an incorrect representation of SE and AE. The biological SE, e.g., is presumably stiffer than the metal spring used in the prototype (Günther and Schmitt, 2010) and has non-linear viscoelastic characteristics (Loram et al., 2007). Increasing stiffness (by factor 10) in the numerical model reduces the deviation in the force-velocity relation, at least for higher forces (Figure 4.5). Although the AE in biological muscle is more complex than modeled here – it shows force-length dependencies, force enhancement and depression effects, and excitation contraction coupling (Section 1.3) – these missing properties cannot account for the deviations as the experiment is designed to disregard them. Finally, the force in the AE used to derive the Hill relation in the model was assumed to decrease linearly with contraction velocity (see figure 5 in Günther and Schmitt, 2010). As our hardware experiment is based on non-changing AE force, further theoretical analysis are necessary to throw light on the found difference between the predicted force-velocity relation, on the one hand, and both the measured and the simulated relations, on the other (Chapter 5).
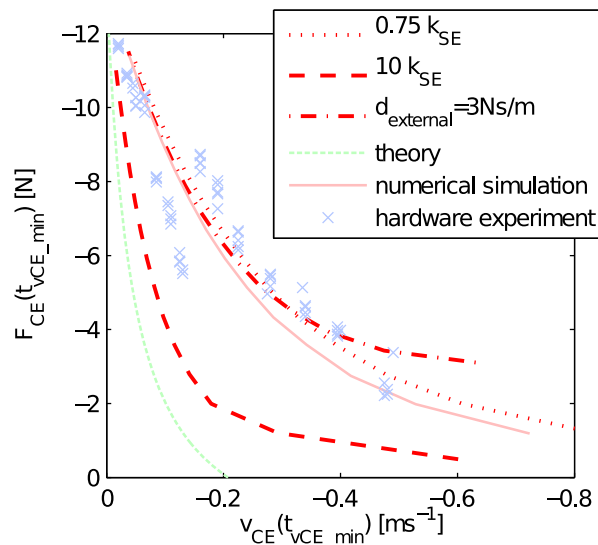
Figure 4.5: Parameter variation in the numerical model. A SE with a 0.75 times lower stiffness can explain some of the deviation between experiment and numerical prediction; the sane can an external damping ($F_{d\_\text{external}} = -d_{\text{external}}\dot{y}_2$). Tenfold higher stiffness of the SE is more realistic with respect to biological muscles and may explain part of the deviation from the theoretical prediction.

4.4.3 Artificial muscles for prosthetics and orthotics

Generally, an improvement in performance of technical systems, e.g. robot arms, walking machines, prostheses, and orthoses are expected from actuators incorporating muscle-like characteristics (Madden, 2007). A more natural movement, generated by such actuators could improve wearability patient acceptance. Therefore, the construction of artificial muscles with biology-like capabilities is one of the most challenging developments in biomedical science.

The force-velocity relation is an outstanding dynamic property of biological muscles. It can be observed in muscles of insects (Ahn and Full, 2002), spiders (Siebert et al., 2010), frogs (Hill, 1938), mammals (van Zandwijk et al., 1996; Günther et al., 2007) and other animals. The relation between force and velocity was always found to be of hyperbolic nature. In Section 1.8 some artificial muscles were reviewed, and it was shown that non exist that has a hyperbolic force-velocity relation as known from biological muscles. The advantage of the artificial muscle concept presented here is that it is based only on a very small number of mechanical elements and an inherently simple control algorithm. Still, it shows already the contraction characteristics of real biological muscle with the incorporation of high robustness and self-stability. With this actuator it is possible to produce movement characteristics similar to that of real biological muscles from the physical structure of the actuator. Moreover, the presented concept is a template, which is not limited to electric drives but also allows the use of smaller, more efficient, more powerful new actuators, for example, combustion engines or dielectric elastomers (Madden, 2007). Therefore, the presented simple and straight forward contractile element concept proves that a more natural movement is technically realizable.

5

Can quick release experiments reveal the muscle structure? A bionic approach

In the previous chapter, a quantitative deviation in contraction dynamics between the theoretical prediction and the hardware implementation of a physical muscle model was found. Furthermore, the numerical simulation of the contraction dynamics supported the findings of the hardware implementation. Therefore, the experimental method of quick release experiments against an inertial mass has to be revisited. In this chapter, the theoretical model is modified and a different type of muscle experiment, isotonic quick release contractions, is utilized to further investigate the origin and meaning of the deviation. Parts of this chapter have been published in the Journal of Bionic Engineering, 9(2), 2012.

5.1 Experiments in muscle physiology

To determine the dynamic properties of muscles, namely, the force-velocity relation, several different experiments are reported in the literature: isokinetic contraction experiments (e.g., Bressler and Clinch, 1974; Ettema and Huijing, 1988; Barclay et al., 1993; Siebert et al., 2008; Till et al., 2008), isotonic quick release experiments (e.g., Jewell and Wilkie, 1958; Cavagna and Citterio, 1974; Ettema and Huijing, 1988; van Zandwijk et al., 1996) and quick release contractions against an inertial mass (Wilkie, 1949; Günther et al., 2007). Each of these experiments is repeated several times, the isokinetic experiments at several velocities, and the quick release experiments with varying external force or mass. The force-velocity relations can only be determined from such a set of experiments, as each experimental condition retrieves one operating point of the muscle.

In the context of phenomenological muscle models, all three experiments should reveal the same force-velocity relation. This is in fact one of the assumptions made to allow a representation of the contractile element in the form of Equation (1.3). However, the physical structure of the theoretical model of Günther and Schmitt (2010) has one additional degree of freedom (length of the active element l_{AE}). The model analytically predicts the operating points without considering the time development of the system (including $l_{AE}(t)$) during the contraction experiment. Therefore, it is not a priori clear, which experiment is adequate for the comparison to this model. It is possible that the deviations between theory and simulation/experiment observed in the previous chapter is a result of an inconsistency with respect

to the experiment. Therefore, in this chapter two types of quick release experiments were performed in simulation and hardware, which represent two extreme cases of the contraction dynamics: against a constant force (isotonic) and against an inertial mass. To allow this in a consistent way, the theory hat to be modified with respect to the force of the active element.

5.2 Methods

5.2.1 New formulation of the theory

In the previous chapter it was demonstrated that the phenomenologically found hyperbolic force-velocity relation (Hill, 1938) of the contractile element (CE) can be derived from the combination of three simple mechanical elements: a force generating active element (AE) to which a damper (PDE) is connected in parallel and, in series to both, a serial element (SE) (Figure 4.1). The following three assumptions are identical to the original formulation of Günther and Schmitt (2010):

(1) The three elements fulfill the force equilibrium (Equation (4.5))

$$F_{CE} = F_{SE} = F_{AE} + F_{PDE} \ ,$$
(5.1)

(2) The kinematic relation for the lengths "l" of the elements is

$$l_{AE} = l_{PDE} = l_{CE} - l_{SE} \ .$$
(5.2)

(3) The kinematic gearing ratio between internal (SE) and external (CE) contraction velocity can be represented by an arbitrary parameter (Equation (4.11))[1]

$$\kappa_v = \frac{\dot{l}_{SE}}{\dot{l}_{CE}} \ .$$
(5.3)

The the parallel damping element was explicitly specified by Günther and Schmitt (2010) (Equations (4.1) and (4.2)). The characteristics of the serial element do not have to be specified.

The active element is the source of mechanical energy. For this element, we simplify the approach of Günther and Schmitt (2010): we now assume[2] the straightforward identity

$$F_{\text{AE}} = q_{\text{AE}} \cdot F_{\text{AE,max}} = F_{\text{CE,0}}$$
(5.4)

with $F_{AE,max}$ being the maximum AE force, $0 \leq q_{\text{AE}} \leq 1$ representing the activity of the muscle (e.g., Zajac, 1989), and $F_{\text{CE,0}}$ denoting the isometric CE force. All simulations and experiments were performed with full activity $q_{\text{AE}} = 1$. This is equal to the assumption

---

[1]In the theoretical derivation κ_v is assumed to be constant. In a real dynamic contraction, it changes over time $\kappa_v(t)$ as will be discussed later.

[2]In contrast to Equation 6 in (Günther and Schmitt, 2010), where the AE force depended on SE length and the damping coefficient: $F_{AE} = F_{CE,0} + d_{PDE}(F_{CE,0}) \cdot \dot{l}_{SE}$. Here, the force of the AE and the isometric force of the CE ($F_{CE,0} = F_{CE}(\dot{l}_{CE} = 0)$) are simply assumed to be the same (input) parameter with no dependencies: $F_{AE} = F_{CE,0}$.

that the muscle fibers are maximally activated and operate at optimal length throughout the experiments, as usually assumed for quick release experiments.

This simplification allows a straightforward numerical and hardware implementation, but also changes the derivation of the hyperbolic force-velocity relation: Substituting Equation (4.1), the explicit dependency of $d_{PDE}(F_{AE})$ on force F_{AE} and model parameters (Equation (4.2)), and Equation (5.3) into Equation (5.1), thereby considering the time derivative of Equation (5.2), makes the force equilibrium Equation (5.1) to constitute a hyperbola

$$(F_{CE} + \frac{R_{PDE}}{1 - R_{PDE}} \cdot F_{AE,max}) \cdot \dot{l}_{CE} = -\frac{1}{1 - R_{PDE}} \cdot \frac{1}{1 - \kappa_v} \cdot \frac{F_{AE,max}}{D_{PDE,max}} \cdot (F_{AE,max} - F_{CE}) \ . \quad (5.5)$$

Comparing this hyperbola to Equation (1.4), the original formulation of Hill (1938),

$$(F_{CE} + \mathcal{A}) \cdot \dot{l}_{CE} = -\mathcal{B} \cdot (F_{CE,0} - F_{CE}) \ , \quad (5.6)$$

with the Hill parameters $\mathcal{A}$, $\mathcal{B}$ and the isometric force $F_{CE,0}$ being positive and $\dot{l}_{CE}$ consistently being negative in the shortening (concentric) case, the Hill parameters can be expressed in terms of the new mechanical parameters

$$\mathcal{A} = \frac{R_{PDE}}{1 - R_{PDE}} \cdot F_{AE,max} \quad (5.7)$$

$$\mathcal{B} = \frac{1}{1 - R_{PDE}} \cdot \frac{1}{1 - \kappa_v} \cdot \frac{F_{AE,max}}{D_{PDE,max}} \ . \quad (5.8)$$

5.2.2 Deriving the mechanical parameters

Through Equations (5.7) and (5.8) the Hill parameters $\mathcal{A}$ and $\mathcal{B}$ are directly related to the parameters of the three elements. If these relations are rearranged, it is possible to determine the mechanical parameters of the PDE from biological muscle experiments:

$$R_{PDE} = \frac{\mathcal{A}}{\mathcal{A} + F_{AE,max}} \quad (5.9)$$

$$(1 - \kappa_v) \cdot D_{PDE,max} = \frac{\mathcal{A} + F_{AE,max}}{\mathcal{B}} \ . \quad (5.10)$$

Here, the possible internal movement at the connection point of the elements introduces an additional degree of freedom, which has not been considered in Hill-type muscle models so far, except (Günther and Schmitt, 2010). This degree of freedom is represented by κ_v, the gearing ratio (Equation (5.3)). Isotonic quick release experiments, which are usually performed with biological muscles, are designed to eliminate the contribution of the serial elasticity. Therefore, it can be assumed that the SE is at constant length ($\dot{l}_{SE} = 0$) in the experiment and hence, $\kappa_v = 0$.

With this assumption, the damper parameters can be determined. For this study, experimental data of a rat gastrocnemius muscle were used: $F_{AE,max} = 13.39\,\text{N}$ and the Hill

constants are $\mathcal{A} = 2.68\,\mathrm{N}$ and $\mathcal{B} = 4.16 \times 10^{-2}\,\mathrm{ms^{-1}}$ (van Zandwijk et al., 1996, Animal 1). The resulting parameters are

$$
\begin{aligned}
R_{PDE} &= 0.17 \\
D_{PDE,max} &= 386.4\,\mathrm{Nsm^{-1}} \ .
\end{aligned}
$$

5.2.3 Numerical model

As in Section 4.2.2, the numerical model of the CE can be expressed by two coupled differential equations. The first describes the internal degree of freedom (according to Equation (4.6)), the second the external degree of freedom. For the external movement (coordinate y_2 representing l_{CE}) two possible scenarios are considered: (a) An isotonic contraction against a constant external force $F_{ext} = $ const. Here, F_{ext} determines the length of the SE via $F_{ext} = F_{SE} = -k_{SE}(l_{SE} - l_{SE,0})$. Hence, $l_{SE} = $ const and therefore

$$
\dot{y}_2 = \dot{y}_1 \ . \tag{5.11}
$$

(b) A contraction against an inertial mass m at the end of the contractile element (y_2) as described by Equation (4.7).

The serial element is modeled as a linear spring (Equation (4.4)) with a stiffness $k_{SE} = 2401\,\mathrm{Nm^{-1}}$ (in accordance to the mechanical setup).

This set of differential equations was solved with Matlab Simulink embedded ODE45 (Dormand-Prince) solver with absolute and relative tolerance of 1×10^{-7}.

5.2.4 Hardware model

The setup was similar to the one described in Section 4.2.4. The only differences were that both active element AE and parallel damping element PDE were implemented with one electric motor (Figure 5.1, compare to Figure 4.2). Also the new isotonic experimental condition was realized with another motor attached to the end of the spring to exert the force $F_{ext} = F_{CE}$.

5.2.5 Experimental protocol

To investigate the force-velocity characteristics of the contractile element two experiments were performed. For both experiments, the AE activity was set to $q_{AE} = 1$ (maximum activity) and the CE length was fixed with the electromagnet in the beginning. This resulted in an AE/PDE contraction and a SE expansion until $F_{CE} = F_{AE,max}$. After this initial isometric contraction at $t_{QR} = 3\,\mathrm{s}$, the electromagnet was released. Then the whole CE started to contract and the two external conditions resulted in the two different experiments: **Isotonic quick release contraction** experiments (QR_F): Here, the CE contracted against a constant external force F_{ext}. External forces between $0.2\,\mathrm{N} < F_{CE} < F_{AE,max}$ were applied in 19 steps. Each force condition was repeated ten times. The contraction velocity was evaluated $0.5\,\mathrm{s}$ after the release. For the **quick release contraction against an inertial mass** m (QR_m) the weight was released and CE contraction velocity and force were recorded as described in Section 4.2.5. Here, the force-velocity relation was extracted from the recorded data at the peak contraction velocity v_{max}.
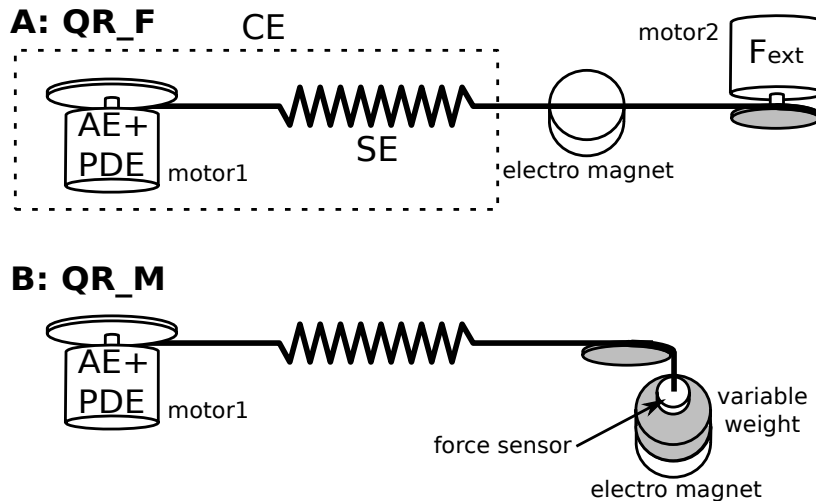
Figure 5.1: Hardware design. Active element AE and parallel damping element PDE forces were generated by an electric motor (Maxon ECmax40) as hardware in the loop. The serial element SE was implemented as a mechanical spring. An electro magnet was used to fix the contractile element length in the isometric part of the quick release contractions. A: For the isotonic experiments (QR_F), a second motor was used to generate a defined external force F_{ext}. B: for the experiments against an inertial mass m (QR_M) a variable weight was used as load. The force sensor measured the contractile element force F_{CE}.

5.3 Results

5.3.1 Isotonic quick release experiments

Isotonic quick-release experiments against a constant force (QR_F) revealed a hyperbolic force-velocity relation for the numerical model and the hardware implementation (Figure 5.2). The numerical force-velocity relation was identical to the analytical prediction and to the fit of the biological muscle data (van Zandwijk et al., 1996) from which the model parameters were derived. This force-velocity relation is also shown in all other figures for reference (theory/biology, red line). The force-velocity data of the hardware implementation (green x) shows a slight deviation towards lower velocities and lower forces. Fitting Equation (5.5) to the data (with $\kappa_v = 0$) results in parameter estimates of $D_{PDE,\text{max,fit}} = 474 \, \text{Ns}^{-1}$ and $R_{PDE,\text{fit}} = 0.15$ (quality of fit: $R^2 = 0.96$), compared to the nominal values $D_{PDE,max} = 386 \, \text{Nsm}^{-1}$ and $R_{PDE} = 0.17$ preset from theory (Section 5.2.2).

5.3.2 Quick release experiments against an inertial mass

Quick-release contractions against an inertial mass (QR_m) resulted in a different force-velocity relation with substantially higher contraction velocities (Figures 5.3) compared to the isotonic quick-release contractions (Figure 5.2). A hyperbolic fit ($R^2 = 0.80$) to the experimental data (green line) gives parameter estimates of $D_{PDE,max,fit} = 162 \, \text{Nsm}^{-1}$ and $R_{PDE,fit} = 0.14$, although the nominal damper parameters were kept identical to the QR_F experiments.

The experimental force vs. velocity trajectories show additional oscillations (Figure 5.5),
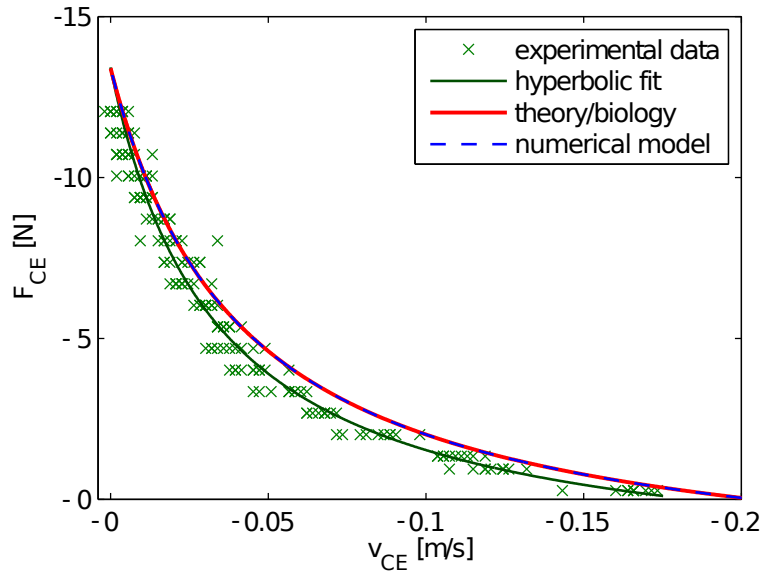
Figure 5.2: Force-velocity relation determined in isotonic quick release experiments (QR_F). The numerical simulation (blue dashed line) resulted in a force-velocity relation identical to the theoretical prediction of the analytical model (red solid line). A fit (green solid line, quality of the fit: $R^2 = 0.96$) to the experimental data (green x) revealed a hyperbolic force-velocity relation also for the hardware model. The deviation between the theoretical prediction of the analytical model and the fit of the experimental data was probably the result of additional internal friction (motors, bearings), which caused a reduction in the contraction velocities and active element forces.

which are not present in the simulation (Figure 5.4). These oscillations originate from additional masses and elasticities introduced by force/position sensor and steel wire connections respectively. The peculiar step in the experimental force-velocity relation (Figure 5.3) is a result of these additional oscillations. As Figure 5.5 shows, there are two prominent maxima in the velocity. For increasing masses, at one point the second maximum becomes the absolute maximum which corresponds to a lower force and therefore results in the step in the force-velocity relation.

5.4 Discussion

In a bionic approach, the function and structure of muscle in quick release experiments were investigated. A new macroscopic model was presented that analytically predicts the hyperbolic force-velocity relation known to characterize the contraction dynamics of active fibers and their assemblies in biological muscles. It was the goal of this study to understand the relationship between the macroscopic model structure and its dynamic role in the contraction. To that end, two types of quick release contraction experiments were performed with a numerical model and a hardware implementation. Both, the numerical model and the hardware implementation confirmed the analytical model. The discrepancies found in Chapter 4 could be resolved.

These results prove that the origin of the hyperbolic force-velocity relation can be me-
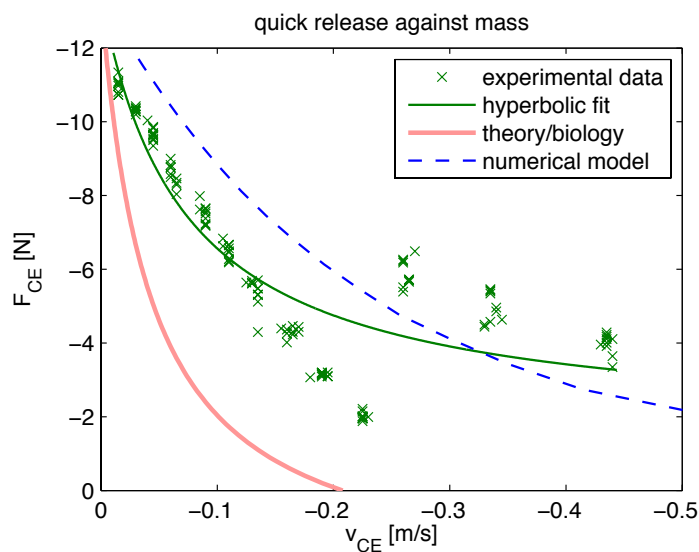
Figure 5.3: Quick release experiments against an inertial mass (QR_m). The force-velocity relation was determined by finding the time index with highest contraction velocity v_{max} and by extracting velocity and force at this time index for each experiment. These data points plotted (and connected, or fitted) represent the force-velocity relation $F_{CE}(v_{max})$ (see also Figure 5.4). The numerical simulation (blue dashed line) resulted in a force-velocity relation with substantially higher velocities than in the isotonic (QR_F) simulations. The experimental data (green x) and a hyperbolic fit (green solid line, quality of the fit: $R^2 = 0.80$) for the hardware model showed a similar trend to higher velocities. The theoretical prediction of the analytical model for $\kappa_v = 0$ isotonic experiments (red line) is drawn for reference.

chanically explained on a macroscopic level by the arrangement of the three mechanical elements active element AE, parallel damper element PDE and serial element SE (Günther and Schmitt, 2010). If the contractile element is considered to be the active engine of the muscle, the analytical model predicts its operating points and the numerical model presents differential equations to predict the dynamic force generation of the contractile element. In contrast to microscopic muscle models, where the hyperbolic force-velocity relation is explained in terms of cross-bridge state and related transition rates and chemical rates (see microscopic muscle models in Section 1.3), it is here explained in terms of fundamental macroscopic mechanical properties. Still, it remains open where in detail the microscopic origin of the mechanical properties are located. Nevertheless, in distinction to other macroscopic Hill-type muscle models, the force-velocity relation is not implemented as an empirical function $F(v)$ (e.g., Hill, 1938; Ettema and Huijing, 1988; van Soest and Bobbert, 1993; Günther et al., 2007) but rather is the dynamical result of the interaction of mechanical elements. Therefore, this model can be seen as a macroscopic muscle model derived from first-order mechanical principles.

From our point of view, the advantages of the model are: (a) It is possible to investigate the contribution of the mechanical muscle characteristics, represent AE, PDE, and SE, to the overall contraction dynamics. (b) The force-velocity operating points can be predicted analytically for different contraction modes. (c) Biological experiments can be interpreted within the framework of the model. (d) As the model is based on mechanical elements,
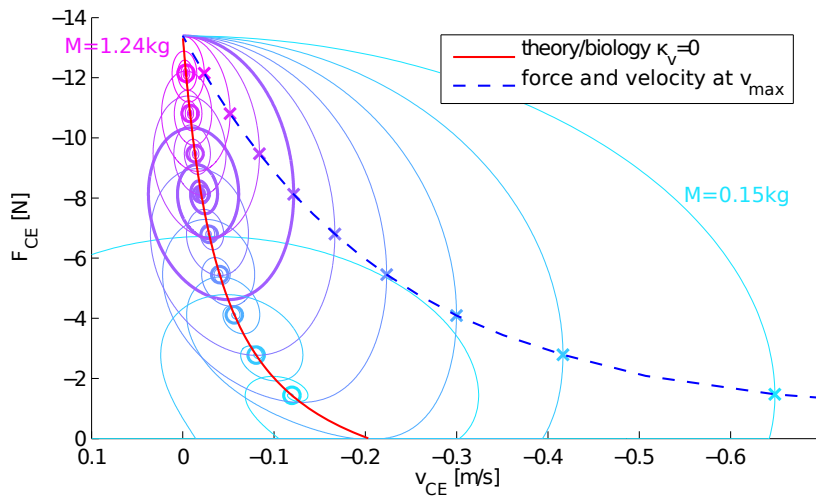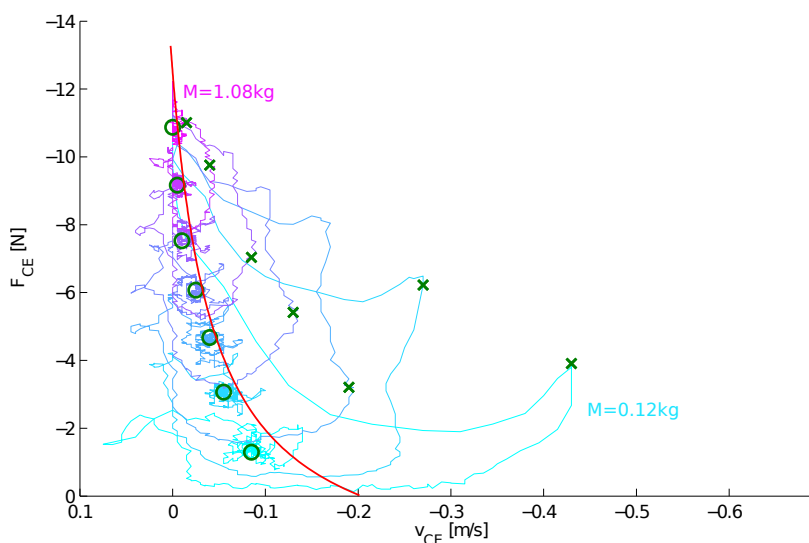
Figure 5.4: Simulated time course of the force-velocity relation in quick release experiments against an inertial mass (QR_m). The color of the line indicates the mass (small mass: light blue, heavy mass: pink). Every experiment starts at $v_{CE} = \dot{l}_{CE} = 0$ and $F_{CE} = F_{AE,max} = 13.39\,\mathrm{N}$ (upper left corner). From there, the contraction velocity increases up to a maximum v_{max} marked with an **X**. Connecting these maxima gives the force-velocity relation determined in QR_m experiments (blue dashed line). The long time convergence points of the force-velocity trajectories are marked with **O**s. These convergence points lie on the force-velocity relation determined by isotonic simulations (QR_F, red line).

it could serve as a template for the construction of bionic artificial muscles with biological contraction dynamics.

5.4.1 Predictions between the extreme experimental conditions

In biological muscle experiments very specific contraction conditions are generated. Isotonic quick release experiments are designed to eliminate the contribution of the serial elasticities to the overall muscle contraction ($\dot{l}_{SEE} = 0$) and thus, allowing to determine the force-velocity characteristics of the contractile element (e.g., Jewell and Wilkie, 1958; Cavagna and Citterio, 1974; Ettema and Huijing, 1988; van Zandwijk et al., 1996). These conditions are consistent with a gearing ratio of $\kappa_v = 0$ (Equation (5.3)). The force-velocity data determined under these conditions are then fitted with the hyperbolic Hill-equation (Equation (5.6)) to determine the parameters $\mathcal{A}$ and $\mathcal{B}$ (Hill, 1938). In order to derive the values of the parameters R_{PDE} and $D_{PDE,max}$ for our model from such a parameter set, an assumption about κ_v has to be made (see Equations. (5.9) and (5.10)). Here $\kappa_v = 0$ was the logical choice as it corresponds to the original biological experiment. These parameters were then used in the numerical model and the hardware experiment. Performing isotonic quick release simulations and experiments and thus, reproducing the $\kappa_v = 0$ condition, resulted in the exact reproduction of the theoretical force-velocity relation (Figure 5.2).

The quick release experiments against an inertial mass (Wilkie, 1949; Günther et al., 2007) on the other hand generated contractions with $\kappa_v \neq 0$. As expected, the force-velocity operating points in this case did not lie on the original force-velocity relation (Figure 5.3). At the peak contractile element contraction velocity, where the force-velocity data were

Figure 5.5: Experimental time course of the force-velocity relation in quick release experiments against varying inertial masses (QR_m). The color of the line indicates the mass (small mass: light blue, heavy mass: pink). Every experiment starts at $v_{CE} = \dot{l}_{CE} = 0$ and $F_{CE} = F_{AE,max} = 13.39$ N. The absolute maximum in the velocity v_{max} is detected for the force-velocity relation and marked with an **X**. These maxima describe the force-velocity relation determined in QR_m experiments. The long time convergence points of the Force-velocity trajectories are marked with a black **O**s. These convergence points lie close to the force-velocity relation determined by isotonic simulations (QR_F, red line).

extracted (Günther et al., 2007), the contraction was mainly governed by the SE ($\kappa_v > 0.81$). This means that AE and PDE almost stay at constant length for the first part of the QR_m contraction. We compared this to a model with locked AE/PDE length, where only the SE spring accelerated the mass (see also appendix). This extreme case of $\kappa_v = 1$ results in a force-velocity relation very similar to the force-velocity relation of the QR_m experiments (gray line, Figure 5.6).

During the QR_m contractions κ_v changed continuously. In fact, points could be extracted from the QR_m experiments, where κ_v reached certain specific values. Interestingly, all force-velocity operating points corresponding to a specific κ_v lie on a new hyperbola (Figure (5.6)). This hyperbola can be exactly predicted from the theory (Equations. (5.6), (5.7), and (5.8)). The surprising fact is that once the material properties $D_{PDE,max}$ and R_{PDE} are defined, the additional free parameter κ_v predicts every force-velocity operating point of the muscle, independent of the experiment.

Therefore, the two quick release experiments QR_F and QR_m can be seen as two extreme cases. In the QR_F experiments the SE does not contribute to the contraction, while in the QR_m it mainly determines the contraction. For normal biological movements, κ_v will lie in between ($0 < \kappa_v < 1$). The theory, the numeric model and the hardware implementation presented here, predict and reproduce the force-velocity operating points for all these situations.

The isotonic experiments show that the specific damper characteristic chosen would provide already a hyperbolic force-velocity relationship without any serial element as it does not
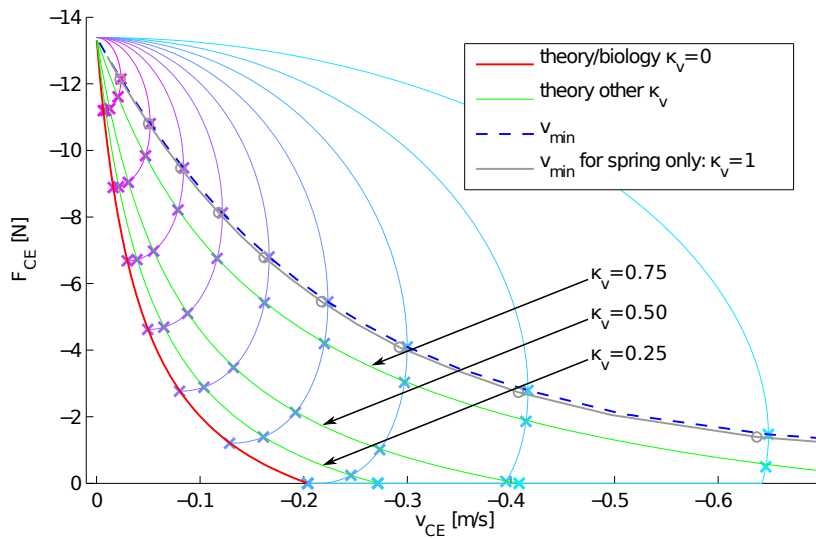
Figure 5.6: During the time course of the contraction in quick release experiments against an inertial mass (QR_m), the internal gearing ratio κ_v changes continuously. From the simulation data, points were extracted where κ_v reached a certain value (marked with **X**s). The theoretical prediction of the hyperbolic force-velocity relation on the other hand depends on the parameter κ_v. Plotting the theoretical predictions for the chosen κ_v values (green lines for $\kappa_v = 0.25$, $\kappa_v = 0.5$ and $\kappa_v = 0.75$) shows that these operating points all correspond to one specific hyperbolic force-velocity relation (intersections of green lines with time traces of the experiment, marked with **X**'s). The extreme case where all contraction happens in the serial element SE ($\kappa_v = 1$) cannot be described by Equation (5.6), as $B \to \infty$ for $\kappa_v \to 1$. But this condition can be described by the isolated contraction dynamics of the spring mass system (SE with external mass). The derivation is explained in the appendix and the results are plotted here (gray line).

contribute to the contraction ($\kappa_v = 0$). Therefore, our model implies on a mathematical level to "switch off the SE". Yet going beyond, our model also demonstrates that this property is inherited by any contractile element structure in which a further arbitrary force bearing element is plugged in serially, which adds an internal degree of freedom to the contractile element structure. By mechanical design, the contractile element structure, thus, gains a manifold of similar force-velocity relations. This also adds function to the structure, namely the potential to profit from the benefits of the force-velocity relation (stabilizing effects Chapter 2 and reduced control effort Chapter 3) during changing loading situations in the real world. Also, mechanical efficiency can be optimized across the whole range of loading situations (Günther and Schmitt, 2010). For this, serial elasticity seems to be particularly beneficial. Our hardware prototype has demonstrated the real world functionality of such a specific implementation of the theoretical structure.

5.4.2 Interpreting biological experiments: muscle structure and κ_v

Both in our technical prototype and our theoretical model, the internal degree of freedom represented by the parameter κ_v can distinguish between different loading modes, e.g., the extremes of an isotonic contraction or a quick-release contraction against an inertial load. Moreover, both approaches can deal with any in-between contraction as a cyclic work-loop,

a stretch-shortening cycle, and an isovelocity or even an isometric contraction during a rise in activity. But do our theoretical model or our technical prototype really map physiological processes in the biological muscle during all these contraction modes?

On the one hand, from a theoretical point of view, we would expect at least slight differences in the results of isotonic and isovelocity experiments, even in a biological muscle. This is because the contraction velocity should immediately change, per definition, during an isotonic contraction. Consequently, the muscle examined is supposed to go through some finite length changes, even though they may be small. Therefore and also keeping muscle's well-known history effects in mind (Abbott and Aubert, 1952; Rode et al., 2009a) when comparing both experimental conditions, the muscle is also supposed to go through a manifold of different states around the operating points examined. This should be reflected by slight differences in force-velocity or velocity-force, respectively, and force- or velocity-enthalpy relations, respectively.

On the other hand, when comparing our theoretical model calculations to enthalpy data of biological muscle, the model predicts a specific parameter value $\kappa_v = 0.85$ for the internal distribution of contraction velocities (Schmitt et al., 2012). This very value is, however, not what would be expected in a real muscle assuming that the model SE represents just serial elastic properties of active muscle fibers. Since pure elastic structures would not change their length during a finite isotonic contraction, meaning $\kappa_v = 0$ (stationary SE length). Although the biological muscle data used for validation had been determined in the isovelocity rather than in the isotonic condition we would yet not expect such a discrepancy when comparing measurements from both conditions in the same muscle. Thus, answering the first part of the above question, our model needs further development.

Any elastic structure is slightly damped in reality. This is e.g. a necessity to suppress load-muscle eigenoscillations (Günther et al., 2007). If, as a consequence of this damping, the SE was rather visco-elastic than purely elastic, better predictions of enthalpy production would be expected. Additionally, such a serial arrangement of dampers would automatically lead to history effects within the contractile element (active muscle). Furthermore, we would like to annotate that this would also mean that an often used assumption should be reconsidered: if there is some damping in any serial element then the isotonic condition does not guarantee that the SE is at constant length during isotonic quick-release experiments, i.e. $\kappa_v > 0$. As a consequence, the measured force-velocity properties can not directly be related to the hypothesized AE in series. Rather, the isotonic measurements would reflect the entangled properties of the whole arrangement including the visco-elasticity of the SE itself, both when asking for the force-velocity characteristics and the heat production. In terms of our model, one would measure a hyperbolic force-velocity relation rather corresponding to one of the green curves in Figure 5.6 than the desired red curve.

Answering the second part of the above question, our current technical prototype was designed to incorporate as little serial damping as possible, using an off-the-shelf spring as SE. However, neither have the damping characteristics of such a real spring been examined so far, although our measured data point to some additional damping in the prototype (Schmitt et al., 2012). Nor is clear as of today whether the built-in damping may suffice to represent potential serial damping of a real muscle. As presented, the latter should be predicted from an improved theoretical model to be validated with measured enthalpy data of biological muscles.

5.4.3 Model assumptions and extendability

This theory focuses on the mechanical origin of the force-velocity relation. Other important features of the muscle contraction dynamics, such as the force-length relation (van Ingen Schenau et al., 1988; Bobbert et al., 1990; Durfee and Palmer, 1994; Zuurbier et al., 1995; Rassier et al., 1999; Rode et al., 2009b), force enhancement and contraction history effects (Forcinito et al., 1998; Meijer et al., 1998; Herzog and Leonard, 2002; Herzog, 2004; Rode et al., 2009a), activation dynamics (e.g., Zajac, 1989), etc. are neglected. However, we expect that including these characteristics in a similar way as it has been done previously in Hill-type models, would enhance the model without principally altering the force-velocity characteristics presented here. The AE force (Equation (5.4)) for example may depend on AE or contractile element length. Here we basically only consider the state in which the contractile element operates at its optimal length. AE force could also depend on muscle activity and the chemical state of the muscle, i.e. the relative number of actively force-producing cross-bridges quantified by the normalized muscle activity $0 \leq q_{\mathrm{AE}} \leq 1$.

The hardware experiment represented AE and PDE combined by a software controlled motor exerting a calculated force on the SE. With respect to a more adequate mechanical representation, we already separated AE and PDE in Chapter 4 by using one separate motor for each element. This made no difference for the QR_m experiments investigated there. In a next step, a real mechanical implementation of the PDE e.g. by a magneto-rheological damper (Garcia et al., 2011), would be desirable. Also the AE could in principle be any other fore generating device/material. Nevertheless, the hardware representation of AE and PDE in this chapter is the simplest possible physical implementation. In the bionic context this step is necessary to verify the real world functionality of the concept (Nachtigall, 2002).

5.4.4 Advantages of biological muscle system design

As stated in the beginning of this thesis, the transfer of the beneficial properties from biological to technical systems it is necessary to (a) determine the characteristics uniquely identifying the biological muscle and (b) evaluate the system design criteria with quantitative and comparable measures.

In the light of our findings we can contribute to (a): at least three basic mechanical characteristics of a biological muscle are necessary to exhibit muscle-like contraction dynamics: (i) a serial structure, with an active part in series to at least one visco-elastic part; (ii) a serial structure in which each part contains some low damping; (iii) a structural assembly including one force-dependent damping part, no matter in which branch of the serial structure. A first simple solution of a bio-inspired functional artificial muscle based on these characteristics was described in (Schmitt et al., 2012). In this context, our model can be seen as a design template for functional artificial muscles.

For (b) see Chapters 2 and 3.

5.4.5 Force- and load-velocity relations of a spring-mass system during quick-release

In this chapter it was shown that an elastic element significantly contributes to the contraction in quick release experiments against an inertial load. To shed some more light on this, we demonstrate in this section that a system of a pre-loaded linear spring which accelerates an inertial mass m during a quick-release situation exhibits a non-linear, hyperbolic-like load-velocity relation. This is basically the extreme case, where $\dot{l}_{AE} = 0$ at all times.

The "load" may be either just the mass m or the weight $m \cdot g$ in case the mass is also exposed to gravity. Let k symbolize the spring stiffness, and y_s the rest length of the spring at which its force

$$F_s = -k\left(y - y_s\right) = -k\,\Delta y \tag{5.12}$$

is zero. There are three contributions to the energy E of the system:

$$E_s(t) \;=\; \frac{1}{2}\,k\,\Delta y^2(t) \tag{5.13}$$

$$E_g(t) \;=\; -m\,g\,\Delta y(t) \tag{5.14}$$

$$E_v(t) \;=\; \frac{1}{2}\,m\,v^2(t)\;, \tag{5.15}$$

where E_s denotes the potential energy stored in the spring, E_g the potential energy of the mass due to gravity, and E_v its kinetic energy when moving with velocity $v = \frac{dy(t)}{dt} = \frac{d\Delta y(t)}{dt}$. The energy of the system characterized by the equation of motion

$$m\,\frac{d^2 y(t)}{dt^2} = m\,\frac{d^2 \Delta y(t)}{dt^2} = F_s(t) + m\,g = -k\,\Delta y(t) + m\,g \tag{5.16}$$

is conserved:

$$E = E_s + E_G + E_v = E_0 = \frac{1}{2}\,k\,\Delta y_0^2 - m\,g\,\Delta y_0 + \frac{1}{2}\,m\,v_0^2\;. \tag{5.17}$$

We identify the initial value of a variable (at $t = 0$) by the index "0". For reasons of conciseness and further on, we omit the symbol "(t)" for the time-dependency of the variables Δy and v (thus, F_s, E_s, E_g, E_v). Now, when substituting the spring force F_s from Equation (5.12) into the terms E_s and E_g on left hand side of Equation (5.17) we find that the latter constitutes the instantaneous non-linear (spring) force-velocity relation

$$F_s^2 + 2\,m\,g\,F_s + k\,m\,v^2 - 2\,k\,E_0 = 0 \tag{5.18}$$

which can be solved for, e.g., the force

$$F_s = -m\,g \pm \sqrt{\left(m\,g\right)^2 + 2\,k\,E_0 - k\,v^2}\;. \tag{5.19}$$

The mass reaches its maximum velocity v_{max} during spring contraction when the spring force F_s just compensates weight force $m\,g$. In this condition, the square root term must vanish that is, we find

$$v_{max}(m, y, v_0) = -\frac{1}{\sqrt{k\,m}}\,\sqrt{\left(m\,g\right)^2 + 2\,k\,E_0}\;. \tag{5.20}$$

In analogy to the force-velocity relation of a contractile element, which represents the velocity response of a contractile element to a given external force (or vice versa), Equation (5.20) is the load-velocity relation characterizing the velocity response of the spring-mass system when the load (m or $m\,g$) is varied. Due to the square root in the denominator the course of this load-velocity relation resembles a hyperbola which has an intersection with the load axis ($v_{max} = 0$). However and in contrast to a contractile element force-velocity relation, v_{max} becomes infinite for a vanishing load, i.e., the load-velocity relation just aligns asymptotically with the velocity axis, a corresponding global $v_{max,m=0}$ does not occur.

Usually, the mass is at rest in the instant of release ($v_0 = 0$). In that case, the energy content $E = E_0$ of the system (Equation (5.17)) can be written as

$$E_0 \;\; = \;\; \frac{1}{2}\,k\,\Delta y_0^2 - m\,g\,\Delta y_0 \tag{5.21}$$

$$= \;\; \frac{1}{k}\left(\frac{1}{2}\,F_{s,0}^2 - m\,g\,F_{s,0}\right)\;, \tag{5.22}$$

where we have substituted the initial force $F_{s,0} = -k\,\Delta y_0$ (maximum force during spring contraction) to get the latter notation. Then, the maximum velocity reached during contraction (Equation (5.20)) is simply

$$v_{max}(m, y_0) = -\frac{F_{s,0} - m\,g}{\sqrt{k\,m}}\;. \tag{5.23}$$

6

Energy management that generates terrain following versus apex preserving hopping in man and machine

In the hopping simulations of Chapters 2 and 3 the leg force of the hopping model (Equation (1.1)) was generated by a muscle model. The nonlinearities of the muscle properties (Equation (2.2)) and the excitation contraction coupling (Equation (1.5)) prohibit an analytical prediction of the energy flow in the system. In this Chapter, the leg force is modeled as a linear spring-damper system, allowing for an investigation of the energy dissipation and supply in stable hopping. This Chapter is a summary of an article published in Biological Cybernetics, 106(1), 2012.

Introduction:
Walking, running, and hopping are human locomotor activities, where the legs periodically hit the ground and push off from it. Until now, it is only incompletely understood as to how these movements are generated physiologically. Even if confining the view solely to the vertical component of these movements, i.e. to hopping, a salient and resilient neurobiological concept that explains hopping is not in sight.

Theoretically, the simplest hopper would be an undamped spring–mass arrangement. On landing, the spring slows down the body's mass and stores its kinetic energy as potential energy, and uses the stored energy for the body's subsequent push off. The spring-loaded inverted pendulum (SLIP) (Blickhan, 1989) is an often-cited example of such a concept.

A handicap of the SLIP is that it models an energetically conservative system, which loses no energy and, therefore, needs no energy replenishment. Real world organisms and machines, however, are inevitably subject to energy dissipation. Hence, SLIP-type modeling is appropriate for simulations; but unless adding practicable energy replenishments, it can neither provide blueprints for a hardware built to check the results of the simulations, nor concepts explaining an organism's locomotion under real world conditions.

To get more insight into the physics of hopping, we outlined two concepts of energy management: "constant energy supply", by which in each bounce – regardless of perturbations – the same amount of mechanical energy is injected, and "lost energy supply", by which the mechanical energy that is going to be dissipated in the current cycle is assessed and replenished.

Two possible hopping styles could be the result of such energy management: "terrain
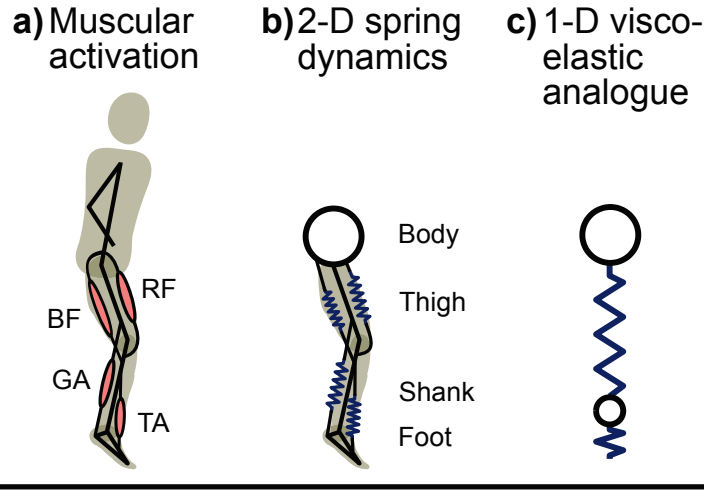
Figure 6.1: Leg representations in hopping. **a)** Three-segmented leg with selected muscles (Rectus Femoris (RF), Biceps Femoris (BF), Tibialis Anterior (TA), and Gastrocnemius (GA)) actuating the hip, knee and ankle joint. **b)** Damped springs instead of muscles make the leg a compliant segmented limb. **c)** One-dimensional arrangement that represents the compliant function of the leg in the vertical direction. The upper spring reflects the compliance accomplished by combining thigh and shank (in the following called "shank"), the lower part the compliance given through the foot. This model is confined to vertical motion.

following" means that the subjects pursued to keep the distance between maximum hopping height (apex) and ground profile constant; "apex-preserving" hopping means that the absolute maximal hopping height is kept constant regardless of changes of the ground level.

The purpose of this study was (i) to get a hint, which one of the hopping styles, apex-preserving hopping or terrain-following hopping, is prevalent in human bouncing, (ii) to propose concepts of energy management that can generate these hopping styles, (iii) to check whether these concepts succeed in a real machine, and (iv) to examine, which concept has the greatest chance to govern also human bouncing.

Methods and Results:
In this study, we followed the test trilogy (Section 1.6).

For the **simulation test**, a cascaded damped spring-mass model (Figure 6.1c) was used. This model offers defined physical structures which allows one to determine their energetic contributions to hopping. In this way, the decrement/increment of the system's mechanical energy E can be determined:

$$E(t+\Delta t)-E(t) = - \int\limits_{t}^{t+\Delta t} \left[b_1 \dot{l}_1^2 + b_2 \dot{l}_2^2 + c_1 \mathrm{sign}(\dot{l}_1)\dot{l}_1 + c_2 \mathrm{sign}(\dot{l}_2)\dot{l}_2 \right] dt + \int\limits_{t}^{t+\Delta t} \left[f_1 \dot{l}_1 + f_2 \dot{l}_2 \right] dt \ ,$$

where l_i are the segment lengths, $\dot{l}_i$ the respective shortening velocities, b_i and c_i are the coefficients of damping and friction, and f_i amendatory forces added from within the subsystems during stance, for example by suitably changing the parameters of the springs, or by extra actuators associated with the springs.
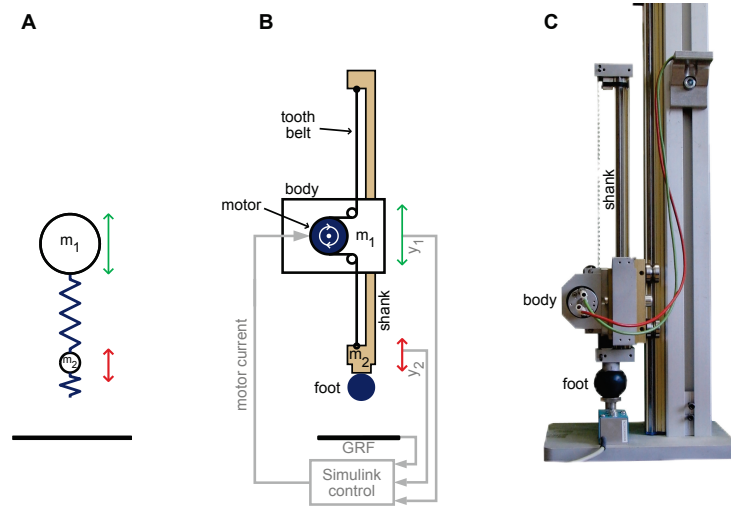
Figure 6.2: The cascaded damped spring-mass model **a)** is the template for the MARCO hopper robot, the home position of which is shown in **c)**, and its functional scheme in **b)**.

Energy supply was managed by manipulating the spring stiffness of the upper segment

$$\Delta k = \frac{6 \cdot \Delta W}{(l_0 - l_{\min})^3} \cdot (l - l_{\min}) \ ,$$

where $l_{\min}$ is the minimal spring length in the stance phase, and l_0 the respective rest length. If the supplied energy ΔW is the same in each cycle, we have "constant energy supply", if it is adjusted to replenish the dissipated energy, we have "lost energy supply".

Simulated hopping with constant energy supply resulted in stable and robust terrain following hopping, while lost energy supply resulted in apex preserving hopping (Figure 6.3b and c).

The **hardware test** was conducted with the MARCO hopper robot (Figure 6.2). Here, constant energy supply also resulted in stable and robust terrain following hopping, while lost energy supply resulted in unstable hopping behavior (Figure 6.3d).

For the **behavior comparison test**, experiments with 12 subjects were conducted. While hopping, the subjects experienced a sudden step down of 5 or 10cm. The resulting hopping pattern resembles terrain following hopping (Figure 6.3a).

Conclusions:
As can be concluded from the behavioral comparison test, human hopping is —under the conditions of the experiment presented— close to terrain following hopping. This suggests that the human hopper adopts constant energy supply to automatically adapt to varying heights of the floor.

If always the same portion of energy is supplied per cycle, the steady state is reached when the losses just come up with that supply. The injection of a predetermined amount of energy ΔW into a spring requires only measurements derivable from length and stretch sensors attached to the spring (called proprioceptors in a biological context).

Such a manner of control as outlined above we call exploitive actuation, which usually gets along with a minimum of computational effort. Please notice, exploitive actuation is not a
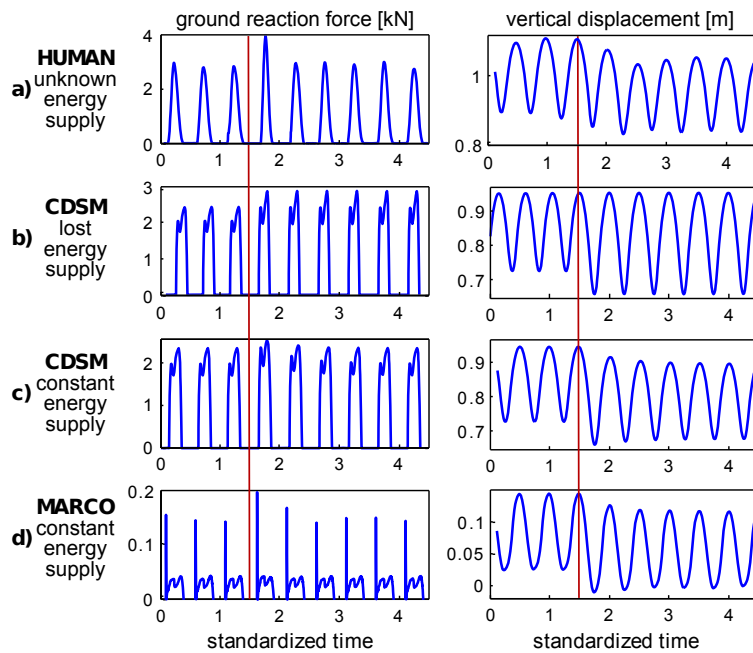
Figure 6.3: Ground reaction force and vertical movement generated by a typical human hopper **a)**, by the cascaded damped spring mass model (CDSM) under lost **b)** and constant energy supply **c)**, by the MARCO hopper robot applying constant energy supply **d)**. The CDSM models **b)**, **c)** are furnished with human parameters. Time is standardized with respect to the length of the hopping cycles. The vertical dashed line indicates the point of time where the floor undergoes a sudden lowering. Vertical movements refer to the y-coordinate of the "body" in the CDSM model and in the MARCO Hopper, and of the center of mass (CoM) in the human hopper. Note that the MARCO hopper's needle shaped peak ground reaction forces at touch down (see **d)**) are caused by the large damping parameter of the adiPRENE® ball taken as foot. Those peaks occur also in the simulated ground reaction forces when the MARCO hopper's parameters are inserted into the CDSM model (respective trajectories are not shown).

control mechanism in the classical sense. For instance, the here proposed solution neither prescribes the hopping height nor provides a machinery to actively enforce a given hopping height. The apex rather emerges dynamically from the conditions around and in the hopper.

Refinements of modeling and further behavioral comparison tests in the framework of the test trilogy are necessary to get a sustainable answer to the question, how intrinsic muscular properties can provide an energy management that physically realizes robustness in human hopping.

7 Conclusions and Remarks

Two major goals are the basis for this thesis. Firstly, to understand which role biological structures play in movement control, and secondly, to derive design concepts allowing a transfer of these findings into technical systems. The presented studies show that dynamic properties of the biological muscle, e.g., the force-velocity relation, contribute to the stability of periodic movements, reduce control effort, are the result of the dynamic interaction of simple mechanical elements, and can be transferred to technical systems.

In more detail, the contribution to these goals is as follows: Chapter 2 investigates different simple control strategies for hopping. This chapter builds upon previous results (Haeufle et al., 2010a), emphasizing the importance of the force-velocity relation for the control of periodic movements. The results show that actuation with an intrinsic force-velocity relation stabilizes hopping with a variety of different simple control approaches. With a biology-like hyperbolic force-velocity relation the resulting hopping patterns are very little influenced by the control method. This implies that the muscle properties dominate the hopping characteristics, at least with respect to stability. Apart from the stabilizing advantage, these results suggest that muscles allow reduced control effort.

Chapter 3 presents a new method to quantify the control effort based on information theory. It basically measures control effort as how detailed the sensory information has to be in order to succeed in movement control. The less neural information processing is required, the less the control effort. This method reveals that the control effort is reduced when generating hopping with a muscle-like actuator incorporating a hyperbolic force-velocity relation. The comparison is made against a DC-motor model with a traditional kinematic PD-control approach. The strength of this new approach is that it can be applied to such different actuation systems.

With the knowledge about the importance of the force-velocity relation, in Chapters 4 and 5 the mechanical origin of this property is investigated. A model, based on Günther and Schmitt (2010) and Haeufle et al. (2012b), is derived, which explains the hyperbolic force-velocity relation originating from the dynamic interaction of three simple mechanical elements. In Chapter 4 the possibility to recreate this mechanical property in a technical system is explored. The numerical results are reproduced by a hardware model as a proof of concept. However, both are only qualitatively similar to the original theoretical model. In Chapter 5, the model and the experimental setup are modified. The quantitative deviation

in the previous chapter is resolved. The difference can be attributed to kinetic energy in the interaction of the elastic element with the external load in the quick release experiments. As the theoretical, the numerical, and the hardware model now predict the same force-velocity relations, the model can bee seen as a design concept for an artificial muscle.

The importance of the hardware test: computer simulation and hardware verification is a powerful combination to test theories of movement generation and control (Section 1.6). In the presented studies the hardware experiments brought important insights which did not become evident in the theory or simulation before:

(1) in the first published version of the mechanical contractile element concept (Günther and Schmitt, 2010) the active element force depended on the contraction velocity of the serial element

$$F_{AE} = F_{CE,0} + d_{PDE}(F_{CE,0}) \cdot \dot{l}_{SE} \ .$$

In the process of implementing the active element in hardware, it seemed more appropriate to describe $F_{AE} = F_{CE,0}$ (current isometric force) as a parameter to be held constant in quick-release experiments. The theory was revised accordingly (Section 5.2.1) and still resulted in a hyperbolic force-velocity relation. However, it describes the active element simpler and more adequate for technical implementation. For the final evaluation whether this model is more realistic than the previous model, other criteria have to be taken into account, e.g., the enthalpy rate and efficiency (see Figures 7.1 and Schmitt et al. (2012)).

(2) For the experimental derivation of the force-velocity relation in quick release experiments, it is generally assumed that after quick release a constant external force is applied to the muscle. This was sometimes done using controlled actuators exerting the force (e.g., Woittiez et al., 1987; Farahat and Herr, 2005) or with a mass in gravity (Wilkie, 1949; Günther et al., 2007), and sometimes transmitting the force through a lever arm (Hill, 1938; McMahon, 1984). As discussed in Chapter 5, the interaction of the muscle's serial elasticity with the inertial load (oscillator) also contributes to the measured velocities and thus to the measured force-velocity relation. This important contribution of the kinetic energy in the external load has to be considered.

(3) Only the hardware test revealed, which type of energy supply in hopping can be realized in a technical system (Chapter 6 and Kalveram et al., 2012).

Furthermore, this approach can be used to iteratively identify essential properties of a system. For example, the mechanical model of the contractile element can only reproduce the force-velocity relation in concentric steady-state contractions so far. The biologically observed force saturation in eccentric contractions cannot be explained by our model. Furthermore, the force-length relation, force-depression, and force-enhancement are currently not explained by the model. Hence, it does not explain all details of the biological muscle, but the functionally important (see Chapter 2 and Haeufle et al. (2010a)) hyperbolic force-velocity relation.

Finally, it has to be remarked that the test trilogy (Section 1.6) has not been applied to all aspects of this thesis. For the new contractile element model, numerical and hardware test were performed, but the behavioral comparison test was only performed with data from the literature. Additionally, the test trilogy applies better to goal oriented movement control and requires revealing perturbations. Both aspects were not given in the study of the contraction behavior of isolated and fully activated muscles. The test trilogy is more applicable to the studies on hopping (Chapters 2, 3, and 6). The study on hopping summarized in Chapter 6
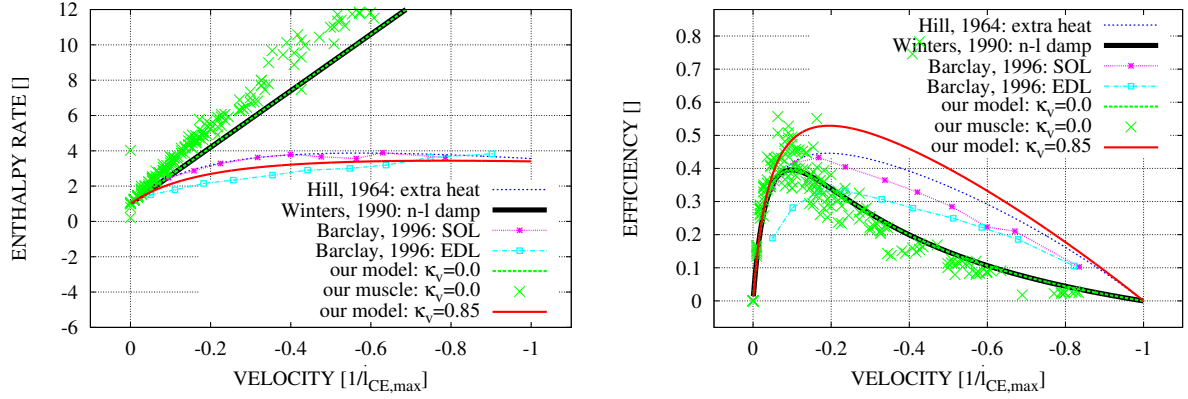
Figure 7.1: Comparison of enthalpy rate and efficiency in contractions between different muscle models and measurements. **A:** Comparison of enthalpy rates $\dot{\mathcal{H}}$ (Equation (1.7)) normalized to the maintenance heat rate $\dot{h}_0$. Experimental data (Barclay, 1996: SOL: M. soleus and EDL: M. extensor digitorum longus) were directly taken from Houdijk et al. (2006) and compared to those predicted by our model, choosing $\kappa_v = 0.85$. Additional data are taken from isotonic experiments of the artificial contractile element and from the model case $\kappa_v = 0.0$ representing exactly Winters' non-linear damper approach (Winters, 1990). Also plotted is data from Hill's refined fit to his measurements (Hill, 1964) (for details about the latter two cases see Günther and Schmitt (2010)). The parameters of our model with $\kappa_v = 0.85$ represent a median piglet muscle (Günther et al., 2007): $F_{AE} = F_{CE,0} = F_{AE,max} = 30\,N$, $R_{PDE} = 0.2$, $D_{PDE,max} = 6667\,Ns/m$. Leaving all other parameter values unchanged, the model case $\kappa_v = 0.0$ implies the same force-velocity relation for a corresponding value $D_{PDE,max} = 1000\,Ns/m$. **B:** Comparison of the respective mechanical efficiencies $\eta_{CE} = -F_{CE} \cdot \dot{l}_{CE}/\dot{\mathcal{H}}$. Note: The heat rate is simply the energy rate dissipated by the damper $\dot{h} = d_{PDE}(F_{CE}) \cdot \dot{l}_{AE}^2$. Maintenance heat rate was assumed to be $\dot{h}_0 = c_{h_0} \cdot F_{CE,0} \cdot \dot{l}_{CE,max}$ (Günther and Schmitt, 2010), with $c_{h_0} = 1/16$ for our specific choice of model parameters. (Figure published in Schmitt et al. (2012)).

consequently follows the test trilogy. In Chapters 2 and 3, however, only the numerical test is discussed. One reason is the reduced complexity of the models.

Reduced model complexity: The simple spring-mass model is able to predict time patterns of the center of mass position (CoM) as well as the ground reaction forces of human and animal hopping, running (Blickhan, 1989), and walking (Geyer et al., 2006). However, it is an energy conservative model incapable of explaining either the biological adaptation to energetic perturbations, or the necessary compensation for inevitable energy losses. More complex forward dynamic models of human locomotion (e.g., Geyer et al., 2003; Günther and Ruder, 2003; van der Krogt et al., 2009; Geyer and Herr, 2010) incorporate leg geometry, muscle-tendon complexes and different control strategies. However, in these models it is difficult to identify the minimal requirements and essential features for locomotion. Hopping models discussed in this thesis fill this gap between the spring-mass model and musculo-skeletal models.

The spring-damper based hopping model (Chapter 6) only adds the complexity of energy management to the spring-mass model. This was done at the level of leg stiffness and viscous energy losses, allowing to quantify the energy lost and supplied in each cycle. From this, fundamental physical insight into the energy management in hopping was gained. The

hopping models studied in Chapters 3 and 2 on the other hand, incorporated intrinsic muscle properties. By stepwise increasing the complexity (constant, linear, non-linear), their role in the control of hopping was studied (see also Haeufle et al., 2010a). The inheritance of the results to more complex models was discussed in detail in Section 2.4.4.

The complexity of the contractile element model (Chapters 4 and 5) is oriented on the complexity of Hill-type muscle models. Usually, the contractile element in Hill-type models is understood only as a black-box element, incorporating the force-length, the force-velocity, and the stimulation-contraction relation (Eq 1.3). Hill's hyperbolic force-velocity relation is described by only three parameters (A, B, F_{max}). Our contractile element requires four parameters, i.e. R_{PDE}, $D_{PDE,max}$, $F_{AE,max}$, and κ_v. Compared to the phenomenological Hill-model, all these parameters have a physical meaning. Furthermore, the gearing ratio κ_V represents an additional degree of freedom, which can be attributed either to the contractile element itself or already to the interaction with the tendon. If the latter is true, our model has the same number of parameters as the Hill-type model. However, it is still open, which attribution is correct.

The relation of such macroscopic muscle models to microscopic muscle models has been discussed from several perspectives in this thesis (Sections 1.3, 1.8 and 5.1). One example may illustrate the relation from a physics point of view: a DC-motor model. One could measure the torque-speed relation, fit a function to the results and use this function as a model. This type of phenomenological black-box model is equivalent to the macroscopic Hill-type muscle models. A detailed study of the electromagnetic forces on the level of atoms and electrons could establish a microscopic model of the principle function. However, it could hardly be used to model a specific DC-motor with all its windings and structural specifics. Most commonly in dynamic simulations, macroscopic models describing the motor by two coupled differential equations (Equation (3.8)) are used. One equation summarizes the electrical current through the windings, and the other one the mechanical position of the rotor. Each parameter in such a macroscopic motor model has a physical meaning. This model is the analog to our contractile element.

Generality of the contractile element model: The strength of Hill's muscle model is that it is applicable to all skeletal muscles of such different animals as frogs and cats and even spiders (Siebert et al., 2010), and also to muscles of very different sizes (Figure 7.2). Because of the mathematically proven identity between Hill's phenomenological model and our mechanical model of the contractile element (see Chapter 5), the actuator design concept could also be the basis for the construction of such different artificial muscles.

Interestingly, a variety of constructs will result in hyperbolic or hyperbolic-like force-velocity relations. The kinematic and dynamic measures alone are therefore not enough to determine the correctness of a muscle model. Energetic and thermodynamic measures must be considered too. In Schmitt et al. (2012) we could show that the enthalpy rate and efficiency indicate a high internal gearing ratio $\kappa_v \approx 0.85$ for the contractile element model in order to fit experimental data. This would mean that most of the actual contraction happens in the SE and not the AE/PDE, and that therefore the SE cannot be purely elastic, a possibility allowed by the theoretical model. This indicates that the internal degree of freedom represented by κ_v is actually intrinsic to the contractile element and not the degree of freedom between contractile element and elastic tendon. Such a degree of freedom has not been considered in Hill-type muscle models so far. The discussion about κ_v seems very
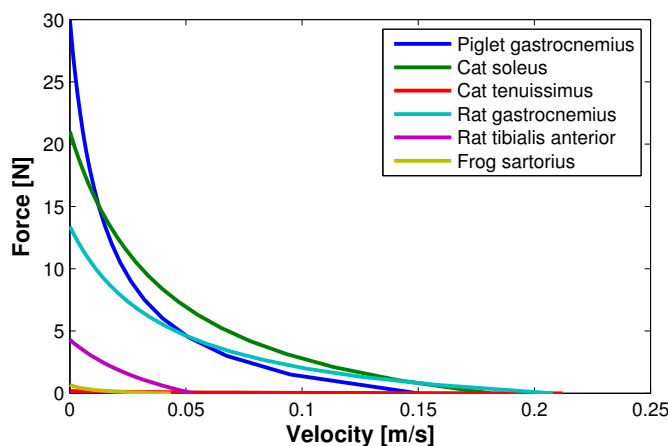
Figure 7.2: Concentric force-velocity relations of different muscles. Although their structural implementation and function is very different, the contraction dynamics of all these muscles can be approximated by Hill's hyperbolic relation. The contractile element model discussed in Chapter 5 is applicable to all these models. (Credit: this figure is based on a literature search done by Matthias Kachel, a former student with our lab: (Günther et al., 2007; Cole et al., 1996; Spector et al., 1980; van Zandwijk et al., 1996; Klute et al., 2002)).

technical but is in fact rather simple: this degree of freedom in our model in principle allows to consistently explain, force-velocity relations and enthalpy rates. Only so far, the mechanical source of the high κ_v values is unclear.

Additionally, the biological representation of the three elements is still not clear. It remains open whether the PDE actually dissipates energy which is at the same time actively produced by the AE, or whether it is intrinsic to the AE and thus rather hinders the AE energy output. This could be a bio-chemical effect as proposed by the rate-equation in the Huxley-type microscopic models or a mechanical effect so far undiscovered.

Making systems comparable by means of processed information: it has been discussed in detail in Section 3.5, how the information theoretical approach to control effort could be applied to different biological and technical systems. In this sense, the new approach to control effort always evaluates a complete moving system, including actuators, controllers, mechanical body, and environment. It finally allows their comparison for one defined movement. To fully compare the properties of several such systems, it is obviously not enough to only compare the control effort. Other criteria have to be considered as well. In Figure 7.3 a spider diagram is proposed for this purpose, here with exemplary data from Chapter 3. Other criteria commonly evaluated in robotics are e.g., workspace, force-torque output, resolution, bandwidth, precision, inertia, weight, damping, elasticity, friction, transparency (capability to suppress feel of resisting forces, or to pretend "free" motion), and safety[1]. Additionally, comparison of systems is often only possible by normalizing results to characteristic system properties, e.g., information per body weight (I/m) or time required for a movement (I/T), or could be related to time (dI/dt) or energy (dI/dE) as an information flow. This would allow e.g., to compare the control effort for locomotion of leopards, snails and robots on the level of information.

---

[1]A list presented by Prof. Gassert (ETH Zürich) with respect to haptic interfaces, June 2012.
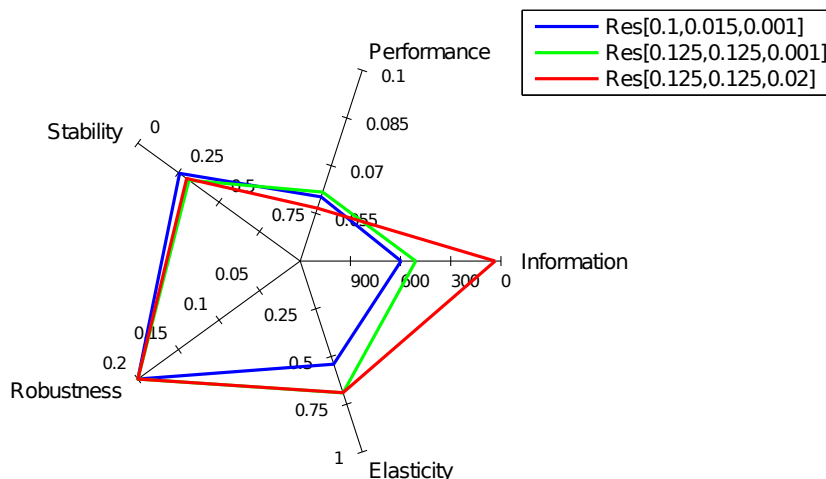
Figure 7.3: Spider diagram for information, performance, stability, robustness, and elasticity in hopping. Here, the muscle is driven by a feed-forward activation pattern $A(t)$. The resolution of the $A(t)$ pattern is varied, as well as the time resolution of the trigger event (take off) detection. Results are shown for the previously published resolution (Haeufle et al., 2010a) (blue), a lower pattern resolution (green) and additionally a lower take-off detection time resolution (red). Resolutions are given as $[\Delta A, \Delta t_{\text{pattern}}, \Delta t_{\text{take-off}}]$. The minimal required information was $I_{\min} = 34$ bit (red). For all characterizing quantities the preferred values lie on the outside of the diagram (little information, high performance, good stability, high robustness, elastic behavior).

This shows how difficult it still is to determine which actuator is "better" than the others. The primary challenge is to determine the most relevant criteria. This has recently become a socially relevant problem when the South African double amputee Oscar Pistorius participated in the 400m sprint and 400m raleigh at the regular Olympic Games (London 2012). The question was, whether or not he has an advantage from his prosthetic legs over regular athletes. The spring-like carbon prostheses are said to be more energy efficient than biological legs. The International Association of Athletics Federations (IAAF) prohibits the use of devices which give an athlete an advantage[2]. The Court of Arbitration for Sport (CAS) interpreted this criterion as an overall net-advantage. From the discussion above it seems almost impossible to determine whether or not he has a net-advantage. The only way this might be possible in the future is by determining which criteria and aspects are most relevant in running.

A step in this direction was proposed in this thesis by determining the relevant actuator properties (e.g., the hyperbolic force-velocity relation) and quantifying their benefit (better stability, less control effort). In this sense, the new approach to control effort is an important step, as it allows a comparison of different actuator types. From my point of view, our results show a disadvantage for Pistorius as the passive prostheses do not incorporate the beneficial properties of muscles. All the more impressive that he made it into the 400m semi finals in London.

---

[2]IAAF competition rule 144.2(e) prohibits the "use of any technical device that incorporates springs, wheels or any other element that provides the user with an advantage over another athlete not using such a device." (IAAF Competition Rules 2008).

Steps towards robotic application: As reviewed in the introduction (Section 1.8), the first step to incorporate compliance in robots was to actively control compliant behavior with stiff actuators. The recent developments in variable compliance actuators, including a large european grant "VIACTORS"[3], promote the incorporation of passive elastic structures in actuators. The next logical step towards bio-inspired actuation is the incorporation of the variable damping characteristics (e.g., Garcia et al., 2011) of biological muscles. Our proposed concept for such an actuator could so far only be proven in a technical test-bed, in size and weight far from the biological counterpart. Here, the next step will be to try new materials, new actuation principles, and new manufacturing processes to come up with a small and powerful actuator comparable to biological muscles. Recent research in new active materials may offer solutions to the engineering challenges involved in this endeavor.

7.1 Personal view on the greater context

"The fact that there is cosmos rather than chaos is the starting point of science."
P.C.W. Davies

In this statement P. Davies summarizes the fascinating observation that the universe comprises many distinct objects that we can name: galaxies, stars, planets, plants, flies[4], muscles etc. They all represent complex recognizable structures and not chaos. Some of them even show a dynamic behavior we call "being alive". All this structure in the universe exists despite the second law of thermodynamics demanding the steady increase of entropy in all thermodynamical systems and thus a steady decrease of structure. Nevertheless, the electro-magnetic interaction of atoms and molecules afford the existence of vast and complex structures, such as the human organism far from thermodynamical equilibrium.

It has been suggested that information plays a crucial role in the formation of such structures (e.g., Bennett, 1985; Polani, 2009). This role becomes a little clearer in the thought experiment of "Maxwell's Demon". The demon is a hypothetical entity controlling the flow of particles between two containers. By allowing only hot particles to pass in one direction and cool particles pass in the other direction, the demon could allow a heat flow from a cooler to a warmer container, which is forbidden by the second law of thermodynamics. The solution to the problem is that the demon needs to measure the particle velocities, allow or forbid the particle passage, and needs to forget the measurement result before the next measurement can be evaluated (Bennett, 1982; Weigand et al., 2010). Even if the measurement and the opening of the passage can be done reversibly, forgetting the information gained in the measurement is an irreversible process generating more entropy than reduced by the sorting of the particles.

This example shows that entropy and information are closely related to each other. Although the physics fundament with the four distinct interactions (see introduction), the conservation laws, and the thermodynamic principles is well established, its application to dynamic systems far from thermodynamical equilibrium is a challenging and fascinating endeavor. The indication that emergence of structures, despite the second law of thermodynamics, is closely related to information suggests that information is a crucial quantity in

---

[3]http://www.viactors.eu/
[4]Flies by the way are annoying me, as they are flying around my head while I'm writing these words.

living organisms. Also research on cybernetics and artificial intelligence particularly emphasizes the role of information (Wiener, 1948; Ashby, 1956; Belis and Guiasu, 1968). In this context, the physics based information approach to control effort (Chapter 3) may offer a connection between biomechanical research and these adjacent fields worthwhile of further research.

But how can complex behavior emerge? Valentino Braitenberg develops in thought experiments self-operating machines, called vehicles, which exhibit complex behavior on the basis of very simple sensor-actuator couplings (Braitenberg, 1986). He attributes to the emerging behavior qualities like "love", "aggression", or "creative thinking", which are commonly thought to only emerge in very complex beings. Looking at it the other way around, it becomes clear that observed complex behavior does not necessarily require complex underlying structures.

In his book Braitenberg focuses on the "neural" sensor-actuator coupling, and thus on what he calls "synthetic psychology". The results of this thesis suggest to also consider mechanical structures and their contribution to movement generation. If they are added to his "vehicles", even more interesting and complex behavior could emerge with even less "neural" contribution. Or, in terms of Chapter 3, very complex behavior can emerge with very little processed information, especially if the agent (or vehicle) incorporates well-designed materials and structures.

Finally, this leads to a question often debated between robotic engineers, biologists, and psychologists: how is the movement generation organized? In industrial robotic engineering it is the goal to exactly know the state of the system at any time in order to use adequate control to generate desired movements. This leads to the requirement of very fast sensor evaluation and motor response, to very stiff systems, and to high demands on the computational side. Interestingly, at least the first two requirements are not fulfilled in biological systems. It is sometimes assumed that the enormous computational power of our brain together with the many sensors could somehow compensate for the slow neural path-ways and the soft and elastic structures in our body. However, to my knowledge nobody has yet proposed a satisfying concept to explain how this could be done. Especially a concept that could pass all tests of the test trilogy (Kalveram and Seyfarth, 2009). Thus, it is questionable whether the industrial robotics concept is at all applicable to biological systems at all.

The results of this thesis and other research propose a different view. Movement generation in biology may be organized in a hierarchical way (Powers, 1973; Kalveram et al., 2012). At the lowest level, mechanical structures together with very simple neural control strategies (reflexes (Prochazka et al., 2002; Geyer and Herr, 2010), central pattern generators (Ijspeert, 2008), or equilibrium point control (Feldman and Levin, 2009)) generates movement primitives (e.g., Degallier and Ijspeert, 2010). The actuator dynamics are non-linear, the neural control has delays, and the elasticities do not allow for an exact determination of the system state. However, these basic "functional units" are reliable and thus easy to "exploit" by the next higher level in the control hierarchy. An example discussed in this thesis is hopping with force-feedback and muscle like properties: once this sensor-actuator loop is engaged, hopping is generated and even stabilized against perturbations without the need of further control. Additionally, by varying only one parameter, namely the feedback gain G_F, the hopping height can be varied. Evidently, these low-level functional units "appear" very simple to the higher-level controller. They may even appear "linear" allowing a very simple

control.

These observations seem very promising. So far, however, this theory has not been proven under the terms of the test trilogy. For locomotion though, there are at least two simulation tests which support this hypothesis: Günther and Ruder (2003) synthesized human walking in a musculo-skeletal simulation with control based on the equilibrium point theory (λ-model), and Geyer and Herr (2010) with control based on simple reflexes. A hardware test is still pending.

In the end effect this would mean that biological structures do not need a high performance brain to generate basic movements like walking or running. But why does evolution then allow such an expensive central brain which consumes about 20% of the metabolic energy (Mink et al., 1981)? Maybe the reason lies in the diversity of movements, actions, and the design and usage of tools that allow us to adapt to many different ecological niches.

The ideas discussed in this section are an attempt to propose spots and links where the puzzle pieces, developed in this thesis, might fit into the big picture of current research questions. These research questions are being posed in the realm where physics, biology, engineering, biomechanics, psychology, cybernetics, and artificial intelligence overlap. Although all these disciplines have contributed to the fascinating puzzle of locomotion, and movement generation in general, the puzzle is still not fully resolved. Much needs to be done before we can predict the gold medal winner of the next Olympic Games via models. Although the research will be continued, I assume that once the olympic fire burns in Rio de Janeiro and we watch the athletes there, we will be puzzled by the elegance, diversity, and complexity of human movements again.

Bibliography

Abbott, B. C. and Aubert, X. M. The force exerted by active striated muscle during and after change of length. *The Journal of Physiology*, 117(1):77–86, 1952.

Ahn, A. N. and Full, R. J. A motor and a brake: two leg extensor muscles acting at the same joint manage energy differently in a running insect. *The Journal of Experimental Biology*, 205(Pt 3):379–89, 2002. PMID 11854374.

Akiyama, Y., Terada, R., Hashimoto, M., Hoshino, T., Furukawa, Y., and Morishima, K. Rod-shaped Tissue Engineered Skeletal Muscle with Artificial Anchors to Utilize as a Bio-Actuator. *Journal of Biomechanical Science and Engineering*, 5(3):236–244, 2010. doi: 10.1299/jbse.5.236.

Albu-Schäffer, A., Eiberger, O., Grebenstein, M., Haddadin, S., Ott, C., Wimbock, T., Wolf, S., and Hirzinger, G. Soft robotics. *IEEE Robotics & Automation Magazine*, 15(3):20–30, 2008. doi: 10.1109/MRA.2008.927979.

Aoi, S., Ogihara, N., Funato, T., Sugimoto, Y., and Tsuchiya, K. Evaluating functional roles of phase resetting in generation of adaptive human bipedal walking with a physiologically based model of the spinal pattern generator. *Biological Cybernetics*, 102(5):373–87, 2010. doi: 10.1007/s00422-010-0373-y. PMID 20217427.

Ashby, W. R. *An introduction to Cybernetics*. Chapman & Hall LTD, London, 1 edition, 1956.

Aubert, X., Roquet, M. L., and Van der Elst, J. The Tension-Length Diagram of the Frog's Sartorius Muscle. *Archives of Physiology and Biochemistry*, 59(2):239–241, 1951. doi: 10.3109/13813455109145002.

Barclay, C. J. Mechanical efficiency and fatigue of fast and slow muscles of the mouse. *The Journal of Physiology*, 497 (Pt 3):781–94, 1996. PMID 9003563.

Barclay, C. J. A weakly coupled version of the Huxley crossbridge model can simulate energetics of amphibian and mammalian skeletal muscle. *Journal of Muscle Research and Cell Motility*, 20(2):163–76, 1999. doi: 10.1023/A:1005464231331. PMID 10412088.

Bibliography

Barclay, C. J., Constable, J. K., and Gibbs, C. L. Energetics of fast- and slow-twitch muscles of the mouse. *The Journal of Physiology*, 472(3):61–80, 1993. PMID 8145164.

Belis, M. and Guiasu, S. A quantitative-qualitative measure of information in cybernetic systems (Corresp.). *IEEE Transactions on Information Theory*, 14(4):593–594, 1968. doi: 10.1109/TIT.1968.1054185.

Bennett, C. Dissipation, information, computational complexity and the definition of organization. In Pines, D., editor, *Emerging Syntheses in Science*, pages 215–233. Addison-Wesley, Redwood City, CA, 1985.

Bennett, C. H. The thermodynamics of computation - a review. *International Journal of Theoretical Physics*, 21(12):905–940, 1982. doi: 10.1007/BF02084158.

Biewener, A. and Daley, M. Unsteady locomotion: integrating muscle function with whole body dynamics and neuromuscular control. *Journal of Experimental Biology*, 210(Pt 17): 2949–60, 2007. doi: 10.1242/jeb.005801. PMID 17704070.

Blickhan, R., Seyfarth, A., Geyer, H., Grimmer, S., Wagner, H., and Günther, M. Intelligence by mechanics. *Philosophical Transactions of the Royal Society of London, Series A*, 365 (1850):199–220, 2007. doi: 10.1098/rsta.2006.1911. PMID 17148057.

Blickhan, R. The spring-mass model for running and hopping. *Journal of Biomechanics*, 22 (11-12):1217–1227, 1989. doi: 10.1016/0021-9290(89)90224-8. PMID 2625422.

Blickhan, R. and Full, R. J. Similarity in multilegged locomotion: Bouncing like a monopode. *Journal of Comparative Physiology A*, 173(5):509–517, 1993. doi: 10.1007/BF00197760.

Blickhan, R., Wagner, H., and Seyfarth, A. Brain or muscles. *Recent Research Developments in Biomechanics*, 1:215–245, 2003.

Blum, Y., Lipfert, S. W., Rummel, J., and Seyfarth, A. Swing leg control in human running. *Bioinspiration & Biomimetics*, 5(2):026006, 2010. doi: 10.1088/1748-3182/5/2/026006. PMID 20498515.

Bobbert, M. F., Ettema, G. C., and Huijing, P. A. The force-length relationship of a muscle-tendon complex: experimental results and model calculations. *European Journal of Applied Physiology and Occupational Physiology*, 61(3-4):323–9, 1990. PMID 2282919.

Bobrow, J. E., Martin, B., Sohl, G., Wang, E. C., Park, F. C., and Kim, J. Optimal robot motions for physical criteria. *Journal of Robotic Systems*, 18(12):785–795, 2001. doi: 10.1002/rob.8116.

Braitenberg, V. *Vehicles: Experiments in Synthetic Psychology*. MIT Press, Cambridge, 1 edition, 1986. ISBN 978-0-262-52112-3.

Bressler, B. H. and Clinch, N. F. The compliance of contracting skeletal muscle. *The Journal of Physiology*, 237(3):477–93, 1974. doi: 10.3892/mmr.2011.495. PMID 4207658.

Brown, I. E., Scott, S. H., and Loeb, G. E. Preflexes—programmable high-gain zero-delay intrinsic responses of perturbed musculoskeletal systems. *Society of Neuroscience, Abstracts*, 21:562, 1995.

Brown, I. and Loeb, G. E. A Reductionist Approach to Creating and Using Neuromusculoskeletal Models. In Winters, J. M. and Crago, P., editors, *Biomechanics and Neural Control of Posture and Movement*, pages 148–163. Springer Verlag, New York, 2000.

Buschmann, T., Lohmeier, S., Kühnlenz, K., Buss, M., Ulbrich, H., and Pfeiffer, F. LOLA - a Performance Enhanced Humanoid Robot (LOLA - ein leistungsgesteigerter humanoider Roboter). *IT - Information Technology*, 49(4):218–223, 2007. doi: 10.1524/itit.2007.49.4.218.

Capdepuy, P., Polani, D., and Nehaniv, C. L. Adaptation of the Perception-Action Loop Using Active Channel Sampling. In *2008 NASA/ESA Conference on Adaptive Hardware and Systems*, pages 443–450. IEEE, 2008. ISBN 978-0-7695-3166-3. doi: 10.1109/AHS.2008.64.

Carpi, F., Raspopovic, S., Frediani, G., and De Rossi, D. Real-time control of dielectric elastomer actuators via bioelectric and biomechanical signals. *Polymer International*, 59 (3):422–429, 2010. doi: 10.1002/pi.2757.

Cavagna, G. A. Elastic bounce of the body. *Journal of Applied Physiology*, 29(3):279–82, 1970. PMID 5451302.

Cavagna, G. A. and Citterio, G. Effect of stretching on the elastic characteristics and the contractile component of frog striated muscle. *The Journal of Physiology*, 239(1):1–14, 1974. PMID 4368635.

Cham, J. G., Bailey, S. A., and Cutkosky, M. R. Robust Dynamic Locomotion through Feedforward-Preflex Interaction. In *ASME IMECE Proceedings*, pages 2–9, Orlando, Florida, USA, 2000.

Chee-Meng, C., Geok-Soon, H., and Wei, Z. Series damper actuator: a novel force/torque control actuator. In *4th IEEE/RAS International Conference on Humanoid Robots*, pages 533–546. IEEE, 2004. ISBN 0-7803-8863-1. doi: 10.1109/ICHR.2004.1442669.

Chin, L., Yue, P., Feng, J. J., and Seow, C. Y. Mathematical simulation of muscle crossbridge cycle and force-velocity relationship. *Biophysical Journal*, 91(10):3653–63, 2006. doi: 10.1529/biophysj.106.092510. PMID 16935957.

Chou, C.-P. and Hannaford, B. Measurement and modeling of McKibben pneumatic artificial muscles. *IEEE Transactions on Robotics and Automation*, 12(1):90–102, 1996. doi: 10.1109/70.481753.

Chuc, N. H., Vuong, N. H. L., Kim, D. S., Moon, H. P., Koo, J. C., Lee, Y. K., Nam, J.-D., and Choi, H. R. Fabrication and Control of Rectilinear Artificial Muscle Actuator. *IEEE/ASME Transactions on Mechatronics*, 16(1):167–176, 2011. doi: 10.1109/TMECH.2009.2038223.

Bibliography

Close, R. I. Activation delays in frog twitch muscle fibres. *The Journal of Physiology*, 313: 81–100, 1981. PMID 7277238.

Cole, G. K., van den Bogert, A. J., Herzog, W., and Gerritsen, K. G. Modelling of force production in skeletal muscle undergoing stretch. *Journal of Biomechanics*, 29(8):1091–1104, 1996. doi: 10.1016/0021-9290(96)00005-X.

Collins, S. H. A Three-Dimensional Passive-Dynamic Walking Robot with Two Legs and Knees. *The International Journal of Robotics Research*, 20(7):607–615, 2001. doi: 10.1177/02783640122067561.

Cooke, R., White, H., and Pate, E. A model of the release of myosin heads from actin in rapidly contracting muscle fibers. *Biophysical Journal*, 66(3):778–788, 1994. doi: 10.1016/S0006-3495(94)80854-9.

Daerden, F. and Lefeber, D. Pneumatic artificial muscles actuators for robotics and automation. *European Journal of Mechanical and Environmental Engineering*, 47(1):1121, 2002.

Daley, M. A., Righetti, L., and Ijspeert, A. J. Modelling the interplay of central pattern generation and sensory feedback in the neuromuscular control of running. *Comparative Biochemistry and Physiology - Part A: Molecular & Integrative Physiology*, 153(2):S135–S135, 2009. doi: 10.1016/j.cbpa.2009.04.243.

Degallier, S. and Ijspeert, A. Modeling discrete and rhythmic movements through motor primitives: a review. *Biological Cybernetics*, 103(4):319–38, 2010. doi: 10.1007/s00422-010-0403-9. PMID 20697734.

Delcomyn, F. Neural basis of rhythmic behavior in animals. *Science*, 210(4469):492–498, 1980. doi: 10.1126/science.7423199. PMID 7423199.

Dickinson, M. H. How Animals Move: An Integrative View. *Science*, 288(5463):100–106, 2000. doi: 10.1126/science.288.5463.100.

du Bois-Reymond, E. *Untersuchungen über thierische Elektricität*. Georg Reimer, Berlin, 1848.

Durfee, W. K. and Palmer, K. I. Estimation of force-activation, force-length, and force-velocity properties in isolated, electrically stimulated muscle. *IEEE Transactions on Biomedical Engineering*, 41(3):205–16, 1994. doi: 10.1109/10.284939. PMID 8045573.

Duysens, J. Neural control of locomotion; Part 1: The central pattern generator from cats to humans. *Gait & Posture*, 7(2):131–141, 1998. doi: 10.1016/S0966-6362(97)00042-8.

Einstein, A. Die Grundlage der allgemeinen Relativitätstheorie. *Annalen der Physik*, 354 (7):769–822, 1916. doi: 10.1002/andp.19163540702.

Ettema, G. C. and Huijing, P. A. Isokinetic and isotonic force-velocity characteristics of rat EDL at muscle optimum length. In Groot, G. D., Hollander, A. P., Huijing, P. A., and Van Ingen Schenau, G. J., editors, *Biomechanics XI-A, International Series on Biomechanics 7-A*, pages 58–62. Free University Press, Amsterdam, 1988.

Ettema, G. C. Mechanical efficiency and efficiency of storage and release of series elastic energy in skeletal muscle during stretch-shorten cycles. *The Journal of Experimental Biology*, 199(Pt 9):1983–97, 1996. PMID 8831144.

Fang, Y. Robust Adaptive Control of Conjugated Polymer Actuators. *IEEE Transactions on Control Systems Technology*, 32(4):1696–612, 2008. doi: 10.1109/TCST.2007.912112.

Farahat, W. and Herr, H. An apparatus for characterization and control of isolated muscle. *EEE Transactions on Neural Systems and Rehabilitation Engineering*, 13(4):473–81, 2005. doi: 10.1109/TNSRE.2005.857686. PMID 16425829.

Farley, C. T. and Morgenroth, D. C. Leg stiffness primarily depends on ankle stiffness during human hopping. *Journal of Biomechanics*, 32(3):267–273, 1999. doi: 10.1016/S0021-9290(98)00170-5.

Farley, C. T., Blickhan, R., Saito, J., and Taylor, C. R. Hopping frequency in humans: a test of how springs set stride frequency in bouncing gaits. *Journal of Applied Physiology*, 71(6):2127–32, 1991. PMID 1778902.

Farley, C. T., Houdijk, H. H., Van Strien, C., and Louie, M. Mechanism of leg stiffness adjustment for hopping on surfaces of different stiffnesses. *Journal of Applied Physiology*, 85(3):1044–55, 1998. PMID 9729582.

Feldman, A. G. and Levin, M. F. The equilibrium-point hypothesis–past, present and future. *Advances in Experimental Medicine and Biology*, 629:699–726, 2009. doi: 10.1007/978-0-387-77064-2_38. PMID 19227529.

Fermi, E. Versuch einer Theorie der Beta-Strahlen. I. *Zeitschrift für Physik*, 88(3-4):161–177, 1934. doi: 10.1007/BF01351864.

Ferris, D. P., Liang, K., and Farley, C. T. Runners adjust leg stiffness for their first step on a new running surface. *Journal of Biomechanics*, 32(8):787–794, 1999. doi: 10.1016/S0021-9290(99)00078-0.

FESTO. Pneumatische Federelementanordnung insbesondere zur Niveauregulierung von Kraftfahrzeugen, 2000.

Feynman, R. *The Character of Physical Law*. Random House, New York, 1994. ISBN 0-679-60127-9.

Fick, A. Neue Beiträge zur Kenntniss von der Wärmeentwicklung im Muskel. *Pflüger, Archiv für die Gesammte Physiologie des Menschen und der Thiere*, 51(11-12):541–569, 1892. doi: 10.1007/BF01663505.

Bibliography

Forcinito, M., Epstein, M., and Herzog, W. Can a rheological muscle model predict force depression/enhancement? *Journal of Biomechanics*, 31(12):1093–1099, 1998. doi: 10.1016/S0021-9290(98)00132-8. PMID 9882041.

Foroughi, J., Spinks, G. M., Wallace, G. G., Oh, J., Kozlov, M. E., Fang, S., Mirfakhrai, T., Madden, J. D. W., Shin, M. K., Kim, S. J., and Baughman, R. H. Torsional carbon nanotube artificial muscles. *Science*, 334(6055):494–7, 2011. doi: 10.1126/science.1211220. PMID 21998253.

Frank, T. and Schilling, C. The development of cascadable microdrives with muscle-like operating behaviour. *Journal of Micromechanics and Microengineering*, 8(3):222–229, 1998. doi: 10.1088/0960-1317/8/3/008.

Friesen, W. O. Central Pattern Generators: Sensory Feedback. *Encyclopedia of Neuroscience*, pages 701–709, 2009. doi: 10.1016/B978-008045046-9.01949-5.

Full, R. J. and Koditschek, D. E. Templates and anchors: neuromechanical hypotheses of legged locomotion on land. *Journal of Experimental Biology*, 202(Pt 23):3325–32, 1999. PMID 10562515.

Full, R. J., Kubow, T., Schmitt, J., Holmes, P., and Koditschek, D. Quantifying Dynamic Stability and Maneuverability in Legged Locomotion. *Integrative and Comparative Biology*, 42(1):149–157, 2002. doi: 10.1093/icb/42.1.149.

Garcia, E., Arevalo, J., Muñoz, G., and Gonzalez-de Santos, P. Combining series elastic actuation and magneto-rheological damping for the control of agile locomotion. *Robotics and Autonomous Systems*, 59(10):827–839, 2011. doi: 10.1016/j.robot.2011.06.006.

Garofalo, G., Ott, C., and Albu-Schäffer, A. Walking control of fully actuated robots based on the Bipedal SLIP model. In *IEEE International Conference on Robotics and Automation*, pages 1456–1463. IEEE, 2012. ISBN 978-1-4673-1405-3. doi: 10.1109/ICRA.2012.6225272.

Gernert, D. Pragmatic Information: Historical Exposition and General Overview. *Mind & Matter*, 4(2):141–167, 2006.

Gerritsen, K. G. M., van Den Bogert, A. J., Hulliger, M., and Zernicke, R. F. Intrinsic muscle properties facilitate locomotor control - a computer simulation study. *Motor Control*, 2(3):206–20, 1998. PMID 9644290.

Geyer, H. and Herr, H. A muscle-reflex model that encodes principles of legged mechanics produces human walking dynamics and muscle activities. *IEEE Transactions on Neural Systems and Rehabilitation Engineering*, 18(3):263–73, 2010. doi: 10.1109/TNSRE.2010.2047592. PMID 20378480.

Geyer, H., Seyfarth, A., and Blickhan, R. Positive force feedback in bouncing gaits? *Proceedings of the Royal Society of London. Series B*, 270(1529):2173–83, 2003. doi: 10.1098/rspb.2003.2454. PMID 14561282.

Geyer, H., Seyfarth, A., and Blickhan, R. Spring-mass running: simple approximate solution and application to gait stability. *Journal of Theoretical Biology*, 232(3):315–28, 2005. doi: 10.1016/j.jtbi.2004.08.015. PMID 15572057.

Geyer, H., Seyfarth, A., and Blickhan, R. Compliant leg behaviour explains basic dynamics of walking and running. *Proceedings of the Royal Society of London. Series B*, 273(1603): 2861–7, 2006. doi: 10.1098/rspb.2006.3637. PMID 17015312.

Goher, K. and Tokhi, M. Modelling, simulation and balance control of a two wheeled robotic machine with static variation in load position. In *Proceedings of the 22nd European Conference on Modelling and Simulation*, volume 5, pages 3–6, Nicosia, Cyprus, 2005.

Gordon, A. M., Huxley, A. F., and Julian, F. J. The variation in isometric tension with sarcomere length in vertebrate muscle fibres. *The Journal of Physiology*, 184(1):170–92, 1966. PMID 5921536.

Grimmer, S., Ernst, M., Günther, M., and Blickhan, R. Running on uneven ground: leg adjustment to vertical steps and self-stability. *The Journal of Experimental Biology*, 211 (Pt 18):2989–3000, 2008. doi: 10.1242/jeb.014357. PMID 18775936.

Gross, D. and Wilczek, F. Ultraviolet Behavior of Non-Abelian Gauge Theories. *Physical Review Letters*, 30(26):1343–1346, 1973. doi: 10.1103/PhysRevLett.30.1343.

Günther, M. and Ruder, H. Synthesis of two-dimensional human walking: a test of the lambda-model. *Biological Cybernetics*, 89(2):89–106, 2003. doi: 10.1007/s00422-003-0414-x. PMID 12905038.

Günther, M. and Schmitt, S. A macroscopic ansatz to deduce the Hill relation. *Journal of Theoretical Biology*, 263(4):407–18, 2010. doi: 10.1016/j.jtbi.2009.12.027. PMID 20045704.

Günther, M., Schmitt, S., and Wank, V. High-frequency oscillations as a consequence of neglected serial damping in Hill-type muscle models. *Biological Cybernetics*, 97(1):63–79, 2007. doi: 10.1007/s00422-007-0160-6. PMID 17598125.

Haeufle, D. F. B., Grimmer, S., and Seyfarth, A. The role of intrinsic muscle properties for stable hopping - stability is achieved by the force-velocity relation. *Bioinspiration & Biomimetics*, 5(1):016004, 2010a. doi: 10.1088/1748-3182/5/1/016004.

Haeufle, D. F. B., Günther, M., Blickhan, R., and Schmitt, S. Proof of concept: model based bionic muscle with hyperbolic force-velocity relation. In *International Conference on Applied Biomechanics and Bionics*, Venice, 2010b.

Haeufle, D. F. B., Grimmer, S., Kalveram, K.-T., and Seyfarth, A. Integration of intrinsic muscle properties, feed-forward and feedback signals for generating and stabilizing hopping. *Journal of the Royal Society, Interface*, 9(72):1458–69, 2012a. doi: 10.1098/rsif.2011.0694. PMID 22219395.

Haeufle, D. F. B., Günther, M., Blickhan, R., and Schmitt, S. Proof of concept: Model based bionic muscle with hyperbolic force-velocity relation. *Applied Bionics and Biomechanics*, 9(3):267–274, 2012b. doi: 10.3233/ABB-2011-0052.

Bibliography

Haeufle, D., Günther, M., Blickhan, R., and Schmitt, S. Can Quick Release Experiments Reveal the Muscle Structure? A Bionic Approach. *Journal of Bionic Engineering*, 9(2): 211–223, 2012c. doi: 10.1016/S1672-6529(11)60115-7.

Ham, R., Sugar, T., Vanderborght, B., Hollander, K., and Lefeber, D. Compliant actuator designs. *IEEE Robotics & Automation Magazine*, 16(3):81–94, 2009. doi: 10.1109/MRA.2009.933629.

Hannaford, B., Jaax, K., and Klute, G. K. Bio-inspired actuation and sensing. *Autonomous Robots*, 11(3):267–272, 2001. doi: 10.1023/A:1012495108404.

Hatze, H. A myocybernetic control model of skeletal muscle. *Biological Cybernetics*, 25(2): 103–119, 1977a. doi: 10.1007/BF00337268. PMID 836914.

Hatze, H. The relative contribution of motor unit recruitment and rate coding to the production of static isometric muscle force. *Biological Cybernetics*, 27(1):21–25, 1977b. doi: 10.1007/BF00357706.

Hatze, H. A general myocybernetic control model of skeletal muscle. *Biological Cybernetics*, 28(3):143–157, 1978. doi: 10.1007/BF00337136.

Heglund, N. C. and Cavagna, G. A. Efficiency of vertebrate locomotory muscles. *The Journal of Experimental Biology*, 115:283–92, 1985. PMID 4031770.

Heglund, N. C. and Cavagna, G. A. Mechanical work, oxygen consumption, and efficiency in isolated frog and rat muscle. *The American Journal of Physiology*, 253(1 Pt 1):C22–9, 1987. PMID 3496797.

Herzog, W. and Leonard, T. R. Force enhancement following stretching of skeletal muscle: a new mechanism. *The Journal of Experimental Biology*, 205(Pt 9):1275–83, 2002. PMID 11948204.

Herzog, W. History dependence of skeletal muscle force production: implications for movement control. *Human movement science*, 23(5):591–604, 2004. doi: 10.1016/j.humov.2004.10.003. PMID 15589623.

Hill, A. V. The heat of shortening and the dynamic constants of muscle. *Proceedings of the Royal Society of London. Series B*, 126(843):136–195, 1938. doi: 10.1098/rspb.1938.0050.

Hill, A. V. The Effect of Load on the Heat of Shortening of Muscle. *Proceedings of the Royal Society of London. Series B*, 159(975):297–318, 1964. doi: 10.1098/rspb.1964.0004.

Hinrichsen, D. and Pritchard, A. J. *Mathematical Systems Theory I*, volume 48 of *Texts in Applied Mathematics*. Springer Berlin Heidelberg, Berlin, Heidelberg, 2010. ISBN 978-3-642-03940-9. doi: 10.1007/b137541.

Hirose, M. and Ogawa, K. Honda humanoid robots development. *Philosophical Transactions of the Royal Society of London, Series A*, 365(1850):11–9, 2007. doi: 10.1098/rsta.2006.1917. PMID 17148047.

Hoffmann, M. and Pfeifer, R. The implications of embodiment for behavior and cognition: animal and robotic case studies. In Tschacher, W. and Bergomi, C., editors, *The Implications of Embodiment: Cognition and Communication*, pages 31–58. Imprint Academic, 1 edition, 2011. ISBN 978-1845402402.

Hogan, N., Bizzi, E., Mussa-Ivaldi, F. A., and Flash, T. Controlling multijoint motor behavior. *Exercise and Sport Sciences Reviews*, 15:153–90, 1987. PMID 3297722.

Hogan, N. and Sternad, D. On rhythmic and discrete movements: reflections, definitions and implications for motor control. *Experimental Brain Research*, 181(1):13–30, 2007. doi: 10.1007/s00221-007-0899-y. PMID 17530234.

Houdijk, H., Bobbert, M. F., and de Haan, A. Evaluation of a Hill based muscle model for the energy cost and efficiency of muscular contraction. *Journal of Biomechanics*, 39(3): 536–43, 2006. doi: 10.1016/j.jbiomech.2004.11.033. PMID 16389094.

Hsu, J., Kueck, J., Olszewski, M., Casada, D., Otaduy, P., and Tolbert, L. Comparison of induction motor field efficiency evaluation methods. *IEEE Transactions on Industry Applications*, 34(1):117–125, 1998. doi: 10.1109/28.658732.

Hurst, J. and Rizzi, A. Series compliance for an efficient running gait. *IEEE Robotics & Automation Magazine*, 15(3):42–51, 2008. doi: 10.1109/MRA.2008.927693.

Huxley, A. F. Muscle structure and theories of contraction. *Progress in Biophysics and Biophysical Chemistry*, 7:255–318, 1957. PMID 13485191.

IAAF. IAAF World Championships: IAAF Statistics Handbook, 2010.

Ijspeert, A. J. Central pattern generators for locomotion control in animals and robots: a review. *Neural Networks*, 21(4):642–53, 2008. doi: 10.1016/j.neunet.2008.03.014. PMID 18555958.

Ivanenko, Y. P., Poppele, R. E., and Lacquaniti, F. Motor control programs and walking. *The Neuroscientist*, 12(4):339–48, 2006. doi: 10.1177/1073858406287987. PMID 16840710.

Jewell, B. R. and Wilkie, D. R. An analysis of the mechanical components in frog's striated muscle. *The Journal of Physiology*, 143(3):515–40, 1958. PMID 13588571.

Johansson, R. and Magnusson, M. Optimal coordination and control of posture and locomotion. *Mathematical Biosciences*, 103(2):203–44, 1991. doi: 10.1016/0025-5564(91)90054-M. PMID 1804446.

Kalveram, K. T. and Seyfarth, A. Inverse biomimetics: how robots can help to verify concepts concerning sensorimotor control of human arm and leg movements. *Journal of Physiology, Paris*, 103(3-5):232–43, 2009. doi: 10.1016/j.jphysparis.2009.08.006. PMID 19665562.

Bibliography

Kalveram, K. T., Schinauer, T., Beirle, S., Richter, S., and Jansen-Osmann, P. Threading neural feedforward into a mechanical spring: how biology exploits physics in limb control. *Biological Cybernetics*, 92(4):229–40, 2005. doi: 10.1007/s00422-005-0542-6. PMID 15834624.

Kalveram, K. T., Haeufle, D. F. B., and Seyfarth, A. From Hopping to Walking - how the Biped Jena-Walker can Learn from the Single-Leg Marco-Hopper. In Marques, L., De Almeida, A., and Tokhi, M. O., editors, *CLAWAR-Advances in Mobile Robotics*, pages 638–645, 2008.

Kalveram, K. T., Haeufle, D. F. B., Grimmer, S., and Seyfarth, A. Energy management that generates hopping. Comparison of virtual, robotic and human bouncing. In *Proceedings of the International Conference on Simulation, Modeling and Programming for Autonomous Robots*, pages 147–156, Darmstadt, 2010. ISBN: 978-3-00-032863-3.

Kalveram, K. T., Haeufle, D. F. B., Seyfarth, A., and Grimmer, S. Energy management that generates terrain following versus apex-preserving hopping in man and machine. *Biological Cybernetics*, 106(1):1–13, 2012. doi: 10.1007/s00422-012-0476-8. PMID 22350535.

Karpelson, M. and Wood, R. J. A review of actuation and power electronics options for flapping-wing robotic insects. *2008 IEEE International Conference on Robotics and Automation*, pages 779–786, 2008. doi: 10.1109/ROBOT.2008.4543300.

Kawato, M. Internal models for motor control and trajectory planning. *Current Opinion in Neurobiology*, 9(6):718–27, 1999. PMID 10607637.

Kawato, M., Maeda, Y., Uno, Y., and Suzuki, R. Trajectory formation of arm movement by cascade neural network model based on minimum torque-change criterion. *Biological Cybernetics*, 62(4):275–288, 1990. doi: 10.1007/BF00201442.

Kerscher, T., Albiez, J., Zollner, J., and Dillmann, R. Evaluation of the Dynamic Model of Fluidic Muscles using Quick-Release. In *The First IEEE/RAS-EMBS International Conference on Biomedical Robotics and Biomechatronics*, pages 637–642. IEEE, 2006. ISBN 1-4244-0040-6. doi: 10.1109/BIOROB.2006.1639161.

Kistemaker, D. a., Van Soest, A. J., and Bobbert, M. F. Is equilibrium point control feasible for fast goal-directed single-joint movements? *Journal of Neurophysiology*, 95(5):2898–912, 2006. doi: 10.1152/jn.00983.2005. PMID 16436480.

Klute, G. K., Czerniecki, J. M., and Hannaford, B. Artificial Muscles: Actuators for Biorobotic Systems. *The International Journal of Robotics Research*, 21(4):295–309, 2002. doi: 10.1177/027836402320556331.

Koditschek, D. E., Full, R. J., and Buehler, M. Mechanical aspects of legged locomotion control. *Arthropod Structure & Development*, 33(3):251–72, 2004. doi: 10.1016/j.asd.2004.06.003. PMID 18089038.

Kolmogorov, A. Three approaches to the quantitative definition of information. *Problemy Peredachi Informatsii*, 1(1):3–11, 1965.

Kukillaya, R., Proctor, J., and Holmes, P. Neuromechanical models for insect locomotion: Stability, maneuverability, and proprioceptive feedback. *Chaos*, 19(2):026107, 2009. doi: 10.1063/1.3141306. PMID 19566267.

Kuo, A. D. An optimal control model for analyzing human postural balance. *IEEE Transactions on Bio-medical Engineering*, 42(1):87–101, 1995. doi: 10.1109/10.362914. PMID 7851935.

Kuo, A. D. The relative roles of feedforward and feedback in the control of rhythmic movements. *Motor Control*, 6(2):129–45, 2002. PMID 12122223.

Lam, T., Anderschitz, M., and Dietz, V. Contribution of feedback and feedforward strategies to locomotor adaptations. *Journal of Neurophysiology*, 95(2):766–73, 2006. doi: 10.1152/jn.00473.2005. PMID 16424453.

Lan, G. and Sun, S. X. Dynamics of myosin-driven skeletal muscle contraction: I. Steady-state force generation. *Biophysical Journal*, 88(6):4107–17, 2005. doi: 10.1529/biophysj.104.056846. PMID 15778440.

Lieber, R. L. Skeletal muscle is a biological example of a linear electroactive actuator. In *Proceedings of SPIE*, volume 3669, pages 19–25. SPIE, 1999. doi: 10.1117/12.349688.

Lilly, J. and Quesada, P. A Two-Input Sliding-Mode Controller for a Planar Arm Actuated by Four Pneumatic Muscle Groups. *IEEE Transactions on Neural Systems and Rehabilitation Engineering*, 12(3):349–359, 2004. doi: 10.1109/TNSRE.2004.831490. PMID 15473198.

Lin, H.-T., Leisk, G. G., and Trimmer, B. GoQBot: a caterpillar-inspired soft-bodied rolling robot. *Bioinspiration & Biomimetics*, 6(2):026007, 2011. doi: 10.1088/1748-3182/6/2/026007. PMID 21521905.

Lipfert, S. W. *Kinematic and Dynamic Similarities between Walking and Running*. Verlag Dr. Kovac, Hamburg, 2010. ISBN 978-3830050308.

Lockhart, D. B. and Ting, L. H. Optimal sensorimotor transformations for balance. *Nature Neuroscience*, 10(10):1329–36, 2007. doi: 10.1038/nn1986. PMID 17873869.

Loeb, G. E. Neural Control of Locomotion. *BioScience*, 39(11):800, 1989. doi: 10.2307/1311186.

Loram, I. D., Maganaris, C. N., and Lakie, M. The passive, human calf muscles in relation to standing: the non-linear decrease from short range to long range stiffness. *The Journal of Physiology*, 584(Pt 2):661–75, 2007. doi: 10.1113/jphysiol.2007.140046. PMID 17823209.

MacKay-Lyons, M. Central pattern generation of locomotion: a review of the evidence. *Physical Therapy*, 82(1):69–83, 2002. PMID 11784280.

Madden, J. D. Mobile robots: motor challenges and materials solutions. *Science*, 318(5853): 1094–7, 2007. doi: 10.1126/science.1146351. PMID 18006737.

Bibliography

Maufroy, C., Maus, H. M., and Seyfarth, A. Simplified control of upright walking by exploring asymmetric gaits induced by leg damping. In *2011 IEEE International Conference on Robotics and Biomimetics*, pages 491–496. Ieee, 2011. ISBN 978-1-4577-2138-0. doi: 10.1109/ROBIO.2011.6181334.

Maxwell, J. C. *A treatise on electricity and magnetism*. Clarendon Press, Oxford, 1 edition, 1873.

McGeer, T. Passive Dynamic Walking. *The International Journal of Robotics Research*, 9 (2):62–82, 1990. doi: 10.1177/027836499000900206.

McMahon, T. A. *Muscles, reflexes, and locomotion*. Princeton Univ Press, 1984.

Meijer, K., Grootenboer, H., Koopman, H., van der Linden, B., and Huijing, P. A Hill type model of rat medial gastrocnemius muscle that accounts for shortening history effects. *Journal of Biomechanics*, 31(6):555–563, 1998. doi: 10.1016/S0021-9290(98)00048-7.

Melvill Jones, G. M. and Watt, D. G. Observations on the control of stepping and hopping movements in man. *Journal of Physiology*, 219(3):709–27, 1971. PMID 5157598.

Mergner, T. Annual Reviews in Control A neurological view on reactive human stance control. *Annual Reviews in Control*, 34(2):177–198, 2010. doi: 10.1016/j.arcontrol.2010.08.001.

Mergner, T., Huethe, F., Maurer, C., and Ament, C. Human Equilibrium Control Principles Implemented into a Biped Humanoid Robot. In Zielinska, T. and Zielinski, C., editors, *Robot Design, Dynamics, and Control, CISM Courses and Lectures 487*, pages 271–279. 2006.

Mink, J. W., Blumenschine, R. J., and Adams, D. B. Ratio of central nervous system to body metabolism in vertebrates: its constancy and functional basis. *The American Journal of Physiology*, 241(3):R203–12, 1981. PMID 7282965.

Moritz, C. T. and Farley, C. T. Passive dynamics change leg mechanics for an unexpected surface during human hopping. *Journal of Applied Physiology*, 97(4):1313–22, 2004. doi: 10.1152/japplphysiol.00393.2004. PMID 15169748.

Nachtigall, W. *Bionik*. Springer, 2 edition, 2002. ISBN 978-3-540-43660-7.

Nelson, W. L. Physical principles for economies of skilled movements. *Biological Cybernetics*, 46(2):135–147, 1983. doi: 10.1007/BF00339982.

Neustadt, L. W. Minimum Effort Control Systems. *Journal of the Society for Industrial and Applied Mathematics, Series A: Control*, 1(1):16, 1962. doi: 10.1137/0301002.

Newton, S. I. *Mathematical principles of natural philosophy*. Cadell and Davies, London, 2 edition, 1802.

Nielsen, J. B. How we walk: central control of muscle activity during human walking. *The Neuroscientist*, 9(3):195, 2003. doi: 10.1177/1073858403251978.

Nigg, B. M. and Herzog, W. *Biomechanics of the Musculo-skeletal System*. Wiley, 2007. ISBN 0470017678.

Niiyama, R., Nishikawa, S., and Kuniyoshi, Y. Biomechanical Approach to Open-Loop Bipedal Running with a Musculoskeletal Athlete Robot. *Advanced Robotics*, 26(3-4):383–398, 2012. doi: 10.1163/156855311X614635.

Nouri, B. M. Y. and Zaidan, A. Computer control of a powered two degree freedom reciprocating gait orthosis. *ISA Transactions*, 45(2):249–58, 2006. PMID 16649569.

Paul, C. Morphological computation: A basis for the analysis of morphology and control requirements. *Robotics and Autonomous Systems*, 54(8):619–630, 2006. doi: 10.1016/j.robot.2006.03.003.

Paul, C., Bellotti, M., Jezernik, S., and Curt, A. Development of a human neuro-musculo-skeletal model for investigation of spinal cord injury. *Biological Cybernetics*, 93(3):153–70, 2005. doi: 10.1007/s00422-005-0559-x. PMID 16133587.

Pearson, K. G., Ekeberg, O., and Büschges, A. Assessing sensory function in locomotor systems using neuro-mechanical simulations. *Trends in Neurosciences*, 29(11):625–31, 2006. doi: 10.1016/j.tins.2006.08.007. PMID 16956675.

Pelrine, R. Dielectric elastomer artificial muscle actuators: toward biomimetic motion. In *Proceedings of SPIE*, volume 4695, pages 126–137. SPIE, 2002. doi: 10.1117/12.475157.

Peuker, F., Maufroy, C., and Seyfarth, A. Leg-adjustment strategies for stable running in three dimensions. *Bioinspiration & Biomimetics*, 7(3):036002, 2012. doi: 10.1088/1748-3182/7/3/036002.

Pfeifer, R. and Iida, F. Embodied Artificial Intelligence: Trends and Challenges. In Iida, F., Pfeifer, R., Steels, L., and Yasuo, K., editors, *Embodied Artificial Intelligence*, chapter 1. 3139/2004 edition, 2004. doi: 10.1007/978-3-540-27833-7_1.

Piazzesi, G. and Lombardi, V. A cross-bridge model that is able to explain mechanical and energetic properties of shortening muscle. *Biophysical journal*, 68(5):1966–79, 1995. doi: 10.1016/S0006-3495(95)80374-7. PMID 7612839.

Piazzesi, G. and Lombardi, V. Simulation of the rapid regeneration of the actin-myosin working stroke with a tight coupling model of muscle contraction. *Journal of Muscle Research and Cell Motility*, 17(1):45–53, 1996. doi: 10.1007/BF00140323.

Polani, D. Information: currency of life? *HFSP Journal*, 3(5):307–16, 2009. doi: 10.2976/1.3171566. PMID 20357888.

Polani, D., Sporns, O., and Lungarella, M. How Information and Embodiment Shape Intelligent Information Processing. In Lungarella, M., Iida, F., Bongard, J., and Pfeifer, R., editors, *Lecture Notes in Computer Science: 50 years of Artificial Intelligence*, pages 99–111. Springer, 2007. doi: 10.1007/978-3-540-77296-5_10.

Bibliography

Politzer, H. Reliable Perturbative Results for Strong Interactions? *Physical Review Letters*, 30(26):1346–1349, 1973. doi: 10.1103/PhysRevLett.30.1346.

Poulakakis, I. Spring Loaded Inverted Pendulum embedding: Extensions toward the control of compliant running robots. *2010 IEEE International Conference on Robotics and Automation*, pages 5219–5224, 2010. doi: 10.1109/ROBOT.2010.5509373.

Powers, W. T. *Behavior: The Control of Perception*. Aldine Transaction, 1973.

Pratt, G. A. and Williamson, M. M. Series elastic actuators. *Proceedings 1995 IEEE/RSJ International Conference on Intelligent Robots and Systems. Human Robot Interaction and Cooperative Robots*, pages 399–406, 1995. doi: 10.1109/IROS.1995.525827.

Pratt, J., Krupp, B., and Morse, C. Series elastic actuators for high fidelity force control. *Industrial Robot: An International Journal*, 29(3):234–241, 2002. doi: 10.1108/01439910210425522.

Prochazka, A. and Yakovenko, S. Predictive and reactive tuning of the locomotor CPG. *Integrative and Comparative Biology*, 47(4):474–481, 2007. doi: 10.1093/icb/icm065.

Prochazka, A., Gritsenko, V., and Yakovenko, S. Sensory control of locomotion: reflexes versus higher-level control. *Advances in Experimental Medicine and Biology*, 508:357–67, 2002. doi: 10.1007/978-1-4615-0713-0_41. PMID 12171131.

Proctor, J. and Holmes, P. Reflexes and preflexes: on the role of sensory feedback on rhythmic patterns in insect locomotion. *Biological Cybernetics*, 102(6):513–31, 2010. doi: 10.1007/s00422-010-0383-9. PMID 20358220.

Proctor, J., Kukillaya, R. P., and Holmes, P. A phase-reduced neuro-mechanical model for insect locomotion: feed-forward stability and proprioceptive feedback. *Philosophical Transactions of the Royal Society of London, Series A*, 368(1930):5087–104, 2010. doi: 10.1098/rsta.2010.0134. PMID 20921014.

Qiu, L., Bernhardsson, B., Rantzer, A., Davison, E., Young, P., and Doyle, J. A formula for computation of the real stability radius. *Automatica*, 31(6):879–890, 1995. doi: 10.1016/0005-1098(95)00024-Q.

Radkhah, K., Maufroy, C., Maus, M., Scholz, D., Seyfarth, A., and von Stryk, O. Concept and design of the BioBiped1 robot for human-like walking and running. *International Journal of Humanoid Robotics*, 08(03):439, 2011. doi: 10.1142/S0219843611002587.

Raibert, M. H. Legged robots. *Communications of the ACM*, 29(6):499–514, 1986. doi: 10.1145/5948.5950.

Rassier, D. E., MacIntosh, B. R., and Herzog, W. Length dependence of active force production in skeletal muscle. *Journal of Applied Physiology*, 86(5):1445–57, 1999. PMID 10233103.

Renjewski, D. and Seyfarth, A. Robots in human biomechanics-a study on ankle push-off in walking. *Bioinspiration & Biomimetics*, 7(3):036005, 2012. doi: 10.1088/1748-3182/7/3/036005. PMID 22510333.

Righetti, L. Programmable central pattern generators: an application to biped locomotion control. In *IEEE International Conference on Robotics and Automation*, pages 1585–1590. IEEE, 2006. ISBN 0-7803-9505-0. doi: 10.1109/ROBOT.2006.1641933.

Rode, C., Siebert, T., and Blickhan, R. Titin-induced force enhancement and force depression: a 'sticky-spring' mechanism in muscle contractions? *Journal of Theoretical Biology*, 259(2):350–60, 2009a. doi: 10.1016/j.jtbi.2009.03.015. PMID 19306884.

Rode, C., Siebert, T., Herzog, W., and Blickhan, R. The Effects of Parallel and Series Elastic Components on the Active Cat Soleus Force-Length Relationship. *Journal of Mechanics in Medicine and Biology*, 09(01):105, 2009b. doi: 10.1142/S0219519409002870.

Rummel, J. and Seyfarth, A. Stable Running with Segmented Legs. *The International Journal of Robotics Research*, 27(8):919–934, 2008. doi: 10.1177/0278364908095136.

Rummel, J., Blum, Y., and Seyfarth, A. Robust and efficient walking with spring-like legs. *Bioinspiration & biomimetics*, 5(4):046004, 2010. doi: 10.1088/1748-3182/5/4/046004. PMID 21079285.

Rutishauser, S., Sprowitz, A., Righetti, L., and Ijspeert, A. J. Passive compliant quadruped robot using Central Pattern Generators for locomotion control. In *IEEE RAS & EMBS International Conference on Biomedical Robotics and Biomechatronics*, pages 710–715. IEEE, 2008. ISBN 978-1-4244-2882-3. doi: 10.1109/BIOROB.2008.4762878.

Rybak, I., Ivashko, D., Prilutsky, B., Lewis, M., and Chapin, J. Modeling Neural Control of Locomotion: Integration of Reflex Circuits with CPG. In *Artificial Neural Networks - ICANN*, pages 99–104, Madrid, 2002. Springer. doi: 10.1007/3-540-46084-5_17.

Sandow, A. Skeletal muscle. *Annual Review of Physiology*, 32:87–138, 1970. doi: 10.1146/annurev.ph.32.030170.000511. PMID 4906128.

Saranli, U., Arslan, O., Ankarali, M., and Morgül, O. Approximate analytic solutions to non-symmetric stance trajectories of the passive Spring-Loaded Inverted Pendulum with damping. *Nonlinear Dynamics*, 62(4):729–742, 2010. doi: 10.1007/s11071-010-9757-8.

Schiehlen, W. Multibody System Dynamics: Roots and Perspectives. *Multibody System Dynamics*, 1(2):149–188, 1997. doi: 10.1023/A:1009745432698.

Schmitt, J. and Holmes, P. Mechanical models for insect locomotion: active muscles and energy losses. *Biological Cybernetics*, 89(1):43–55, 2003. doi: 10.1007/s00422-003-0404-z. PMID 12836032.

Schmitt, S., Haeufle, D. F. B., Blickhan, R., and Günther, M. Nature as an engineer: one simple concept of a bio-inspired functional artificial muscle. *Bioinspiration & Biomimetics*, 7(3):036022, 2012. doi: 10.1088/1748-3182/7/3/036022. PMID 22728876.

Bibliography

Schouten, A. C., de Vlugt, E., van der Helm, F. C. T., and Brouwn, G. G. Optimal posture control of a musculo-skeletal arm model. *Biological Cybernetics*, 84(2):143–152, 2001. doi: 10.1007/s004220000202. PMID 11205351.

Schwind, W. J. *Spring loaded inverted pendulum running: A plant model*. PhD thesis, University of Michigan, 1998.

Seyfarth, A., Geyer, H., Günther, M., and Blickhan, R. A movement criterion for running. *Journal of Biomechanics*, 35(5):649–655, 2002. doi: 10.1016/S0021-9290(01)00245-7. PMID 11955504.

Seyfarth, A., Geyer, H., Lipfert, S. W., Rummel, J., Minekawa, Y., and Iida, F. Running and walking with compliant legs. *Fast Motions in Biomechanics and Robotics*, 340(2006): 383–401, 2006. doi: 10.1007/978-3-540-36119-0_18.

Seyfarth, A., Kalveram, K. T., and Geyer, H. Simulating muscle-reflex dynamics in a simple hopping robot. In *Proceedings of Fachgespräche Autonome Mobile Systeme*, page 294300. Springer, 2007.

Shannon, C. and Weaver, W. *The Mathematical Theory of Communication*. University of Illinois Press, 1949.

Shannon, C. E. A Mathematical Theory of Communication. *Bell System Technical Journal, reprint with corrections*, 27(7,10):379–423,623–656, 1948. doi: 10.1145/584091.584093.

Sherwood, L. *Fundamentals of Human Physiology*. Cengage Learning, Belmont, CA, 2 edition, 2011. ISBN 0840062257.

Siciliano, B., Sciavicco, L., Villani, L., and Oriolo, G. *Robotics*. Advanced Textbooks in Control and Signal Processing. Springer London, London, 2009. ISBN 978-1-84628-641-4. doi: 10.1007/978-1-84628-642-1.

Siebert, T., Rode, C., Herzog, W., Till, O., and Blickhan, R. Nonlinearities make a difference: comparison of two common Hill-type models with real muscle. *Biological Cybernetics*, 98 (2):133–43, 2008. doi: 10.1007/s00422-007-0197-6. PMID 18049823.

Siebert, T., Weihmann, T., Rode, C., and Blickhan, R. Cupiennius salei: biomechanical properties of the tibia-metatarsus joint and its flexing muscles. *Journal of Comparative Physiology B*, 180(2):199–209, 2010. doi: 10.1007/s00360-009-0401-1. PMID 19756652.

Spector, S. A., Gardiner, P. F., Zernicke, R. F., Roy, R. R., and Edgerton, V. R. Muscle architecture and force-velocity characteristics of cat soleus and medial gastrocnemius: implications for motor control. *Journal of Neurophysiology*, 44(5):951–60, 1980. PMID 7441324.

Sreenath, K., Park, H.-W., and Grizzle, J. W. Design and experimental implementation of a compliant hybrid zero dynamics controller with active force control for running on MA-BEL. In *2012 IEEE International Conference on Robotics and Automation*, pages 51–56, Saint Paul, MN, 2012. IEEE. ISBN 978-1-4673-1405-3. doi: 10.1109/ICRA.2012.6224944.

Stein, R. Peripheral Control of Movement. *Physiological Reviews*, 54(1):215, 1974. PMID 4271683.

Strogatz, S. H. *Nonlinear Dynamics And Chaos: With Applications To Physics, Biology, Chemistry, And Engineering.* Westview Press, 1 edition, 2001.

Takuma, T., Izawa, R., Inoue, T., and Masuda, T. Mechanical Design of a Trunk with Redundant and Viscoelastic Joints for Rhythmic Quadruped Locomotion. *Advanced Robotics*, 26(7):745–764, 2012. doi: 10.1163/156855312X626352.

Taylor, M. D. *A Compact Series Elastic Actuator for Bipedal Robots with Human-Like Dynamic Performance.* Master's thesis, Carnegie Mellon University, 2011.

Till, O., Siebert, T., Rode, C., and Blickhan, R. Characterization of isovelocity extension of activated muscle: a Hill-type model for eccentric contractions and a method for parameter determination. *Journal of Theoretical Biology*, 255(2):176–87, 2008. doi: 10.1016/j.jtbi.2008.08.009. PMID 18771670.

Tishby, N., Pereira, F. C., and Bialek, W. The information bottleneck method. In *37th Annual Allerton Conference on Communication, Control and Computing*, Illinois, 1999. Urbana-Champaign.

Tondu, B. and Lopez, P. Modeling and control of McKibben artificial muscle robot actuators. *IEEE Control Systems Magazine*, 20(2):15–38, 2000. doi: 10.1109/37.833638.

Tondu, B. and Zagal, S. McKibben artificial muscle can be in accordance with the Hill skeletal muscle model. In *The First IEEE/RAS-EMBS International Conference on Biomedical Robotics and Biomechatronics*, pages 714–720, Pisa, 2006. IEEE. ISBN 1-4244-0040-6. doi: 10.1109/BIOROB.2006.1639174.

Touchette, H. and Lloyd, S. Information-Theoretic Limits of Control. *Physical Review Letters*, 84(6):1156–1159, 2000. doi: 10.1103/PhysRevLett.84.1156. PMID 11017467.

Touchette, H. and Lloyd, S. Information-theoretic approach to the study of control systems. *Physica A*, 331(1-2):140–172, 2004. doi: 10.1016/j.physa.2003.09.007.

van den Bogert, A. J. Analysis and simulation of mechanical loads on the human musculoskeletal system: a methodological overview. *Exercise and Sport Sciences Reviews*, 22 (403):23–51, 1994. PMID 7925545.

van der Krogt, M. M., de Graaf, W. W., Farley, C. T., Moritz, C. T., Casius, L. J. R., and Bobbert, M. F. Robust passive dynamics of the musculoskeletal system compensate for unexpected surface changes during human hopping. *Journal of Applied Physiology*, 107 (3):801–8, 2009. doi: 10.1152/japplphysiol.91189.2008. PMID 19589956.

van Ingen Schenau, G., Bobbert, M., Ettema, G., de Graaf, J., and Huijing, P. A simulation of rat edl force output based on intrinsic muscle properties. *Journal of Biomechanics*, 21 (10):815–824, 1988. doi: 10.1016/0021-9290(88)90014-0. PMID 3225268.

Bibliography

van Soest, A. J., Bobbert, M. F., and Van Ingen Schenau, G. J. A control strategy for the execution of explosive movements from varying starting positions. *Journal of Neurophysiology*, 71(4):1390–1402, 1994. PMID 8035223.

van Soest, A. J. and Bobbert, M. F. The contribution of muscle properties in the control of explosive movements. *Biological Cybernetics*, 69(3):195–204, 1993. doi: 10.1007/BF00198959. PMID 8373890.

van Zandwijk, J. P., Bobbert, M. F., Baan, G. C., and Huijing, P. A. From twitch to tetanus: performance of excitation dynamics optimized for a twitch in predicting tetanic muscle forces. *Biological Cybernetics*, 75(5):409–417, 1996. doi: 10.1007/s004220050306. PMID 8983162.

Vanderborght, B., Verrelst, B., Van Ham, R., and Lefeber, D. Controlling a bipedal walking robot actuated by pleated pneumatic artificial muscles. *Robotica*, 24(04):401–410, 2006a. doi: 10.1017/S0263574705002316.

Vanderborght, B., Verrelst, B., van Ham, R., Vermeulen, J., and Lefeber, D. Dynamic Control of a Bipedal Walking Robot actuated with Pneumatic Artificial Muscles. In *Proceedings of the 2005 IEEE International Conference on Robotics and Automation*, pages 1–6. IEEE, 2006b. ISBN 0-7803-8914-X. doi: 10.1109/ROBOT.2005.1570087.

Vogel, H. *Gerthsen Physik*. Springer-Lehrbuch. Springer-Verlag, Berlin/Heidelberg, 2006. ISBN 3-540-25421-8. doi: 10.1007/3-540-29973-4.

Volkenstein, M. V. *Entropy and Information*. Birkhäuser Basel, Basel, 2009. ISBN 978-3-0346-0077-4. doi: 10.1007/978-3-0346-0078-1.

Wai, R.-J. Robust Neural-Fuzzy-Network Control for Robot Manipulator Including Actuator Dynamics. *IEEE Transactions on Industrial Electronics*, 53(4):1328–1349, 2006. doi: 10.1109/TIE.2006.878297.

Wakeling, J. M., Lee, S. S. M., Arnold, A. S., de Boef Miara, M., and Biewener, A. a. A Muscle's Force Depends on the Recruitment Patterns of Its Fibers. *Annals of Biomedical Engineering*, 40(8):1708–20, 2012. doi: 10.1007/s10439-012-0531-6. PMID 22350666.

Walcott, S. and Sun, S. X. Hysteresis in cross-bridge models of muscle. *Physical Chemistry Chemical Physics*, 11(24):4871–81, 2009. doi: 10.1039/b900551j. PMID 19506762.

Walker, D. S. and Niemeyer, G. Examining The benefits of variable impedance actuation. In *IEEE/RSJ International Conference on Intelligent Robots and Systems*, pages 4855–4861. IEEE, 2010. ISBN 978-1-4244-6674-0. doi: 10.1109/IROS.2010.5652500.

Wang, Q.-m. and Cross, L. E. Performance analysis of piezoelectric cantilever bending actuators. *Ferroelectrics*, 215(1):187–213, 1998. doi: 10.1080/00150199808229562.

Weber, E. Muskelbewegung. In Wagner, R., editor, *Handwörterbuch der Physiologie mit Rücksicht auf physiologische Pathologie.*, pages Vol 3, 1–222. Vieweg, Braunschweig, 1846.

Weigand, B., Köhler, J., and von Wolfersdorf, J. *Thermodynamik kompakt.* Springer, Heidelberg, 2 edition, 2010. ISBN 978-3-642-13112-7. doi: 10.1007/978-3-642-13113-4.

Wiener, N. *Cybernetics or control and communication in the animal and the machine.* Hermann et Cie, Paris, 1948.

Wilkie, D. R. The relation between force and velocity in human muscle. *The Journal of Physiology*, 110(3-4):249–80, 1949. PMID 15406429.

Winters, J. M. *Hill-based muscle models: a systems engineering perspective*, pages 69–93. Springer-Verlag Berlin and Heidelberg GmbH & Co. K, 1990.

Woittiez, R., Brand, C., de Haan, A., Hollander, A., Huijing, P. A., van Der Tak, R., and Rijnsburger, W. A multipurpose muscle ergometer. *Journal of Biomechanics*, 20(2): 215–218, 1987. doi: 10.1016/0021-9290(87)90312-5.

Wyeth, G. Demonstrating the safety and performance of a velocity sourced series elastic actuator. In *IEEE International Conference on Robotics and Automation*, pages 3642–3647. IEEE, 2008. ISBN 978-1-4244-1646-2. doi: 10.1109/ROBOT.2008.4543769.

Zacher, S. and Reuter, M. *Regelungstechnik für Ingenieure*. Vieweg+Teubner, Wiesbaden, 13 edition, 2011. ISBN 978-3-8348-0900-1. doi: 10.1007/978-3-8348-9837-1.

Zajac, F. E. Muscle and tendon: properties, models, scaling, and application to biomechanics and motor control. *Critical Reviews in Biomedical Engineering*, 17(4):359–411, 1989. PMID 2676342.

Zehr, E. P. Neural control of rhythmic human movement: the common core hypothesis. *Exercise and Sport Sciences Reviews*, 33(1):54–60, 2005. PMID 15640722.

Zuur, A. T., Lundbye-Jensen, J., Leukel, C., Taube, W., Grey, M. J., Gollhofer, A., Nielsen, J. B., and Gruber, M. Contribution of afferent feedback and descending drive to human hopping. *Journal of Physiology*, 588(Pt 5):799–807, 2010. doi: 10.1113/jphysiol.2009.182709. PMID 20064857.

Zuurbier, C., Heslinga, J., Lee-de Groot, M., and Van der Laarse, W. Mean sarcomere length-force relationship of rat muscle fibre bundles. *Journal of Biomechanics*, 28(1): 83–87, 1995. doi: 10.1016/0021-9290(95)80009-3. PMID 7852444.

Credits

Ehrenwörtliche Erklärung

Ich erkläre, dass ich diese Dissertation, abgesehen von den ausdrücklich bezeichneten Hilfsmitteln und den Ratschlägen von den jeweils namentlich aufgeführten Personen, selbständig verfasst habe.

Stuttgart, den 20.12.2012   der Autor